Dissertation
submitted to the
Combined Faculties for the Natural Sciences and for Mathematics
of the Ruperto-Carola University of Heidelberg, Germany
for the degree of
Doctor of Natural Sciences

Put forward by

Dipl.-Phys. Conradin Langbrandtner
Born in Heidelberg

Oral Examination: June 22th 2011

Background, Sensitivity and Directionality Studies for the Double Chooz Experiment

Referees:

Prof. Dr. Manfred Lindner

&

Prof. Dr. Klaus Blaum

Kurzfassung

Das Double Chooz Experiment hat das Ziel den Neutrinomischungswinkel θ_{13} zu messen, von dem bis jetzt nur eine Obergrenze bekannt ist. Zwei Reaktoren eines Kernkraftwerks im französischen Chooz dienen als Quelle der Elektronantineutrinos, deren Fluss in einem nahen und fernen Detektor gemessen wird. Während der ferne Detektor sensitiv auf die Neutrinooszillation ist, minimiert der nahe Detektor verschiedene systematische Fehler. Im Frühjahr 2011 wird mit der Messung am fernen Detektor begonnen, der nahe Detektor wird etwa 18 Monate später folgen. Entscheidend für die Sensitivität des Experimentes ist ein möglichst kleiner systematischer Fehler, für den das Verständnis der Untergrundereignisse von großer Bedeutung ist. In dieser Doktorarbeit werden die vorkommenden Untergrundereignisse charakterisiert und verschiedene Methoden der Untergrundunterdrückung auf ihre Effektivität untersucht. Darüber hinaus werden unterschiedliche Möglichkeiten vorgestellt, die Untergrundrate aus den experimentellen Daten zu gewinnen. Diese Arbeit prüft außerdem die Auswirkung verschiedener Untergrundraten auf die Sensitivität des Experimentes. Ein weiteres zentrales Thema ist die Richtungsrekonstruktion von Neutrinoereignissen. Diese Arbeit zeigt, dass schon nach einigen Monaten die Lage der beiden Reaktoren mithilfe der Neutrinoereignisse bestimmt werden kann. Durch eine genaue Charakterisierung der Neutrino Richtungsrekonstruktion liefert diese Arbeit wichtige Erkenntnisse ihrer Anwendbarkeit auch für zukünftige große Szintillatorexperimente bei geo- und astrophsikalischen Fragestellungen.

Abstract

The goal of the Double Chooz experiment is the measurement of the neutrino oscillation angle θ_{13}. So far, only an upper limit for its magnitude is known. Two reactors of a nuclear power plant at the French Chooz village provide a source of electron antineutrinos, whose flux is measured with a near and far detector. While the far detector is sensitive to neutrino oscillation, the near detector minimizes different systematic errors. In spring 2011 the far detector will start collecting data, while the near detector will follow roughly 18 months later. For the sensitivity of the experiment it is crucial to minimize the systematic error. Therefore, knowledge on background events is important. In this thesis the different sources of background are characterized and the efficiency of various rejection techniques is investigated. Furthermore, different options to determine the background rate from the experimental data are analyzed. The influence of different background rates on the sensitivity of Double Chooz is calculated. Another central aspect of this thesis is the directional reconstruction of neutrino events. It is demonstrated that the direction of the two reactors can be resolved with neutrino events within the first few months. This thesis designs a precise reconstruction of neutrino directions and thus provides an important benchmark for the applicability of future large scale scintillator experiments in both geo- and astrophysics.

Für Gesa

Contents

Introduction

Among the great successes of the Standard Model of Particle Physics is the prediction of the W and Z bosons, the gluon, and the top and charm quarks. Furthermore, the Standard Model precisely predicts the anomalous magnetic moment of the electron, that agrees with experimental measurements at the level of ten decimals. This is one of the best agreements in all of physics. However, there are indications for physics beyond the Standard Model. For example, it offers no candidate for the so called Dark Matter, no mechanism to stabilize the Higgs mass against radiative corrections and it fails to explain the Baryon asymmetry of the universe.
The first and up to now most conclusive indication for physics beyond the Standard Model is caused by neutrino oscillation, which was first proposed in 1957 by Pontecorvo [1], motivated by the $K^0 \leftrightarrows \overline{K}^0$ transition phenomenon, where the strangeness quantum number is oscillating [2]. The only possible oscillation Pontecorvo could think of at that time were $\nu \leftrightarrows \overline{\nu}$ oscillations for Majorana neutrinos, which was motivated by the rumor of Davis's successful observation of $\overline{\nu} + {}^{37}\mathrm{Cl} \rightarrow {}^{37}\mathrm{Ar} + \mathrm{e}^-$ with reactor neutrinos (which turned out to be false [3]) as a result of $\overline{\nu} \rightarrow \nu$ oscillation and a subsequent $\nu + {}^{37}\mathrm{Cl} \rightarrow {}^{37}\mathrm{Ar} + \mathrm{e}^-$ reaction.
A more realistic description of neutrino oscillations became available with the assumption that ν_e and ν_μ are mixed states of two mass eigenstates, which was proposed by Z. Maki, M. Nakagawa and S. Sakata in 1962 [4]. The theory of neutrino oscillations was finally developed in 1976 by S. Eliezer and A. R. Swift [5], H. Fritzsch and P. Minkowski [6] and S. M. Bilenky and B. Pontecorvo [7].
The theoretical effort was driven from experimental side by the so called "solar neutrino problem" which was discovered in the late 1960s at the Homestake experiment [8], confirmed at the end of the 1990s by the gallium experiments and SuperKamiokande [9; 10; 11] and finally model-independently solved by the SNO experiment in 2002 [12]. The depletion of solar neutrinos was found to be caused by the oscillations of ν_e into ν_μ and ν_τ inside the Sun by the MSW resonance conversion effects [13; 14].
The first model-independent proof of neutrino oscillations has been given in 1998 by the SuperKamiokande experiment by measuring precisely the up-down asymmetry of muon-neutrinos produced in the earth's atmosphere [15].
By today, we have good knowledge on five of a total of eight active parameters which control oscillations (the three mixing angles, the two independent mass differences, their signs and the CP violating phase δ_{CP}). The remaining three parameters are the

mixing angle θ_{13}, δ_{CP} and the sign of Δm_{31}. So far, for θ_{13} only an upper limit exists measured by the CHOOZ experiment in 1999 [16]. The next step in the neutrino community will be a precision determination of the already fairly well known values but also the measurement of the remaining three unknown parameters.
Here θ_{13} has a special relevance as the discovery of the important CP-violating phase δ_{CP} strongly depends on the magnitude of θ_{13}. If that oscillation angle turns out to be very small, there is no detection possibility in the near future for δ_{CP}.
The Double Chooz reactor experiment starts taking data in spring 2011 and aims to measure the value of θ_{13} or alternatively to establish a new upper limit with an unreached precision. This will be done by measuring the electron antineutrino flux emerging from the Chooz nuclear power plant with a liquid scintillator detector at 1 km distance, located roughly at the first oscillation maximum. The major improvement of the Double Chooz experiment is the application of a near detector at 400 m distance, measuring the nearly unoscillated antineutrinos. The far detector will start to take data in spring 2011 and the near detector is planned to start operation 1.5 years later. The uncertainty in the neutrino flux is the dominating systematic error in the first 1.5 years without having the near detector. The measurement with two detectors, which are constructed as identical as possible, will reduce the systematic errors considerably as only relative normalization errors remain.
A limiting factor for the sensitivity towards θ_{13} are different kinds of backgrounds causing an adulteration of event rate and measured positron energy spectrum. These contain the relevant information of θ_{13} in the Double Chooz experiment. Thus, it is crucial for the experiment to precisely determine rate and energy spectrum of all backgrounds. By using different rejection methods as the veto system, spatial cuts or pulseshape analysis one can reject background to some degree but on the other side one has to carefully control the influence of the used cuts on the neutrino events. One important background is the Spill In current, which occurs when a neutrino event outside the target volume is falsely counted as a target event. This background is difficult to determine by means of calibration or simulation and, therefore, other analysis techniques must be applied to characterize the Spill In current.
It is a manifestation for the success of neutrino physics in the last decades that we now have the ability to reconstruct the direction of a particle which was believed to be undetectable at the time of its theoretical invention [17]. Starting with the Gösgen experiment, undoubtedly demonstrating the possibility of pointing neutrinos after inverse beta decay [18] up to the imaging of the Sun in its "neutrino light" at the SuperKamiokande detector [19], the neutrino direction reconstruction is nowadays a well established technique whose potential is far from being exhausted. Double Chooz is able to measure the neutron displacement after inverse beta decay, which is the central parameter of neutrino direction reconstruction, with an unreached precision. Thus, Double Chooz will demonstrate the potential of future large scale detectors to resolve the neutrino direction, which will give important insights in geo- and astrophysics.

It is the main objective of this thesis to give a complete view on the background of the Double Chooz experiment. To do so, all sources of background are discussed and the influence of different cuts is demonstrated. When cuts are unsuitable, alternative analysis methods are considered to determine the rate of the background. Consequently, also the influence of backgrounds on the sensitivity of the experiment is considered. The second objective of this thesis is to demonstrate the potential of neutrino direction reconstruction for the Double Chooz experiment and to evaluate its feasibility. The thesis is structured as follows:
In chapter 1 the oscillation formalism is presented. Furthermore, an overview of current or future experiments to measure θ_{13} is given including their competing and complementary physics potential. In chapter 2 the Double Chooz detector setup and detection principle is described in detail. Chapter 3 demonstrates, how well neutrino direction reconstruction works in liquid scintillator detectors and applications for the Double Chooz experiment and future large scale detectors are discussed. In chapter 4 rate and energy spectrum of all main sources of background are presented based to a large extent on simulations. Various cuts, rejection techniques and their influence on the neutrino events are considered. Special attention is given to methods characterizing the Spill In current. Finally, in chapter 5 the influence of different backgrounds and systematics on the sensitivity of the experiment is analyzed using a χ^2-analysis. The main part of the thesis ends with a summary.
This PhD effort started with hardware work on photomultiplier-tubes (PMTs) calibration and simulation, which is compendiously summarized in Appendix A. Part of this PMT calibration and simulation work is already published [20] or will be submitted in the near future [21; 22].

1 Neutrino Oscillation Physics

The main purpose of this chapter is to demonstrate the importance of measuring θ_{13} with a reactor experiment like Double Chooz. It is not a detailed theoretical description of neutrino oscillation or of its influence on the development of the Standard Model.[1] For that the reader might be referred to the standard text books like [24; 25; 26].
The basic theoretical principle of neutrino oscillation is given in section 1.1. Then an overview of the general potential of reactor experiments is presented in section 1.2 and of accelerator experiments in section 1.3. Afterward the complementary of both reactor and accelerator experiments will be demonstrated in section 1.4. Other possibilities to measure θ_{13} will be explained in section 1.5 and the chapter ends with a short outlook to future neutrino oscillation experiments like Neutrino Factories in section 1.6.

1.1 Theoretical Description

The flavor eigenstates of neutrinos (ν_e, ν_μ and ν_τ) can be presented by linear combinations of the three mass eigenstates (ν_1, ν_2 and ν_3) as given by

$$\underbrace{\begin{pmatrix}\nu_e\\ \nu_\mu\\ \nu_\tau\end{pmatrix}}_{\text{flavor}} = \underbrace{\begin{pmatrix}U_{e1} & U_{e2} & U_{e3}\\ U_{\mu1} & U_{\mu2} & U_{\mu3}\\ U_{\tau1} & U_{\tau2} & U_{\tau3}\end{pmatrix}}_{U} \times \underbrace{\begin{pmatrix}\nu_1\\ \nu_2\\ \nu_3\end{pmatrix}}_{\text{mass}}, \tag{1.1}$$

[1] Neutrino masses are set to zero in the Standard Model. The existence of neutrino masses is the first solid experimental fact requiring physics "beyond the Standard Model" [23].

with U being the neutrino mixing matrix (PMNS-Matrix). Assuming the unitary of the mixing matrix[2], U can be written as

$$\begin{aligned} U &= \begin{pmatrix} 1 & 0 & 0 \\ 0 & c_{23} & s_{23} \\ 0 & -s_{23} & c_{23} \end{pmatrix} \times \begin{pmatrix} c_{13} & 0 & s_{13}e^{-i\delta_{CP}} \\ 0 & 1 & 0 \\ -s_{13}e^{i\delta_{CP}} & 0 & c_{13} \end{pmatrix} \times \begin{pmatrix} c_{12} & s_{12} & 0 \\ -s_{12} & c_{12} & 0 \\ 0 & 0 & 1 \end{pmatrix} \\ &\times \begin{pmatrix} e^{-i\frac{\phi_1}{2}} & 0 & 0 \\ 0 & e^{-i\frac{\phi_2}{2}} & 0 \\ 0 & 0 & 1 \end{pmatrix}, \end{aligned} \tag{1.2}$$

with $s_{ij} = \sin\theta_{ij}$ and $c_{ij} = \cos\theta_{ij}$, where θ_{ij} are the three mixing angles. ϕ_1 and ϕ_2 are the CP violating Majorana phases. As they can not be measured in oscillation experiments [27] one can neglect them in the further work.
Neutrinos with flavor $|\nu_\alpha\rangle$ emitted by a source at $t = 0$ develop with time into a state

$$|\nu(x,t)\rangle = \sum_i U_{\alpha i} \mathrm{e}^{-\mathrm{i}E_i t} |\nu_i\rangle = \sum_{i,\beta} U_{\alpha i} U^*_{\beta i} \mathrm{e}^{-\mathrm{i}px} \mathrm{e}^{-\mathrm{i}E_i t} |\nu_\beta\rangle. \tag{1.3}$$

Using elementary quantum dynamics one gets for the oscillation probability of a state $|\nu_\alpha\rangle$ into state $|\nu_\beta\rangle$

$$P(\alpha \to \beta) = \delta_{\alpha\beta} - 4 \sum_{j>i} U_{\alpha i} U_{\alpha j} U_{\beta i} U_{\beta j} \sin^2 \left(\frac{\Delta m^2_{ij}}{4} \frac{L}{E} \right), \tag{1.4}$$

with E being the neutrino energy and L the distance of the source to the detector. The same result can be achieved by a more sophisticated wave packet treatment [28]. Of the 8 active parameters, listed in table 1.1, which control oscillations (the 3 angles of the MNS matrix, the two independent mass differences, their signs and the CP violating phase δ_{CP}) one has so far determined 5. The remaining 3 are the mixing angle θ_{13}, δ_{CP} and the sign of Δm^2_{31}.
However, it should be remarked that we are not just filling out tables for the sake of completeness, but are trying to understand the underlying physics generating neutrino mixing:

- The goal of the Double Chooz experiment is to measure **the unknown oscillation angle θ_{13}** or to improve the upper limit of the former CHOOZ experiment. Right now it is known that from the three mixing angles two (θ_{12} and θ_{23}) are quite large while θ_{13} is quite small. However, within the existing errors the three numbers look like random numbers in the allowed range and carry little

[2] One of the reasons to measure θ_{13} precisely is to clarify that.

Osc. Parameter	Value
θ_{23}	$\begin{matrix}45.6^\circ \\ 46.2^\circ\end{matrix} \pm 3.4^\circ$
θ_{12}	$34.0^\circ \pm 1.0^\circ$
θ_{13}	$< 10.1^\circ$ at 90% C.L. [29]
Δm^2_{31}	$\begin{matrix}2.45 \pm 0.09 \\ -2.34^{+0.10}_{-0.09}\end{matrix} \times 10^{-3}\,\mathrm{eV}^2$
Δm^2_{21}	$7.59^{+0.20}_{-0.18} \times 10^{-5}\,\mathrm{eV}^2$
Dirac Phase δ_{CP}	$\in [0^\circ, 360^\circ]$

Table 1.1: Oscillation parameters with 1σ errors from a global analysis of solar, atmospheric long-baseline and reactor experiments presented in [30]. For θ_{23} and Δm^2_{31} the upper (lower) row corresponds to normal (inverted) neutrino mass hierarchy.

information of the underlying physics. Reducing the errors one may find that θ_{13} is close to zero and θ_{23} is maximal, which point to an underlying symmetry that a more fundamental theory must explain (e.g. [31]).

- The problem of **neutrino mass hierarchy** (the sign of Δm^2_{31}) is a tantalizing dualism of the normal ordering and the inverted one where the former (latter) implies that a pair of neutrinos with a mass gap responsible for solar neutrino oscillations is lighter (heavier) than the third neutrino. Picking out one from the two alternatives of neutrino mass patterns may bring us one of the most significant hints for underlying physics of neutrino mass.

- Even there is no model-independent connection between the **CP-violating phase** δ_{CP} and the majorana phases, however, a measurement of a nonzero δ_{CP} would still demonstrate that CP violation exists in the neutrino sector, being an important step for the credibility of leptogenesis and the question where the matter in the universe comes from, one of the greatest mysteries in fundamental physics today.

In section 1.3 it will be shown that there are ambitious plans to measure δ_{CP} and $\mathrm{sgn}(\Delta m^2_{31})$ with large accelerator experiments. But since the observable effects of δ_{CP} always appear multiplied by $\sin^2 2\theta_{13}$ and also the sensitivity of $\mathrm{sgn}(\Delta m^2_{31})$ is depending on $\sin^2 2\theta_{13}$ [32] finding a non-zero value of θ_{13} is a critical step for these efforts.

1.2 Reactor Experiments

Typically 5% of the heat produced per fission in a nuclear power plant is carried away by $\overline{\nu}_e$. All reactor experiments are necessarily disappearance experiments measuring $P(\overline{\nu}_e \to \overline{\nu}_e)$ as their energy (some MeV) is far below the threshold for producing μ and τ.
Using equation 1.2 and 1.4 one can calculate the survival probability for the electron antineutrinos from reactors to

$$P(\overline{\nu}_e \to \overline{\nu}_e) \simeq 1 - \underbrace{\sin^2 2\theta_{13} \sin^2 \frac{\Delta m^2_{31} L}{4E}}_{\theta_{13}\text{-dominated}} - \underbrace{\cos^4 \theta_{13} \sin^2 2\theta_{12} \sin^2 \frac{\Delta m^2_{21} L}{4E}}_{\theta_{12}\text{-dominated}}, \qquad (1.5)$$

neglecting terms of higher order in $\Delta m^2_{21}/|\Delta m^2_{31}|$ [33; 34].
With a mean neutrino energy of 3.6 MeV and the values of Δm^2_{21} and $|\Delta m^2_{31}|$ of table 1.1 one finds that at short baselines in the order of $\mathcal{O}(1)$ km the last term of equation 1.5 gets negligible and one has a very clean window into the mixing angle θ_{13} and the Δm_{31}-mass-difference (if θ_{13} is not too small). In the order of $\mathcal{O}(100)$ km the mixing angle θ_{12} and the Δm^2_{21}-mass-difference get measurable. At this distance it is not possible to measure θ_{13} as the neutrino oscillation is blurred with the energy and one can only measure the average oscillation probability. This is illustrated in figure 1.1.

θ_{13}-dominated Experiments

There has been a quite long and successful tradition of reactor experiments at the $\mathcal{O}(1)$ km distance. Starting in 1956 with the first observation of neutrinos at the Cowan-Reines experiment [35] up to the CHOOZ experiment finding the so far best upper limit on θ_{13} [16] there have been several reactor experiments of this type improving the knowledge of the neutrino. A review can be found in [36].
The far detector of Double Chooz will be located 1055 m from the two reactor cores. At this distance the second term of equation 1.5 gets negligible and, therefore, one is able to measure θ_{13} without the influence of any other mixing angle.
Not only the simple counting of electron neutrino events but also the visible energy spectrum[3] contains information about neutrino oscillation due to the energy dependence of the survival probability as illustrated in figure 1.2. In fact with growing statistics the shape of the observed neutrino energy spectrum contains more information than the pure rate of events.

[3] The visible energy E_{vis} will be introduced in more detail later but it shell already be remarked that E_{vis} is directly connected with the neutrino energy E_ν due to $E_\nu = E_{\text{vis}} + 0.78\,\text{MeV}$.

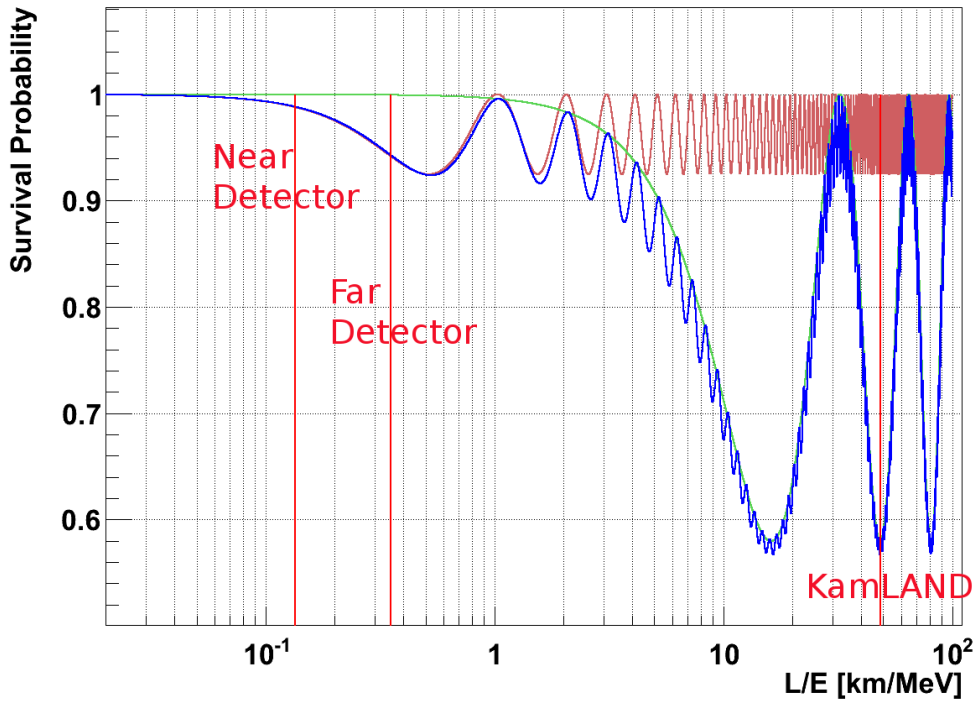

Figure 1.1: Survival probability of $\overline{\nu}_e$ of equation 1.5. In blue for $\sin^2 2\theta_{13} = 0.15$ and $\sin^2 2\theta_{12} = 0.32$. In green the for $\sin^2 2\theta_{13} = 0$ and in red for $\sin^2 2\theta_{12} = 0$. The three vertical red lines indicate the L/E position of the near and far detector of Double Chooz and the averaged KamLAND detector position. The used values of Δm_{21} and Δm_{31} are given in table 1.1.
At the position of the near and far detector of Double Chooz there is no influence of the θ_{12} mixing angle.

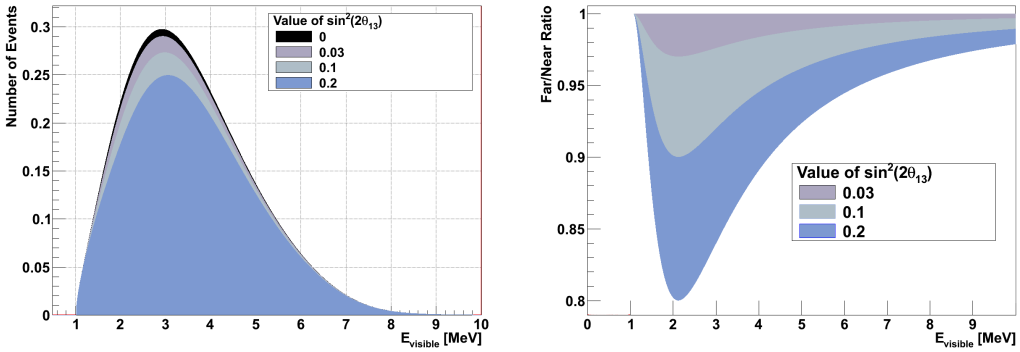

Figure 1.2: **Left:** Deformation of the observed visible energy spectrum in the far detector of Double Chooz for different values of $\sin^2 2\theta_{13}$.
Right: Ratio of the observed visible energy spectrum in the near and far detector.

θ_{12}-dominated Experiments

The KamLAND experiment [37] measures the neutrino flux of 53 Japanese power reactors resulting in an average baseline of roughly 175 km. At this distance KamLAND provides the best possible measurement of Δm^2_{21} for the foreseeable future. Further background reductions may even lead to a sensitivity of KamLAND for θ_{12} obtained in solar neutrino experiments [38]. The big achievement of KamLAND was the exact measurement of Δm^2_{21} and thus to indicate that the oscillation parameters lie in the MSW LMA (Large Mixing Angle) region [38]. This was achieved in a combined analysis of KamLAND and the solar neutrino experiments as illustrated in figure 1.3.

1.3 Accelerator Experiments

Present accelerator experiments produce ν_μ or $\overline{\nu}_\mu$ by hadron (mainly pion and kaon) decay. The hadrons were produced by an intense beam of protons with a kinetic energy of around 100 GeV colliding with a target (e.g. graphite). The positively charged hadrons are focused into a beam and travel down a several 100 m long decay pipe where the beam particles decay primarily to μ and ν_μ. At the end of the decay pipe the remaining muons and hadrons are ranged out in concrete absorber or rock while the neutrinos travel to the detector [25].
Measuring $P(\nu_\mu \to \nu_\mu)$ gives a very precise window into $|\Delta m^2_{31}|$ and θ_{23}. In fact the most precise measurement of $|\Delta m^2_{31}|$ results so far from the accelerator experiment MINOS [39].

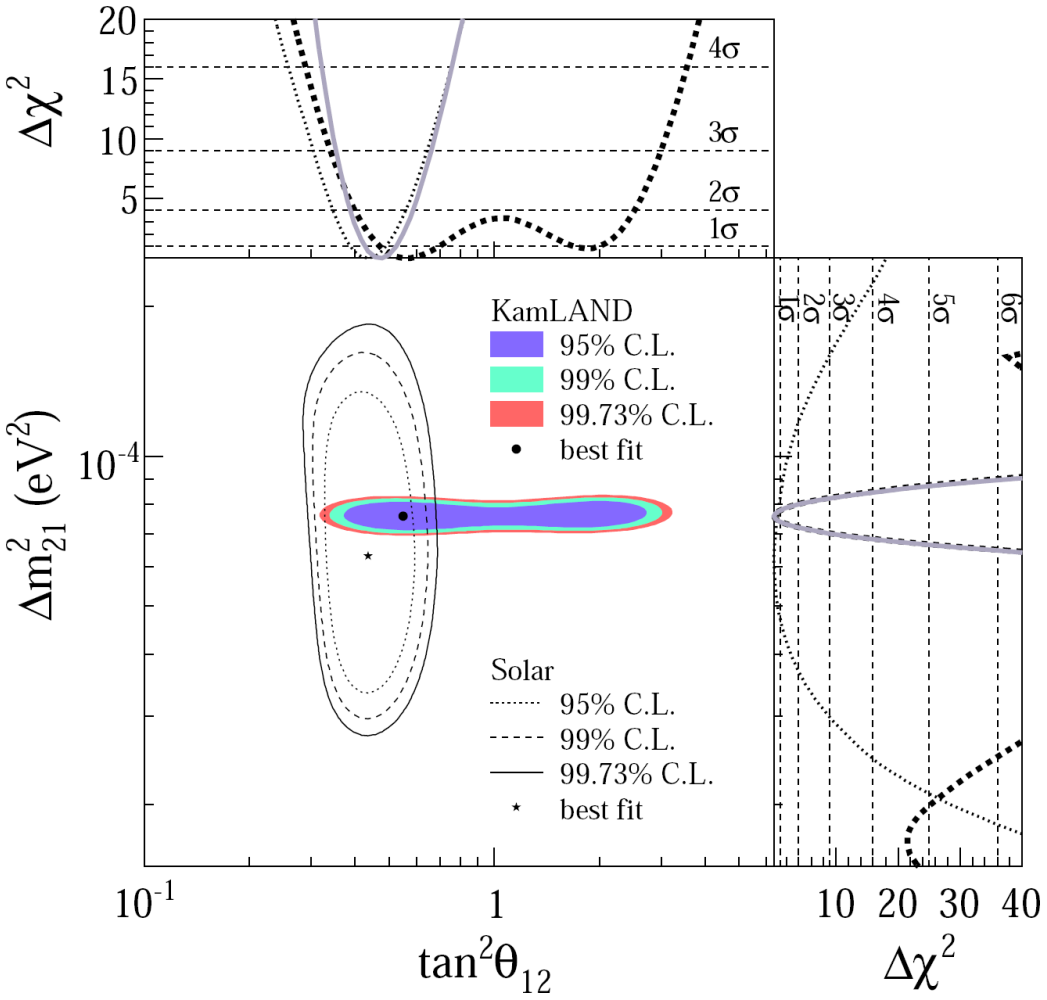

Figure 1.3: Region for neutrino oscillation parameters from KamLAND and solar neutrino experiments. The side-panels show the Δ^2-profiles for KamLAND (dashed) and solar experiments (dotted) individually, as well as the combination of the two (solid) [37].

In the three-flavor oscillation framework, measuring $P(\nu_\mu \rightarrow \nu_e)$ is a very sensitive probe for θ_{13}.

$$P\left(\nu_\mu \rightarrow \nu_e\right) = \sin^2\theta_{23}\sin^2 2\theta_{13}\sin^2\frac{\Delta m^2_{31}L}{4E} + \text{not small terms}(\delta_{CP}, \text{sgn}(\Delta m^2_{31})) \tag{1.6}$$

The exact formula is given e.g. in [23].
It was already mentioned that beneath θ_{13} also the CP-violating phase δ_{CP} and the sign of Δm^2_{31} are not yet determined. For both a combined measurement of the $\nu_\mu \rightarrow \nu_e$ *and* $\overline{\nu}_\mu \rightarrow \overline{\nu}_e$ channel is crucial.
ν_μ and $\overline{\nu}_\mu$ can be produced in large number in accelerators with a quite sharp energy distribution of 3 to 10 GeV and a high pureness[4] at energies of several GeV. Thus, searching for the appearance of ν_e or $\overline{\nu}_e$ in the ν_μ or $\overline{\nu}_\mu$ beam is a very sensitive probe for θ_{13}, δ_{CP} and the sign of Δm^2_{31} using long baselines of several 100 km.

1.3.1 Present Accelerator Experiments

Present accelerator experiments use ν_μ beams to search for ν_μ-disappearance at a baseline of 250 km (K2K [40]) or 735 km (MINOS [39]) and to search for ν_τ-appearance at a baseline of 730 km(OPERA [41]). These experiments will improve the present oscillation parameters and especially increase the lower limit of θ_{23} to clarify if this angle is maximal.
Furthermore, using equation 1.6, they are also able to measure θ_{13}:

- **K2K** found an upper limit of $\sin^2 2\theta_{13}$ consistent with the CHOOZ-result (but slightly larger)[42].

- In 2009 **MINOS** reported 35 ν_e-like events with a background of 27 ± 5(stat.)$\pm$ 2(syst.) events corresponding to a 1.5σ excess which could be explained by a nonzero value of θ_{13} [43]. However, one year later having larger statistics and better understood systematics the MINOS collaboration reported the observation of 54 ν_e-like events with an expected background of 49.1 ± 7.0(stat.) $\pm$ 2.7(syst.), thus reducing the excess above background to only 0.7σ [44].

- Beneath the direct detection of ν_τ appearance from $\nu_\mu \rightarrow \nu_\tau$ oscillation [45] (in summer 2010 the first observation of a ν_τ was published [46]) the **OPERA** detector can also search for the sub-leading $\nu_\mu \rightarrow \nu_e$ oscillation. Thanks to the high granularity and density of the emulsion cloud chamber the OPERA detector is even better suited for electron detection compared to the MINOS experiment and can reach $\sin^2 2\theta_{13} \leq 0.06$ at 90% C.L. after 5 years exposure to the CNGS beam at nominal intensity [47].

[4] Roughly 1% of a ν_μ-beam are ν_e due to the decay of the kaons and of muons [38].

1.3.2 The Superbeam Generation

The main disadvantages of the existing accelerator experiments presented above are the limited power of the proton driver and the intrinsic ν_e-contamination of the beam. In particular the CNGS beam of OPERA, which has been optimized for τ production, has a mean energy about ten times larger than the first $\nu_\mu \rightarrow \nu_e$ oscillation peak at a baseline of 732 km.
The running or planned Superbeam experiments T2K and NOνA are optimized for the of ν_e appearance in a ν_μ beam to measure above all θ_{13}, δ_{CP} and the mass hierarchy. Both experiments have the big advantage to use an increased beam power of 750 kW (roughly twice the power of conventional beams) and to operate off-axis leading to larger flux in the atmospheric L/E, reducing the background due to quasi-elastic scattering at large energies and reducing the intrinsic ν_e contribution in the ν_μ beam.
It should be mentioned that the Superbeam program will furthermore measure the atmospheric parameters θ_{23} and Δm^2_{31} with a so far unreached precision using the $\nu_\mu \rightarrow \nu_\mu$ disappearance channel. The error on the mass difference should be $\sim 2\%$ within a few years, while the error on θ_{23} depends strongly on the value of θ_{23} itself but should be around $\sim 1\%$ [48].

T2K

The T2K experiment can be considered as an upgrade of the K2K experiment. A high intensity ν_μ beam is sent from J-PARC facility to the SuperKamiokande detector located 295 km away with an off-axis angle of 2.5°. That off-axis angle has been chosen to maximize the sensitivity of the experiment to θ_{13}. Beneath the far detector (the SuperKamiokande water-Cherenkov detector) T2K has two near detectors at 280 m [48]. One is on-axis (INGRID) to control the neutrino direction precisely ($<$1 mrad) as a deviation of the beam direction would create a different spectral shape at the far detector. The second near detector (ND280) is off-axis at the same angle as the far detector. The goal of this detector is to measure the ν_μ flux (5% accuracy), the ν_e contamination (2% accuracy) and to measure precisely the π_0 production cross-section as the 2γ-decay of the π_0 is the main background for the ν_e detection [38].
T2K has detected the first neutrino at the end of February 2010 [49]. The θ_{13}-sensitivity for normal hierarchy, $\delta_{CP} = 0$ and $\Delta m^2_{31} = 2.43 \cdot 10^{-3}$ is quoted with $\sin^2 2\theta_{13} = 0.006$ at 90% C.L. after 5 years of data taking.
An upgrade of the experiment is foreseen called T2HK [50], using the HyperKamiokande detector [51] with an enlarged detection volume of roughly 1 Mton and an increased beam-power up to 4 MW.

NOνA

The NOνA experiment will be located at the Ash River facility and observes a neutrino beam with 700 kW and a mean energy of 2 GeV from NuMI located 810 km away. It was proposed to reach a sensitivity for ν_e appearance 10 times better than MINOS [52].
The detector will be a 15 kton segmented plastic scintillator placed 0.8° off-axis. Due to the longer baseline and the larger energy compared to T2K, NOνA will be more sensitive to matter effects and thus to the sign of Δm^2_{31}. Data taking is expected to start 2013. The experiment is planned to run 3 years in ν_μ mode and then again 3 years producing $\overline{\nu}_\mu$ to be sensitive to δ_{CP}. The sensitivity for θ_{13} is quoted with $\sin^2 2\theta_{13} = 0.007$ for normal hierarchy, $\delta_{CP} = 0$ and $\Delta m^2_{31} = 2.43 \cdot 10^{-3}$ at 90% C.L. after 3 years of data taking.

1.4 Complementarity of Superbeams and Reactor Experiments

Many authors have already discussed the degeneracy problem occurring in superbeam experiments [32; 53; 54] and here the combination of reactor and superbeam experiments to resolve the degeneracy problem will only be shortly summarized and motivated.
A measurement of the appearance probability $P(\nu_\mu \to \nu_e) = P_{\mu e}$ for an experiment at a fixed baseline L and energy E can not be used to determine uniquely the oscillation parameters. Taking $(\overline{\theta}_{13}, \overline{\delta}_{CP})$ as the true values, the equation

$$P_{\mu e}\left(\overline{\theta}_{13}, \overline{\delta}_{CP}\right) = P_{\mu e}\left(\theta_{13}, \delta_{CP}\right) \tag{1.7}$$

has a continuous number of solutions as illustrated in figure 1.4 on the left side. The strong correlation of the oscillation parameters defines a strip of solutions $P_{\mu e}\left(\theta_{13}, \delta_{CP}\right)$ in the $(\theta_{13}, \delta_{CP})$-plane compatible with $P_{\mu e}\left(\overline{\theta}_{13}, \overline{\delta}_{CP}\right)$.
In principle T2K and NOνA can also produce a beam of antineutrinos. As one can see on the right side of figure 1.4 the continuum degeneracy reduces then to a twofold degeneracy. Still two solutions are possible for a measured appearance probability $P_{\mu e}$.
In general one can resolve this twofold degeneracy by an independent measurement at a different L/E or by measuring the neutrino energy spectra very precisely and bin them. Each bin then corresponds to a different L/E. The last method will not work at T2K since the energy reconstruction is not sufficient [55] (one rather need a liquid-argon detector as proposed in [56]).
T2K together with NOνA could resolve this twofold degeneracy as shown in figure 1.5. However, first results of NOνA are not expected before 2016 and T2K just has

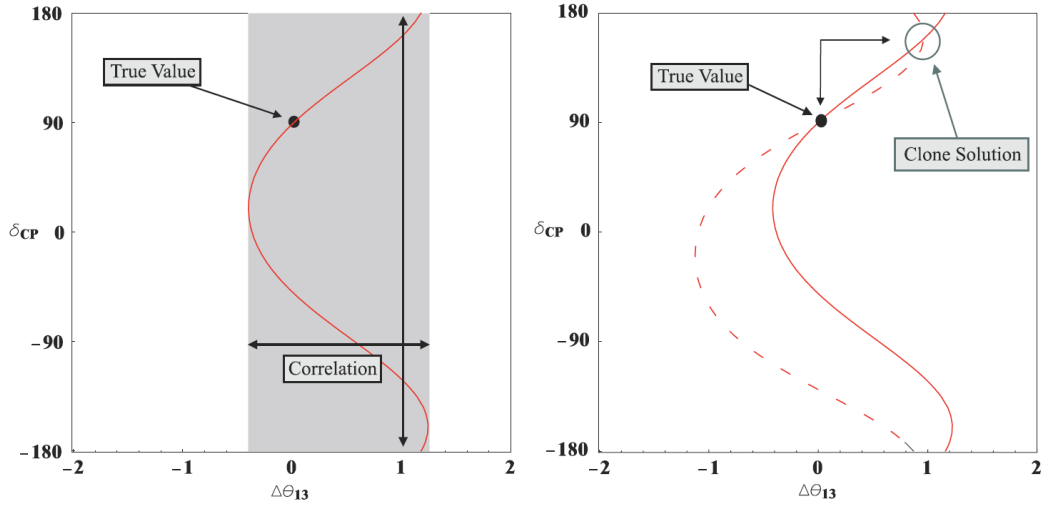

Figure 1.4: **Left:** Correlation of δ_{CP} and θ_{13} if only neutrinos (or antineutrinos) are measured, causing continuum degeneracy.
Right: Correlation if both neutrinos (full line) and antineutrinos (dashed line) are measured, causing twofold degeneracy [55].

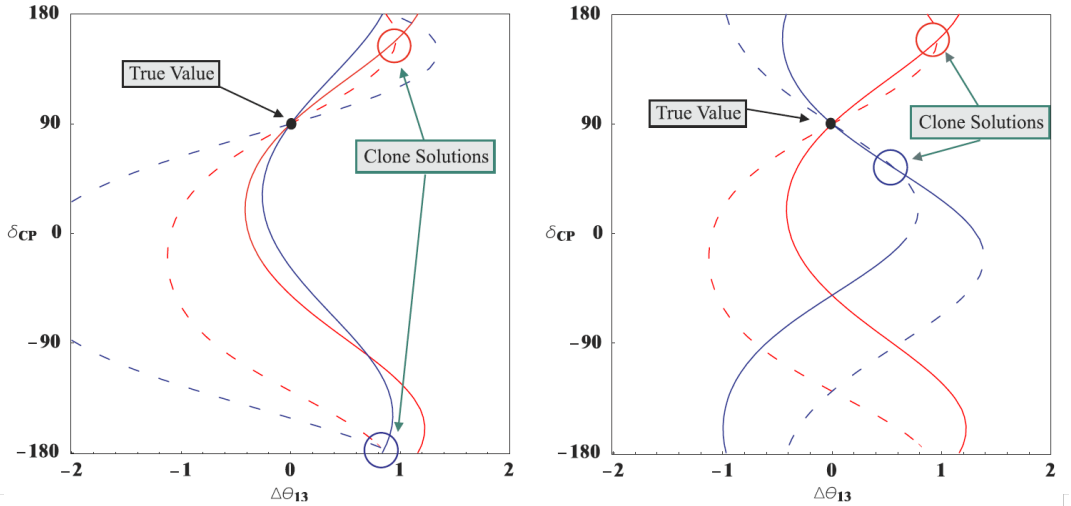

Figure 1.5: **Left:** Solving the degeneracy by using the same channel but at two different baselines.
Right: Solving the degeneracy by using the same baseline but using two different channels (e.g. the "platinum" ($\nu_\mu \rightarrow \nu_e$) and "silver" ($\nu_\mu \rightarrow \nu_\tau$) channel) [55].

started measurements in the neutrino mode. Furthermore, antineutrino running has the disadvantage of a much lower statistics since the neutrino cross section is larger than the anti-neutrino cross section. To accumulate similar statistics the antineutrino mode has to run much longer than the neutrino mode.
Instead of resolving the $\sin^2 2\theta_{13}$ and δ_{CP} correlation with the antineutrino beam and two baselines it was proposed in [32] to resolve it with a precision measurement at a reactor experiment like Double Chooz or Daya Bay [57].
One should point out that using reactor experiments as "clean laboratories for θ_{13}-measurements" [34] can enhance the detection potential of Superbeams by excluding a large part of the $(\delta_{CP}, \theta_{13})$-plane assuming a not too small value of $\sin^2 2\theta_{13}$.
However, the situation gets even more complicated including the unknown sign of Δm^2_{31} and the not exact known value of θ_{23}. Adding the "sign degeneracy" of Δm^2_{31} and the "octant degeneracy" of θ_{23} results in the so called "eight-fold degeneracy". To resolve all degeneracies, several measurements with high precision are needed combining different neutrino oscillation channels [58].

1.5 Other Methods to measure θ_{13}

Beneath using reactors and accelerators to search for the θ_{13} there exist other possibilities.

1.5.1 Atmospheric Neutrinos

The MSW effect [59] of neutrinos crossing the earth matter can produce an enhanced oscillation probability of atmospheric ν_μ into ν_e. Assuming θ_{13} to be at the CHOOZ limit and a neutrino energy of 2-10 GeV it can lead to a 40% excess of upward going ν_e at 7 GeV [60].
So far SuperKamiokande has observed no evidence for this effect [61]. The achieved limit is $\sin^2 2\theta_{13} < 0.15$ and, therefore, close to the CHOOZ limit.

1.5.2 Solar Neutrinos

- A similar effect could produce a day-night asymmetry in the solar neutrino flux due the "regeneration effect" effect in the earth [62]. This asymmetry is proportional to $\cos^2 \theta_{13}$ and, thus, another probe of θ_{13}. However, such an effect was not observed so far in SNO and Borexino [63][64].

- Figure 1.6 shows a comparison of the KamLAND data with the results of the solar experiments. While there is perfect agreement in Δm^2_{21} there appears a mismatch in the favored value of θ_{12}. In [65] it was pointed out that this

mismatch can be lifted by a non-zero value of θ_{13}. Assuming $\theta_{13} > 0$ the KamLAND spectrum can be well fitted with a smaller value of θ_{12}.
However, one must notice that the better agreement between solar and KamLAND analysis for $\theta_{13} \neq 0$ has to be contrasted with a worsening of the global description of the solar neutrino data also given in [65]. As a consequence the best-fit value of θ_{13} and also the statistical significance of the combined solar and KamLAND data is lowered to:

$$\sin^2\theta_{13} = \begin{cases} 0.021 \pm 0.017 & \text{for GS98} \\ 0.017 \pm 0.017 & \text{for AGSS09} \end{cases} \tag{1.8}$$

Due to quite large statistical uncertainties and the dependence of the used solar model there is so far only a quite weak indication for $\theta_{13} \neq 0$ from combined analysis of the solar and long-baseline experiments.

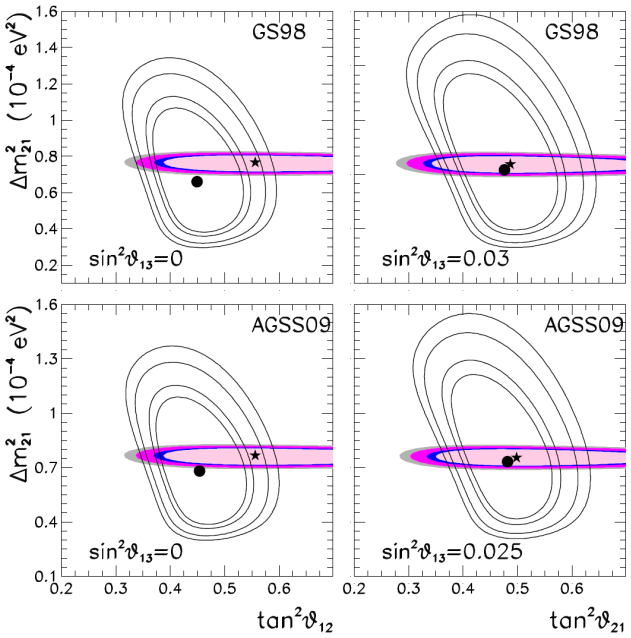

Figure 1.6: Allowed parameter regions (at 90%, 95%, 99% and 99.73% C.L.) from analysis of KamLAND (colored regions with best-fit marked with a star) and solar (void regions with best-fit marked by a dot) data for two different valued of $\sin^2\theta_{13}$ as labeled in the figure. GS98 and AGSS09 are the two different solar models used [44].

1.5.3 Supernova Neutrinos

The neutrino flux of a supernova explosion is dependent on θ_{13} through the MSW effect in the supernova [66]. However, there are other parameters as the density profile of the star influencing the neutrino flux and, therefore, an isolated measurement of the θ_{13} information gets difficult. Experiments aiming to measure θ_{13} from a supernova need, thus, a very good spectral resolution combined with large statistics. Huge water Cherenkov detectors doped with Gadolinium are the best detectors for this purpose. The θ_{13} effect occurs for $\sin^2 2\theta_{13} < 10^{-3}$. Therefore, a supernova explosion observed by the detector just described would tell us if $\sin^2 2\theta_{13}$ is above or below this limit.

1.6 Future Neutrino Oscillation Experiments

The now or in not too far future starting neutrino oscillation experiments will remeasure θ_{12}, θ_{23}, Δm^2_{21}, $|\Delta m^2_{31}|$ with high precision, possibly clarify the sign of Δm^2_{31} and (if not too small) the value of θ_{13}. However, as it was stated before, due to the degeneracies in the $\nu_\mu \rightarrow \nu_e$ channel the measurement of δ_{CP} is limited.
The "era of precision" [67] will use new generations of neutrino sources (Neutrino Factories and Beta Beams [23; 68]) and detectors [69] to resolve the degeneracies and measure all oscillation parameters with an unreached precision.
One possible way was proposed in [58]. They suggest to have two detectors, one detector at about 4000 km which is optimized for measurements of CP violation and determination of θ_{13} and the second detector to be at the "magic baseline" of 7500 km. The "magic baseline" is about 7300-7600 km. At this distance the CP-violating phase is not present and a clean determination of θ_{13} and the neutrino mass hierarchy is possible. Using this detector setup neutrino factories have a sensitivity down to $\sin^2 2\theta_{13} < 10^{-5}$ and can observe the neutrino mass hierarchy and CP violation for $\sin^2 2\theta_{13} > 10^{-4}$ [58].

2 The Double Chooz Experiment

The CHOOZ experiment had taken data between April 1997 and July 1998 and became famous for investigating the so far best upper limit on $\sin^2 2\theta_{13}$.[1] However, the sensitivity of CHOOZ was limited by various factors. The uncertainty of the reactor flux (2%) was the main limitation on the systematic side resulting in an overall systematical error of 2.7%. On the other side it was limited by statistics as the optical properties of the scintillator absorption length continuously degraded. CHOOZ stopped data taking after having collected about 2700 neutrino candidates. These limitations and problems of CHOOZ are substantially improved at Double Chooz. Using an identical near detector to measure precisely the reactor flux and an improved monitoring and shielding of the background events push the overall systematical error to 0.5%. On the other side an enlarged target volume will increase the event rate by roughly a factor of 2. An improved scintillator composition should result in a stability of several years.
Double Chooz will start data taking with the far detector alone for a period of roughly 1.5 years, as the assembly of the near detector has just started. This period is called Phase-I and will reach the CHOOZ-sensitivity of $\sin^2 2\theta_{13} = 0.15$ already after 2-3 month of good data taking and achieve after 1.5 years a sensitivity of $\sin^2 2\theta_{13} \approx 0.06$. Again the main limitation will be the reactor flux uncertainty. In the Phase-II both detectors will be operating. The direct comparison of the unoscillated neutrino spectrum in the near detector with the one measured at the far detector will bring the sensitivity below $\sin^2 2\theta_{13} = 0.03$ after in total 5 years data taking.
In this chapter an overview of the used detection method and the detector setup of Double Chooz is given. Therefore, in section 2.1 the general working principle of the experiment is presented. The production and detection of $\overline{\nu}_e$ is explained in section 2.2 and 2.3. Special attention is given to the kinematics of the inverse beta decay (IBD) as it is of central importance for the neutrino direction reconstruction. Then the structure of the Double Chooz detector and of the simulation package is given in section 2.4 and 2.5.

[1] Over 860 citations of the main article "Limits on neutrino oscillations from the CHOOZ experiment" [16].

2.1 Working Principle

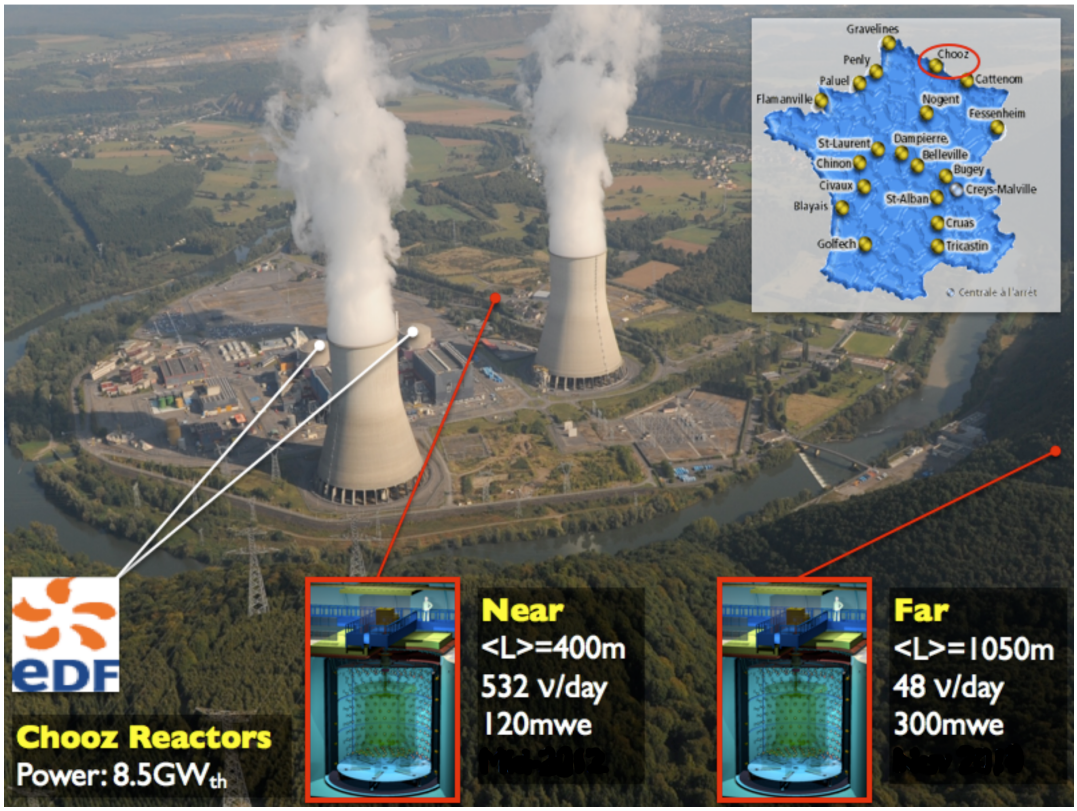

Figure 2.1: The reactor and Double Chooz detector topology.

The basic idea of Double Chooz is the same as in the legendary Reines-Cowan experiment in 1956 [35]: In a volume of liquid scintillator the neutrino undergoes IBD with a proton producing a positron-neutron pair. The positron immediately loses its kinetic energy by scattering with the scintillator molecules and than annihilates with an electron producing light in both processes. The light of this so called prompt signal is detected by photomultiplier tubes observing the scintillator.
The neutron after IBD has only $\mathcal{O}(10\,\mathrm{keV})$ kinetic energy. It is captured some tens to hundreds of μs after IBD dominantly on Gadolinium, which has been added to the scintillator exactly for this reason, producing gammas with in total 8 MeV energy. The light of the capture process is again detected by the photomultipliers and is called late event.
The signal of an neutrino event is, therefore, a coincidence of a prompt and late event in a timewindow of 200μs. The prompt energy is between

0.5 and 8 MeV and the late event energy around 8 MeV.
After IBD the positron is emitted nearly isotropic, while the neutron preserves a memory of the neutrino incoming direction.
While the positron contains the information on the neutrino energy, one can use the neutron to reconstruct the neutrino incoming direction.
Alternatively one could also have used elastic scattering on electrons, quasi-elastic scattering on a proton or deuteron or even on a nucleus to detect the antineutrinos from a reactor. The choice of the IBD was driven by the fact that elastic scattering on electrons has a lower cross section[2], because the interaction with $^{2}_{1}$H has a too high energy threshold of 2.2 MeV and because the interaction on a nucleus is hardly detectable (a few keV of nucleus recoil energy). But the main argument for using the IBD is that one can use the coincidence measurement of the prompt and late event to considerably reduce the background.

2.2 Production of Electron Antineutrinos in a Nuclear Reactor

The Chooz nuclear power plant is a "pressurized water reactor" and each reactor core has a thermal power of 4.27 GW. It is located close to the small village called Chooz in the Ardennes region in the northeast of France, close to the Belgium border.
In a nuclear reactor electron antineutrinos are produced dominantly by the beta decay of the fission products from the four isotopes l=^{235}U, ^{239}Pu, ^{238}U and ^{241}Pu.[3]
The flux from isotope l is given by $\Phi_l(E_\nu)$ in units of antineutrinos per fission and MeV. If the initial composition of the reactor fuel is known, the individual contribution to Φ of each isotope l can be calculated at the different burn-up stages by core simulation codes better than 1% [71].
In [72; 73] the beta spectra from the fission products of ^{235}U, ^{239}Pu and ^{241}Pu were measured from the exposure of these isotopes to thermal neutrons.[4] Subsequently these beta spectra have to be converted into antineutrino spectra including the large number of beta branches involved. The resulting spectra and rates are in excellent agreement with the direct measurement of the antineutrino spectrum at the Bugey reactors [75]. The synthesis of published experiments at reactor-detector distances

[2] The measurement of the scattering of reactor antineutrinos with electrons was e.g. performed at the MUNU experiment to provide information on basic features of the weak interaction and on neutrino properties such as the magnetic moment [70]
[3] The next to leading contributions come from the isotopes ^{240}Pu and ^{242}Pu at the order of 0.1% or less [36].
[4] As ^{238}U undergoes only fast neutron fission no similar measurements exist so far and one has to rely on theoretical calculations. The group of the TUM actually tries to measure this spectrum experimentally [74].

<100 m leads to a good agreement in the ratio of observed event rate to predicted rate with 0.979±0.029 [76].[5]
The neutrino flux spectrum Φ can be written as

$$\Phi(E_\nu) = \exp\left(\sum_{k=1}^{K_l} a_{kl} E_\nu^{k-1}\right). \tag{2.1}$$

K_l stands for the isotopes ^{235}U, ^{239}Pu, ^{238}U and ^{241}Pu. Using the parametrization a_{kl} of [71] one gets for the flux $\Phi(E_\nu)$ the behavior of figure 2.2.
For the CHOOZ experiment the error on the total neutrino flux was about 2% being one of the main contributors for the limitation of the sensitivity. For the Phase-I of Double Chooz a similar systematic error on the total neutrino flux is expected.

2.3 Neutrino Detection at Double Chooz

2.3.1 Neutrino Energy

Reactor antineutrinos have energies of the order of the MeV and are detected at Double Chooz by the IBD reaction:

$$\overline{\nu}_e + p \rightarrow e^+ + n \tag{2.2}$$

The threshold of the IBD is $\Delta + m_e = 1.806\,\text{MeV}$, where $\Delta = m_n - m_p$ is the mass difference of neutron and proton.
The outcome of an IBD is a positron and a neutron. As calculated in [78] and shown in figure 2.3 on the right side the neutron has only a negligible kinetic energy of $\mathcal{O}(10\,\text{keV})$ and thus contains no observable information of the neutrinos energy. Therefore, one finds for the energy of the positron:

$$E_{e^+} = E_{\overline{\nu}} - \Delta. \tag{2.3}$$

As the positron travels through the scintillator light is produced by interaction of the charged positron with the scintillation molecules. Finally the positron annihilates

[5] Recently new reactor antineutrino spectra have been provided for ^{235}U, ^{238}U, ^{239}Pu and ^{241}Pu increasing the mean flux by about 3% [77]. This shifts the ratio to 0.937±0.027, leading to a deviation from unity at 98.4%. In [76] this phenomenon was called "reactor antineutrino anomaly" and the compatibility of that result with a fourth non-standard neutrino state driving neutrino oscillations at short distances was discussed. However, it was also stressed there that other explanations are possible, such as a correlated artifact in the reactor experiments or an erroneous prediction of the antineutrino flux models.
In [30] a combined analysis of new MINOS results and the relevant solar, atmospheric and reactor experiments were presented including the "reactor antineutrino anomaly". However, the hint for a non-zero θ_{13} stays weak at $2.2(2.3)\sigma$ for normal (inverted) hierarchy.

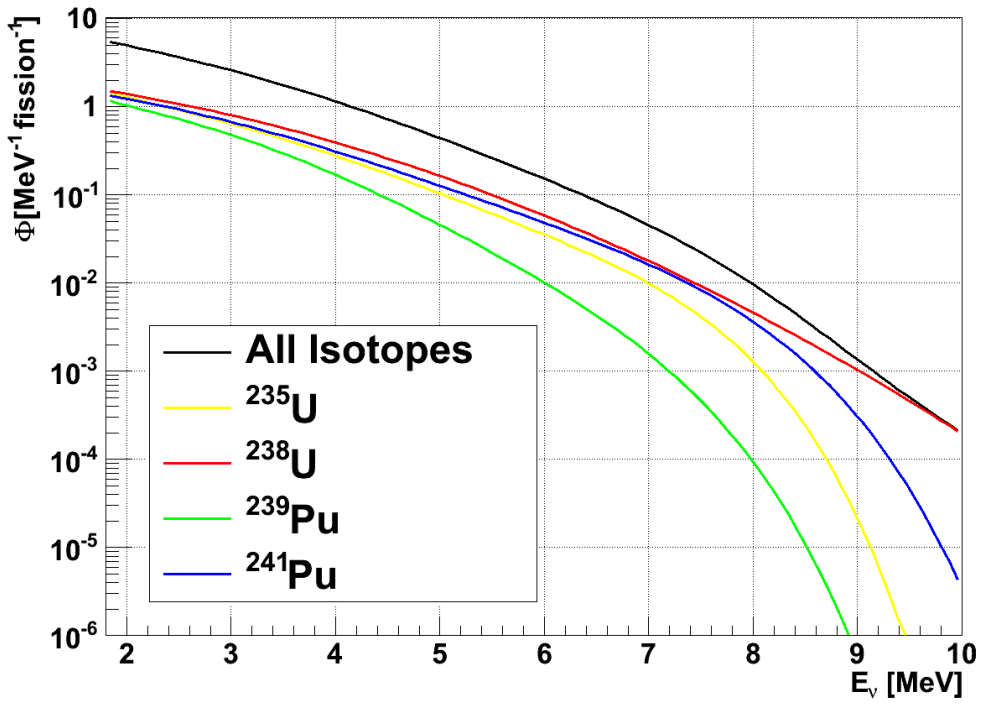

Figure 2.2: Energy Spectrum of the neutrino flux of the 4 isotopes involved in the antineutrino production.

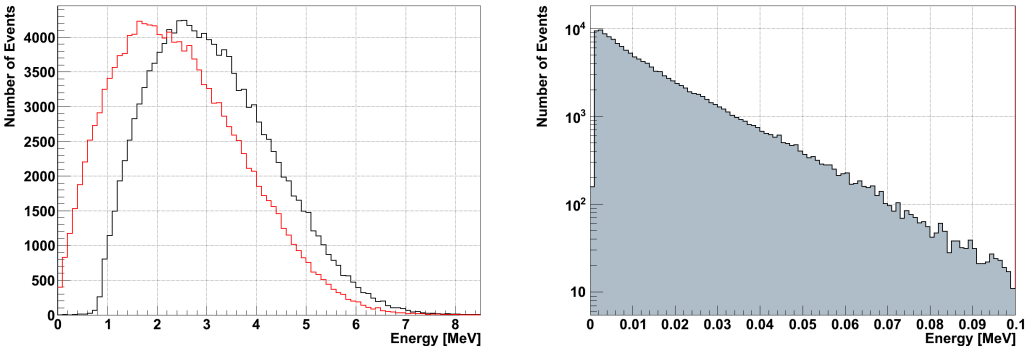

Figure 2.3: **Left:** Simulated kinetic (red) and visible energy (black) of positrons after IBD in the target.
Right: Simulated kinetic energy of neutrons after IBD.

with an electron emitting two gammas again producing scintillation light. Therefore, the visible energy E_{vis} (which one can reconstruct from the observed number of photoelectrons at the photomultiplier tubes) is proportional to the positron energy:

$$E_{vis} = E_{e^+} + m_e. \tag{2.4}$$

Both the positron kinetic energy ($E_{e^+} - m_e$) and the visible energy are shown in figure 2.3 on the left side.
Thus, the neutrino energy and the visible energy are directly connected and independent from the negligible neutron energy:

$$E_{\overline{\nu}} = E_{vis} + \Delta - m_e = E_{vis} + 0.78\,\mathrm{MeV}. \tag{2.5}$$

It should be remarked that the translation of detected photoelectrons into E_{vis} of the scintillating particle is non-trivial because it is influenced by different variables as the position in the detector and the particle type.
The energy dependent cross section of the IBD reaction is [79]

$$\sigma_{\mathrm{IBD}}\left(E_\nu\right) = K \cdot \left(E_\nu - \Delta\right) \sqrt{\left(E_\nu - \Delta\right)^2 - m_e^2} \tag{2.6}$$

and, therefore, proportional to E_ν^2. $K = (9.559 \pm 0.009) \cdot 10^{-44}\mathrm{cm}^2\mathrm{MeV}^{-2}$ is directly related to the neutron life time.
The number of positron events for a measured time T in a given positron energy bin i can be calculated to

$$N_i = \frac{n_p T}{4\pi L^2} \sum_l N_l^{fis} \int \mathrm{d}E_\nu \sigma\left(E_\nu\right) \phi_l\left(E_\nu\right) R_i\left(E_\nu\right) P_{ee}\left(E_\nu, L, \theta_{13}\right), \tag{2.7}$$

with n_p as the proton number in the target, L the detector distance to the source, N_l^{fis} the number of fissions per second of isotope l, $\phi_l\left(E_\nu\right)$ the antineutrino flux, $R_i\left(E_\nu\right)$ the detector response function and $P_{ee}\left(E_\nu, L, \theta_{13}\right)$ the antineutrino survival probability of equation 1.5 .
Using this equation together with equation 2.5 one receives the visible energy spectrum at the Double Chooz detector applying different values for $\sin^2 2\theta_{13}$ in figure 1.2.

2.3.2 Kinematics of the Inverse Beta Decay

In [78] the positron angular distribution after IBD in laboratory frame is calculated to

$$\mathcal{P}(\theta_e) = \mathrm{const} \times (1 - 0.102\,\beta\,\cos\theta_e), \tag{2.8}$$

with the positron velocity β and angle θ_e relative to the neutrino direction. In [80] the anisotropy for positrons from reactor neutrinos is obtained to roughly $-0.05\,\mathrm{cm}$

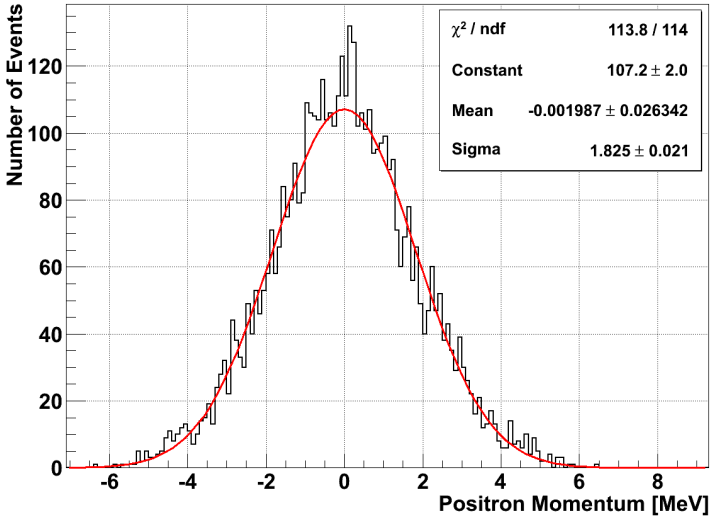

Figure 2.4: Simulated positron momentum in neutrino direction after IBD fitted with a Gaussian. There is no observable preferred direction of the positron after the IBD.

with respect to the neutrino incoming direction. So the positron displacement remains negligibly small. The positrons are emitted nearly homogeneous (figure 2.4) and their small and unmeasurable displacement does not influence the further conclusions of our studies.
Since in the laboratory system the proton is at rest it is a consequence of momentum conservation that

$$\vec{p}_\nu = \vec{p}_e + \vec{p}_n. \tag{2.9}$$

With

$$|\vec{p}_e| \leq \sqrt{(E_\nu - \Delta)^2 - m_e^2} < E_\nu \tag{2.10}$$

one can calculate that the neutron is always emitted in the forward hemisphere relative to the neutrino incoming direction. In [78] the maximum angle between the neutrino and the initial neutron direction is calculated neglecting $\mathcal{O}(1/m_n)$ (where m_n is the neutron mass) to

$$\cos(\theta_n)_{\max} = \frac{\sqrt{2E_\nu\Delta - (\Delta^2 - m_e^2)}}{E_\nu}. \tag{2.11}$$

In figure 2.5 this theoretical value is shown together with simulated neutron events after IBD in the target and shows a good agreement.
At the IBD-threshold of 1.8 MeV the neutron direction is purely forward and at higher energies still largely so.

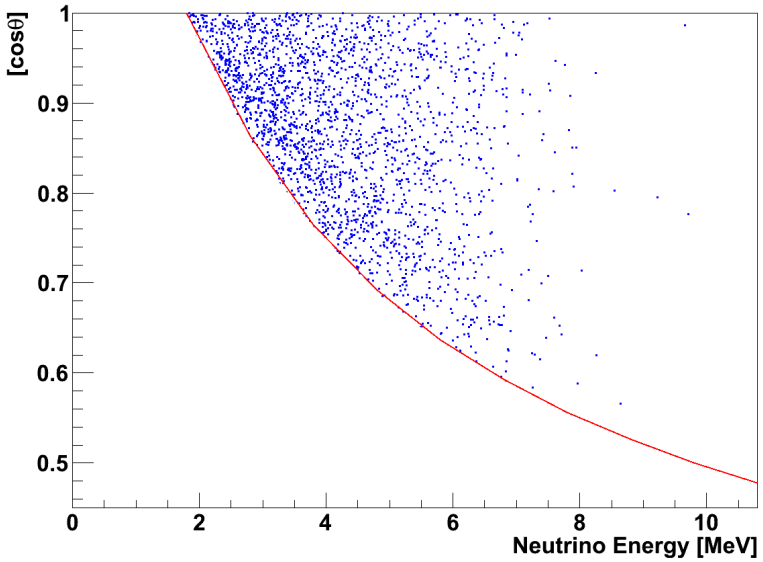

Figure 2.5: Simulated $\cos\theta_n$ of neutrons after IBD (blue) and the theoretical value of $\cos(\theta_n)_{\max}$ of equation 2.11 (red).

2.4 The Double Chooz Detector

2.4.1 Detector Design

The Double Chooz detector illustrated in figure 2.6 has been inspired by the CHOOZ setup with an optimization towards a higher neutrino event rate and a larger signal to background ratio. Therefore, the detector components were chosen in order to have a radioactivity background level of $\leq 10\,\mathrm{Bq}$ in the detection volumes. The Double Chooz detector consists of 4 cylindrical volumes namely the target, gamma catcher, buffer and the inner veto with different functionalities, described below:

Target

The target vessel is an acrylic-cylinder of 2.46 m height, 2.30 m diameter and 8 mm thickness filled with $10.3\,\mathrm{m}^3$ of organic liquid scintillator. The acrylic vessel is transparent to ultra-violet and visible photons with wavelengths above ≈300 nm.
The liquid scintillator in the target is composed of 20% PXE ($C_{16}H_{18}$) and of 80% dodecane ($C_{12}H_{26}$), thus the number ratio of C:H is approximately 1:2. The fluors PPO and Bis-MSB are added as wavelength shifters to prevent the reabsorption of the scintillation light and to bring the wavelength in the sensitive region of the PMTs.

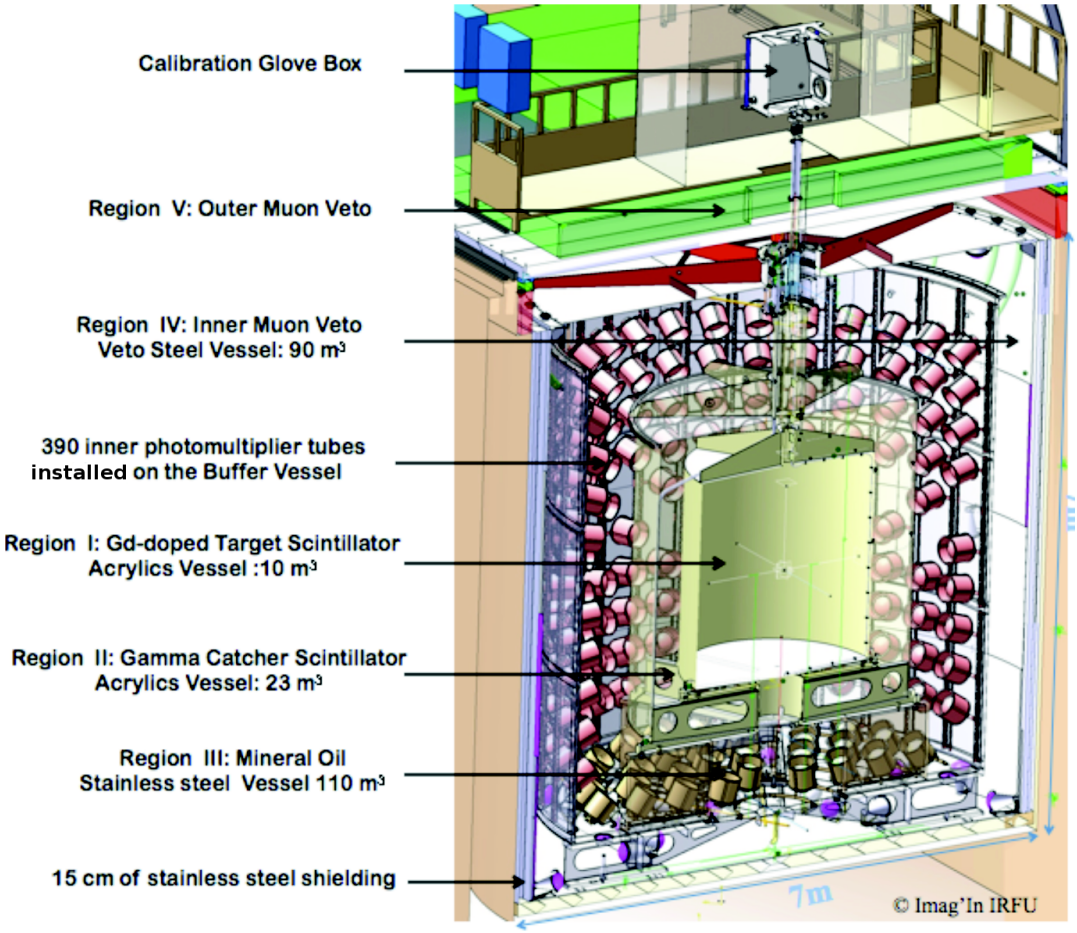

Figure 2.6: The Double Chooz detector design.

The target also contains Gadolinium (Gd) as it has a very large capture cross-section for neutrons roughly $1.5{\cdot}10^5$ times larger than hydrogen [81]. With the used concentration of 1g/l roughly 80% of the neutrons in the target will be captured on Gd. Adding Gd in the target scintillator has several advantages:

- The hydrogen after having absorbed a neutron decays by the emission of only one gamma with the energy of 2.2 MeV, while Gd decays in around 3 gammas with a total energy of 8 MeV and is, therefore, far above the energy of typical background events (<3 MeV). Thus, the background rate is reduced considerably.
- The large neutron cross section of Gd reduces the neutron capture time from roughly 180 μs to roughly 30 μs allowing more restrictive cuts between the prompt and late event and thus again reduces the background rate.
- The vertex reconstruction is based on calculating the place in the detector with the largest likelihood for the observed charge and time distribution at the inner detector PMTs. That reconstruction of the neutron vertex gets improved for neutrons captured on Gd. The one 2.2 MeV gamma of the hydrogen capture travels several cm before the first Compton-scattering produces light. Hence, there is always a bias in the vertex reconstruction of neutron captures on H. On the other side, the 3 gammas of the Gd are emitted in random directions, therefore, the center of mass of light production is in average much closer to the original vertex. Additionally as more light is produced in the Gd capture one has more statistics for the likelihood-maximization procedure.

The disadvantage of a reduced light yield by adding Gd is, thus, by far compensated.

Gamma Catcher

The cylindrical gamma catcher acrylic vessel surrounds the target volume and has the function to collect gammas from IBDs in the target near to the acrylics wall so that their energy is not lost for analysis. In this scintillating volume of 22.3 m^3 no Gd is loaded. Therefore, IBD events in the gamma catcher are not seen by the analysis as only Gd events fulfill the late event energy cut.
However, there occur so called Spill In events, if an IBD takes place in the gamma catcher but the neutron travels into the target and is captured there on Gd. Such an event appears in the analysis as a target event. It can happen the way around that neutrons from IBD in the target reach the gamma catcher and, therefore, can not be detected, called Spill Out. Both effects do not cancel each other and one observes a net Spill In current. This phenomenon will be discussed in section 4.4 in more detail. As the light yield and density of gamma catcher and target has to be the same the

composition of the gamma catcher was chosen to fulfill these conditions (30% dodecane, 66% mineral oil and 4% PXE together with the wavelength shifters PPO and Bis-MSB).

Buffer

The main function of the 105 cm thick buffer volume of 114 m^3 is to shield the target and gamma catcher region from single gammas (mainly from the PMTs) and neutrons created in the rock by cosmic muons. This non-scintillating volume filled with mineral oil is the major improvement over the CHOOZ design.
390 Photomultiplier tubes are mounted on a dedicated support structure on the inside of the buffer vessel. The R7081 from Hamamatsu are 10“ PMTs with low radioactivity glass. Their number were chosen to fulfill the energy resolution requirements of the experiment of $10\%/\sqrt{E\,(\mathrm{MeV})}$. The PMTs have been extensively tested and calibrated and their charge and time characteristics were simulated during this thesis. In the appendix these studies are summarized.

Inner Veto

The main purpose of the optical isolated inner veto (IV) volume with 90 m^3 is to detect muons and fast neutrons entering the detector from the outside. It is filled with liquid scintillator of roughly 50% n-alkanes and 50% LAB[6] with PPO and Bis-MSB as wavelength shifters. It is observed by 78 8“ PMTs (Hamamatsu R1408). To increase the light efficiency both sides of the inner veto have been covered with reflective foils and paint.

Outer Veto

The outer veto is a further improvement of the experiment compared to CHOOZ. It detects muons entering the scintillation volume from above and is made of 6.4×12.8 m^2 plastic scintillation stripes covering the detector. The stripes are crossed in the x-y-plane to have the possibility to track the muon. Furthermore, near-miss muons can be detected and thus identify fast neutron events created by the muons faking neutrino events.

Passive Shielding

The outside of the detector is surrounded by a 15 cm thick low activity and demagnetized steel shielding to protect the detector from natural radioactivity of the

[6] linear alkyl benzene

surrounding rock. The steal replaces low-radioactivity sand, which had the same function in the CHOOZ experiment.

2.4.2 Calibration Systems

The understanding of the detector efficiency and energy scale is crucial for the experiment. The overall goal is a relative error on the detection efficiency of ∼0.5% and an absolute one better than ∼1.5% [79]. For that purpose a good understanding of the energy scale, detector response and trigger efficiency is crucial. Calibration sources allow to check the detector behavior with events having a well known energy, particle type and position.
The calibration sources can be divided in two kinds:

1. Natural cosmic muon products, especially Michel electrons, ^{12}B and spallation neutrons:
   The Michel electrons and the ^{12}B can be used to calibrate the high energy part (>7 MeV) of the IBD energy range. Spallation neutron captures can be tagged by muons entering the detector some μs before and used to calibrate the neutron energy scale at 2.2 MeV and 8 MeV.

2. Man-made gamma, neutron sources and light injection systems:
   At a later stage of the experiment the gamma, beta and neutron sources can in general be placed everywhere in the target by using a so called articulated arm. In earlier stages of the experiment only the central vertical z-axis can be used.
   Furthermore, one can deploy calibration sources in the gamma catcher and buffer tube with the guide tube and buffer tube. The guide tube is installed in the gamma catcher, one part close the target acrylic vessel and the other part close to the gamma catcher acrylic vessel. The buffer tube is a vertical tube installed in the buffer.
   LED light injection systems are installed at the buffer wall next to the PMTs illuminating the whole scintillation volume and allowing, therefore, to check the PMT timing, gain and quantum efficiency and to monitor the speed of light and attenuation length of the scintillator. Another light source is a laser ball illuminating homogeneously the scintillation volume. It can be moved along the z-axis. Additionally, a central LED coupled to a diffuser is mounted.
   The calibration sources will be the same for the two detectors and introduced through the glovebox (figure 2.6). This system will be located above the outer veto.

2.4.3 The Readout and Trigger System

Light produced in the scintillation volume is detected by the inner detector PMTs. This signal is then delivered to the front end electronic (FEE) that amplify the signal to match the dynamic range of the Flash-ADC (FADCs).[7] Meanwhile the signals are summed and sent to the trigger units which after computation send a trigger-signal to the FADCs to store the event in the FADC internal memories. The memories are read out by the online software before the analysis of the events can start. Figure 2.7 shows an overview of that readout process.
The 390 inner detector PMTs are divided into 12 sectors containing each 32 PMTs, 6 sectors for the upper part of the detector, 6 for the bottom part. Half of the PMTs of a given sector are connected to the triggerboard A while the other PMTs are connected with triggerboard B. The choice of the PMTs grouping in a sector is done in order always to have an A-PMT surrounded by B-PMTs and vice versa. Therefore, each of the two trigger boards makes a trigger decision based on the half of the inner detector PMTs. There exist four general trigger decisions depending on the collected charge of the PMTs and they are only enabled if the multiplicity is larger than 2 (at least two sectors should be hit):

- Very high energy deposition (>50 MeV) indicating a muon hit in the detector.
- High energy deposition (>5 MeV) implying e.g. a neutron capture on Gd.
- Low energy deposition (>0.5 MeV) indicating e.g. a positron event.
- Very low energy deposition (>0.3 MeV) to monitor the low energy trigger efficiency and the single background.

For details of the triggerboards the reader might be referred to [82] and for details on the FADCs to [83].

2.5 The Double Chooz Simulation Software

In the preparation of an experiment but also during the data analysis the Monte Carlo simulation plays a crucial role for the experiment to understand the detector response and background characteristics. Therefore, it is important to check and tune the simulation as detailed as possible to get the best agreement between data and simulation. **A not understood difference between real data and simulation indicates a not understood physical or technical problem.**
During this thesis the simulated charge and time response of the PMTs was tuned to achieve the best possible agreement between the simulated and real PMT signal

[7] Analog to digital converter.

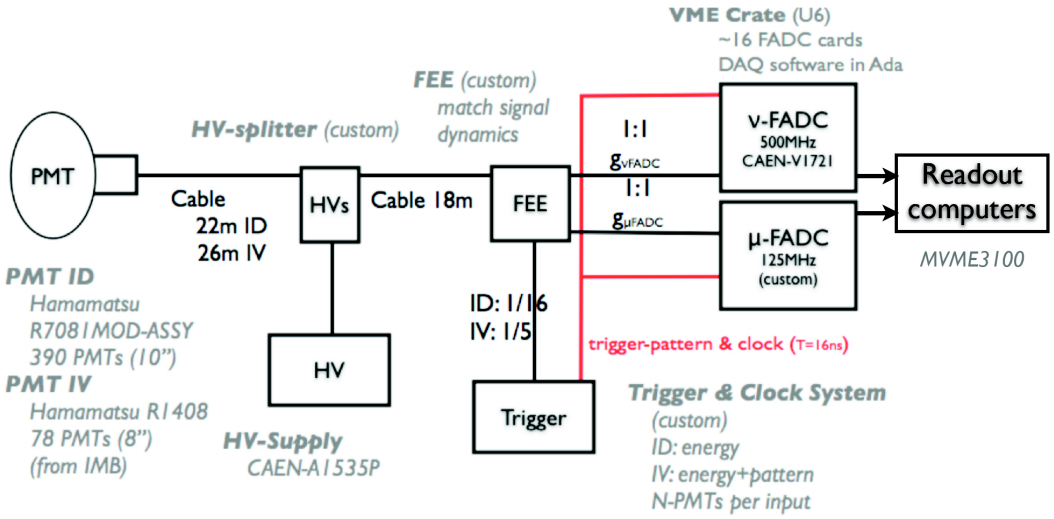

Figure 2.7: The Double Chooz Read Out system [83].

behavior. That is shown in more detail in the appendix.
In the following the main parts and working principles of the Double Chooz simulation software (DOGS) [84] are explained, an overview is given in figure 2.8:

DCNuGen2 With the neutrino generator one can simulate the reactor antineutrino flux and energy. A neutron-positron pair can be produced everywhere in the detector with the correct energy and momentum distribution.

DCGLG4sim The Double Chooz Generic Liquid Scintillator Geant4 simulation is based on GLG4sim, the simulation package of the KamLAND experiment. It describes movement and light production of particles in different detector volumes. E.g. one could use DCNuGen to produce an IBD in target scintillator, afterward using DCGLG4sim to simulate the light production of both particles.
The output of DCGLG4sim are photoelectrons produced at the inner detector PMTs or inner veto PMTs.

DCRoSS The Double Chooz Read-Out Simulation Software simulates the PMT and Read-Out behavior. RoSS completes the detector simulation as the output of RoSS are FADC and trigger signals in the same data format as the experimental data.

DCRecoPulse DCRecoPulse can be applied to both real and simulated data. It reconstructs the number of photoelectrons and time from a given FADC signal.

DCReco This package includes the vertex reconstruction codes e.g. the RecoBAMA algorithm.

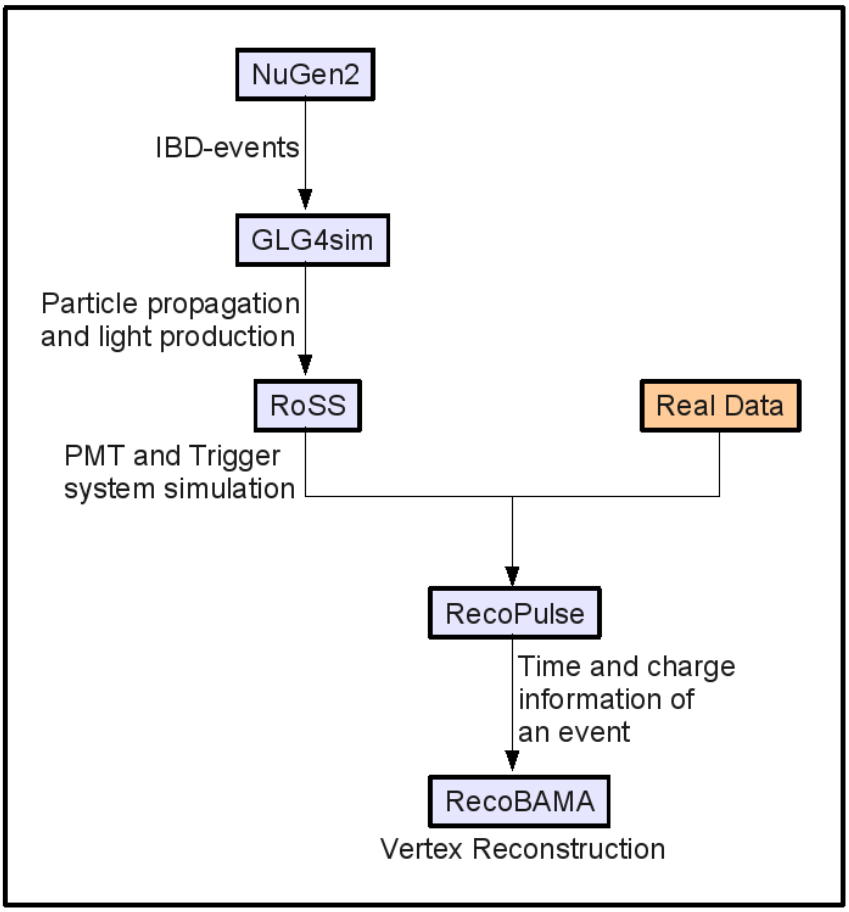

Figure 2.8: The DOGS simulation chain as explained in the text.

3 Neutrino Direction Reconstruction

The Gösgen reactor antineutrino experiment (finished measurements in 1985) was the first one demonstrating the possibility of direction reconstruction for neutrinos after IBD at the 10σ-level [18]. This was possible because the detector was composed of alternating walls of scintillator and ^{3}He neutron detectors. For a given wall of scintillator in which the reaction occurred and the positron was detected more neutrons were observed in the ^{3}He slab away from the reactor than towards the reactor (in fact, the ratio was 2:1). A similar effect was observed in the Bugey 3 experiment, also using a segmented detector [85]. The first unsegmented reactor experiment measuring the neutron displacement after IBD was the CHOOZ experiment, which determined the direction of the reactors with a precision of 18° (1σ) [80].
There are several reasons for a measurement of the neutrino direction at the Double Chooz experiment:
The understanding and proof of direction reconstruction mechanism gives important aspects for tuning the Monte Carlo and the understanding of neutron moderation and diffusion movement in the scintillator as it is explained in section 3.1. A successful determination of the neutrino direction consistent with the Monte Carlo would increase the confidence in detector performance, data analysis and simulation. The possibility of pointing the reactors at Double Chooz will be studied in section 3.2. Furthermore, there is the possibility of using the isotropy of background events and the anisotropy of neutrino events for background reduction. This was already performed at the Palo Verde experiment [86; 87]. This application for Double Chooz will be investigated in section 3.3. Future large scale neutrino experiments like LENA plan to measure the direction of supernova and geo neutrinos using the IBD reaction. Double Chooz is able to measure the important parameters for the direction reconstruction with a so far unreached precision as demonstrated in section 3.4.

3.1 Neutron Moderation and Diffusion

The neutron produced in IBD with some keV undergoes several collisions with the scintillator atoms reducing the energy to thermal equilibrium. This moderation phase is a non-isotropic process which preserves a memory of the initial neutron direction. In

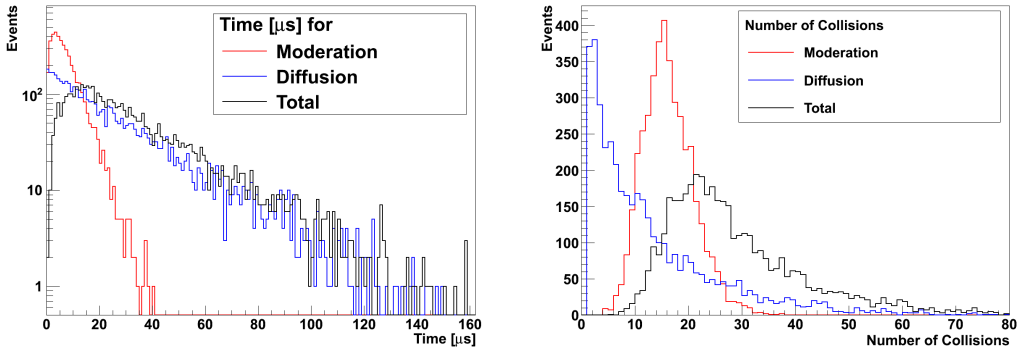

Figure 3.1: Time (left) and number of collisions (right) needed for moderation (red), diffusion (blue) and for being captured (black) of 5000 simulated neutrons in the target volume.

each elastic scattering the average cosine of the neutron with respect to its incoming direction is

$$\cos\overline{\theta_n} = \frac{2}{3\,\mathrm{A}}, \tag{3.1}$$

where A is the the atomic number of the scattering nucleus [88]. Therefore, the directionality is best preserved by scattering with hydrogen which has at energies below 1 MeV the larger cross section compared to carbon [89]. After being moderated the diffusion process begins. There is now in each collision a certain probability to be captured either by gadolinium, by hydrogen or carbon.
For a better understanding of this processes a Monte Carlo simulation was performed using GEANT4. 5000 neutrons with 10 keV kinetic energy, which is the mean of the kinetic energy of neutrons produced in IBD of reactor-$\overline{\nu}_e$, were produced in the center of the target with the momentum vector in the positive y-direction.
In figure 3.1 on the left side one can see the moderation time needed to reach the thermal energy of 0.03 eV. That is 4 μs in the mean with a 1σ-width of 5 μs. The diffusion time is an exponential distribution (the caption probability is now a constant in each collision) with $\tau = 25\,\mu$s.
In figure 3.1 on the right side the number of collisions for the different processes is shown. Since in each collision the neutron looses a certain amount of energy the distribution is a Gaussian with a mean of 15 and a 1σ-width of 5 collisions. The diffusion curve is again an exponential with a slope of 12 collisions.
Figure 3.2 shows the expansion of the neutron cloud in the x-y-plane after different collision numbers. One can see that the y-displacement of 1.72 cm is reached after $\sim$10 scatterings, which is still the moderation phase. The diffusion as a random walk just spreads the distribution, while the average displacement remains.

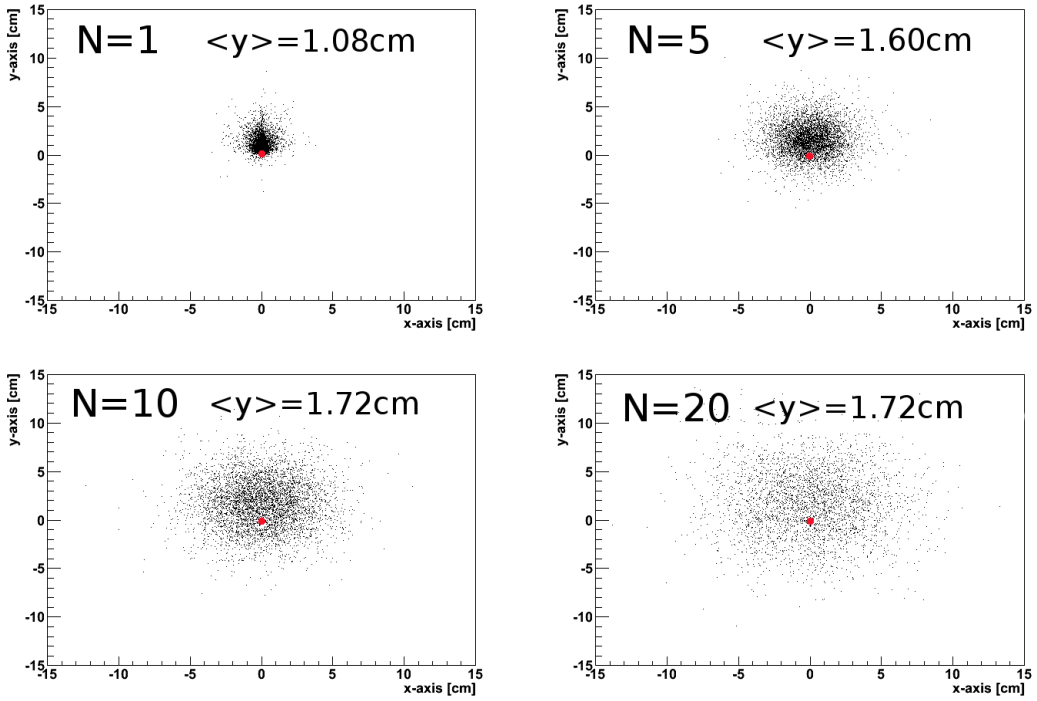

Figure 3.2: Simulation of the neutron displacement evolution after N=1,5,10 and 20 collisions with the scintillator atoms. The red point indicates the neutron start position (0,0). The initial neutron momentum was in positive y-direction.

As it will be demonstrated, the displacement value is one of the very important parameters for detecting the direction of the neutrino. For 10 keV neutrons this value is 1.72 cm (with a negligible statistical error) and is fully reached after the moderation phase.

3.2 Measurement of the Neutrino Direction at Double Chooz

3.2.1 Principle of Direction Reconstruction

As it was pointed out in section 2.3.2 the positron vertex is nearly identical with the vertex of the IBD and the neutron preserves a memory of the neutrino direction. Therefore, the principle of determining the neutrino direction at Double Chooz is to

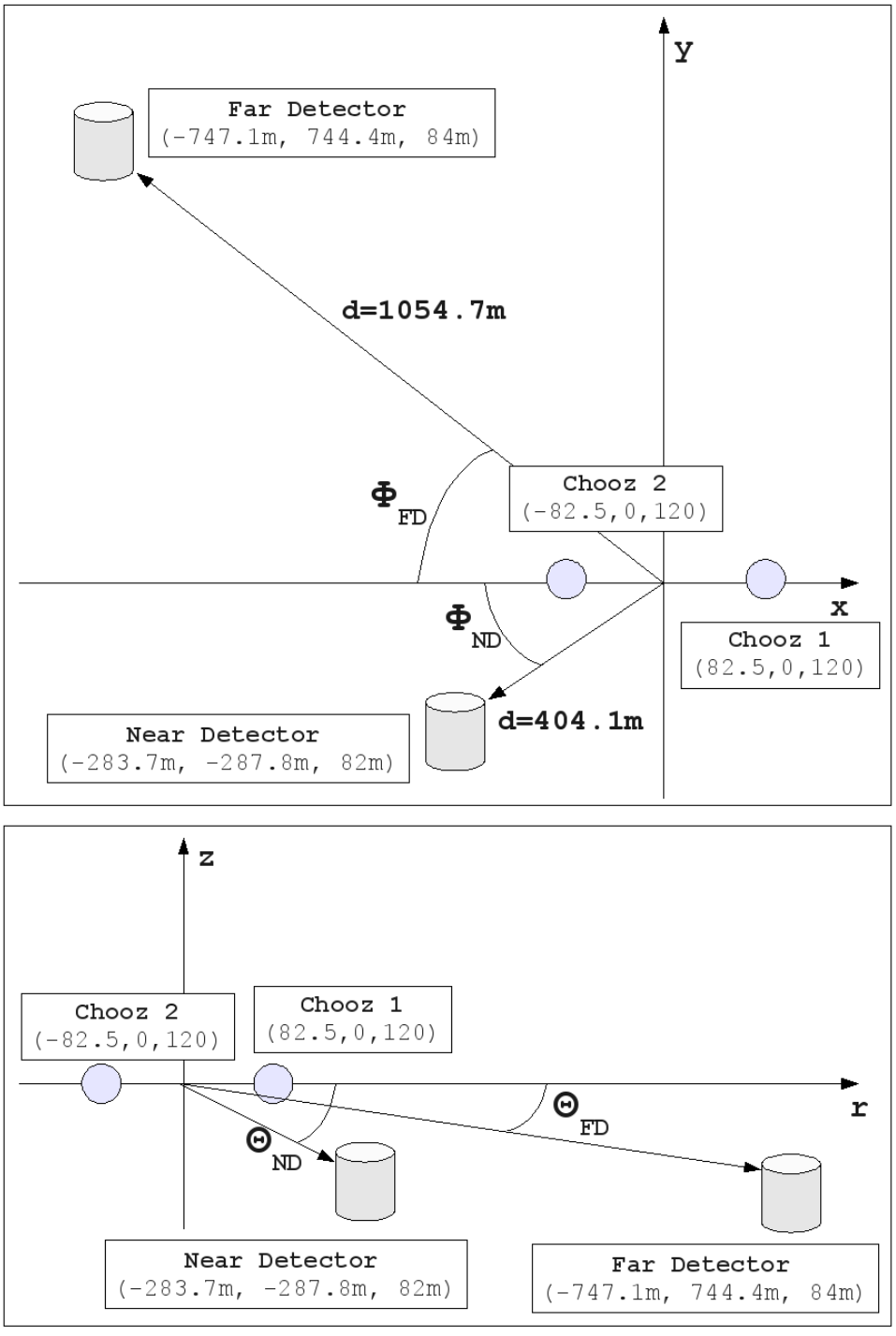

Figure 3.3: The Double Chooz Geometry:
Top: Top view with the azimuth angle ϕ.
Bottom: Side view defining the zenith angle θ.

measure the average $\vec{p}$ of the positron-neutron vectors $\overrightarrow{X}^i_{e-n} = \overrightarrow{X}^i_n - \overrightarrow{X}^i_e$ with $\overrightarrow{X}^i_n$ and $\overrightarrow{X}^i_e$ being the vertex of the neutron and positron of event-number i:

$$\boxed{\vec{p} = \frac{1}{N}\sum_{i=1}^{N} \overrightarrow{X}^i_{e-n} \quad \textbf{Average Positron-Neutron Vector}} \tag{3.2}$$

with N being the total number of events. The resulting reconstructed neutrino direction is the direction of $\vec{p} = (p_x, p_y, p_z)$. One expects for the probability distribution $f(p_i)$ of p_x, p_y and p_z a Gaussian form with

$$\begin{aligned} f(p_x) &= \frac{1}{\sqrt{(2\pi)}P} \exp\left[\frac{(p_x - |\vec{p}| \cdot \cos\phi\cos\theta)^2}{2P^2}\right] \\ f(p_y) &= \frac{1}{\sqrt{(2\pi)}P} \exp\left[\frac{(p_y - |\vec{p}| \cdot \sin\phi\cos\theta)^2}{2P^2}\right] \\ f(p_z) &= \frac{1}{\sqrt{(2\pi)}P} \exp\left[\frac{(p_z - |\vec{p}| \sin\theta)^2}{2P^2}\right] \end{aligned} \tag{3.3}$$

with the average neutron displacement $|\vec{p}|$ and the width of the Gaussian P. As the azimuth angle ϕ and the zenith angle θ are given from the geometry of the experiment (figure 3.3) the only two free parameters are $|\vec{p}|$ and P. Both are measurable values at the experiment and influence strongly the possibility of direction reconstruction. If $|\vec{p}|$ is too small compared with a too large P one will not have the possibility to reconstruct the neutrino direction.

To have an estimation of that parameters for the Double Chooz experiment one year data taking at the far detector was simulated using DOGS and for the vertex reconstruction the RecoBAMA algorithm. To estimate both parameters as realistic as possible the most probable cuts of 1 MeV for the prompt event, 6 MeV for the late event and $\Delta T < 200\,\mu$s were applied. For each pair of prompt and late event passing these cuts $\overrightarrow{X}_{e-n}$ was calculated using the truth information (directly after GLG4sim and without any PMT and vertex reconstruction uncertainties) and from that $|\vec{p}|$ using equation 3.2.

P was calculated from the width of the simulated p_x, p_y and p_z distribution applying now the full chain of the DOGS simulation (PMT and vertex reconstruction uncertainties). Because of the symmetry of the Double Chooz detector P is expected to be nearly the same in x,y and z-direction, which was approved by simulation. The result from simulation is: $|\vec{p}| = 1.48 \pm 0.03(\text{stat})\,\text{cm}$ and $P = 15.38 \pm 0.13(\text{stat})\,\text{cm}$.

In figure 3.4 the distribution of $\cos\eta$ is shown for one year data taking using the full chain of DOGS. η is the angle of the detected positron-neutron vector $\overrightarrow{X}_{e-n}$ to the true incoming direction of the neutrino. Clearly one can see the tendency of $\overrightarrow{X}_{e-n}$ to point in the direction of the neutrinos ($\cos\eta = 1$).

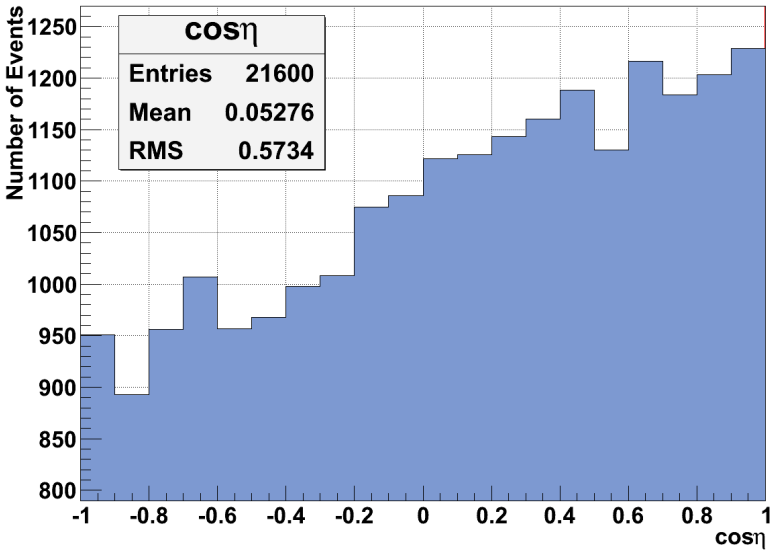

Figure 3.4: Simulated $\cos\eta$ of 1 year data taking in Double Chooz using the full reconstruction algorithm of DOGS.

Systematical Error The simulation of neutrons in the eV region has quite large uncertainties which has a possible influence on the parameters important for the neutrino direction reconstruction namely $|\vec{p}|$ and P.
It was demonstrated in section 3.1 that the neutron has made its displacement already in the moderation phase and so if the neutron code is imprecisely at eV-scale this will affect only the width of the diffusion cloud and leave $|\vec{p}|$ constant. Moreover one can compare the simulation result with the CHOOZ result of $1.9 \pm 0.4\,\text{cm}$ [80] and a theoretical value of 1.5 cm [78] and finds a good consistence. Hence, a not too large systematical uncertainty of 20% should be adequate.
To avoid a misunderstanding: Also the measured 1.72 cm displacement of 10 keV neutrons in section 3.1 is in a good agreement with the IBD-neutron result presented here. In IBD the struck neutron is not exactly forward but has $\langle\cos\theta_n\rangle \simeq 0.9$ for reactor energies [78] (The Monte Carlo simulation gets $\langle\cos\theta_n\rangle = 0.85$). Taking that into account the displacement of 10 keV neutrons emitted strictly in the forward direction in section 3.1 reduces to 1.55 cm which is then in good agreement with the simulation using neutrons from IBD.
Also P will not affected significantly by the uncertainties of the simulation as this value is influenced not only by the neutron moderation and diffusion width, which was in section 3.1 found to be 3.5 cm. Much more influence comes due to the uncertainty in

the positron (σ_e) and neutron (σ_n) vertex reconstruction that is for positrons $\sim 8.5\,\mathrm{cm}$ and for neutrons $\sim 13.5\,\mathrm{cm}$. The total value of P results from

$$P = \sqrt{\sigma_\mathrm{diff}^2 + \sigma_\mathrm{n}^2 + \sigma_\mathrm{e}^2}. \tag{3.4}$$

Therefore, an eventually incorrect treatment of neutron moderation and diffusion in GEANT4 does not have a strong impact on the result. If one assumes a 20 % systematic error in the neutron moderation and diffusion width σ_diff that will only result in a less than 1 % systematic error in P. This results in

$$\boxed{|\vec{p}| = 1.48 \pm 0.03(\mathrm{stat}) \pm 0.3(\mathrm{syst})\,\mathrm{cm}} \tag{3.5}$$

and

$$\boxed{P = 15.38 \pm 0.13(\mathrm{stat})\,\mathrm{cm}} \tag{3.6}$$

which are the values used for the rest of this work.

3.2.2 Angular Resolution at the Far Detector

At the far detector the separation angle between the two reactors is for the azimuth angle only 6.9° and for the zenith angle only 0.2°. As both angles are too close to be separated with the far detector one can try to observe the average azimuth angle $\phi = 44.9°$ and the average zenith angle $\theta = -2.0°$ (figure 3.3).

Analytic Estimates

After measuring $\vec{p} = (p_x, p_y, p_z)$ at the far detector with equation 3.2 one can calculate the reconstructed **azimuth angle**

$$\tan\phi = \frac{\overline{p}_y}{\overline{p}_x} \tag{3.7}$$

and the **zenith angle**

$$\tan\theta = \frac{\overline{p}_z}{\sqrt{\overline{p}_x^2 + \overline{p}_y^2}}. \tag{3.8}$$

with $\overline{p}_i$ as the mean of the measured displacement distribution in direction $i = x, y, z$. To estimate the possibility of direction reconstruction for different runtimes at the far detector one has to estimate $\Delta\phi$ and $\Delta\theta$. For $\Delta\tan\phi$ one calculates:

$$\begin{aligned} \Delta\tan\phi &= \sqrt{\left(\frac{\partial\tan\phi}{\partial\overline{p}_x}\Delta\overline{p}_x\right)^2 + \left(\frac{\partial\tan\phi}{\partial\overline{p}_y}\Delta\overline{p}_y\right)^2} \\ &= \sqrt{\left(\frac{\overline{p}_y}{\overline{p}_x^2}\Delta\overline{p}_x\right)^2 + \left(\frac{1}{\overline{p}_x}\Delta\overline{p}_y\right)^2} \end{aligned} \tag{3.9}$$

with $\Delta\overline{p}_i = P/\sqrt{N}$, $(i = x, y)$.

$$\Delta \tan\phi = \sqrt{\left(\frac{P \cdot \overline{p}_y}{\sqrt{N}\overline{p}_x^2}\right)^2 + \left(\frac{P}{\sqrt{N}\overline{p}_x}\right)^2} \tag{3.10}$$

and similar for $\Delta \tan\theta$. From equation 3.3 and 3.5 one can calculate $\overline{p}_x = -1.05\,\text{cm}$, $\overline{p}_y = 1.04\,,\ \overline{p}_z = -0.08\,\text{cm}$. $P = 15.38\,\text{cm}$ is known from simulation. From that one get for one year data (N$\sim$20.000):

$$\Delta \tan\phi \approx \Delta \tan\theta \approx 0.146 \tag{3.11}$$

which is equivalent to

$$\boxed{\boldsymbol{\Delta\phi \approx \Delta\theta \approx 4.2^\circ \text{ for one year data taking (68\% C.L.).}}} \tag{3.12}$$

The analytic result for $\Delta\phi$ depending on different runtimes of Double Chooz is given in figure 3.5 in the red curve.

Monte Carlo Simulation

A Monte Carlo simulation was performed based on the Double Chooz geometry for the near and far detector and the two reactor cores assuming 55 neutrino events per day. The two reactors were assumed to have the same power. For each event the p_x, p_y and p_z-distributions were randomly created using the PDFs of equation 3.3. Afterward the three resulting histograms were fitted with a Gaussian and the resulting values of $\left(\overline{p}_x^{MC}, \overline{p}_y^{MC}, \overline{p}_z^{MC}\right)$ were used to calculate θ and ϕ using equation 3.7 and 3.8. A run is comparable to one Double Chooz Experiment. To estimate the distribution of $\Delta\phi$ and $\Delta\theta$ 5000 runs were processed.
The result for the zenith and azimuth angle after one year data taking can be seen is figure 3.6. The 1σ resolution is here $\sim 4.2^\circ$ for both angles and in agreement with the analytical calculation. The 1σ distribution for different runtimes is shown in figure 3.5. This is a promising result as Double Chooz will be able to measure the neutrino direction already after a short time of data taking with good precision.

3.2.3 Measurement of the Neutron Displacement $|\vec{p}|$

The average neutron displacement $|\vec{p}|$ in a liquid scintillator is a very important parameter for the possibility of direction reconstruction at present and future neutrino experiments. After the coordination transformation $(x, y, z) \longmapsto (x', y', z')$ (figure 3.7 left side) one can get $|\vec{p}|$ by measuring $\overline{p}_{y'}$. This is possible with a precision of

$$\sigma_{|\vec{p}|} = \frac{P}{\sqrt{N}}. \tag{3.13}$$

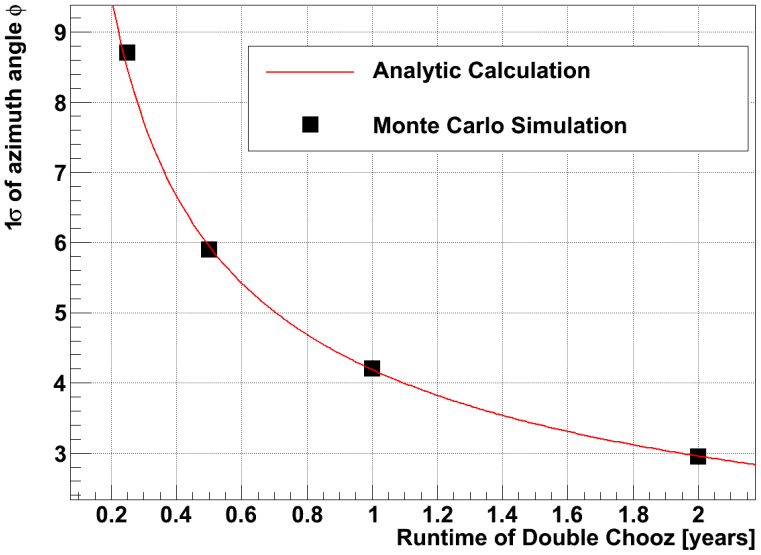

Figure 3.5: 1σ evolution of the azimuth angle ϕ for different runtimes.

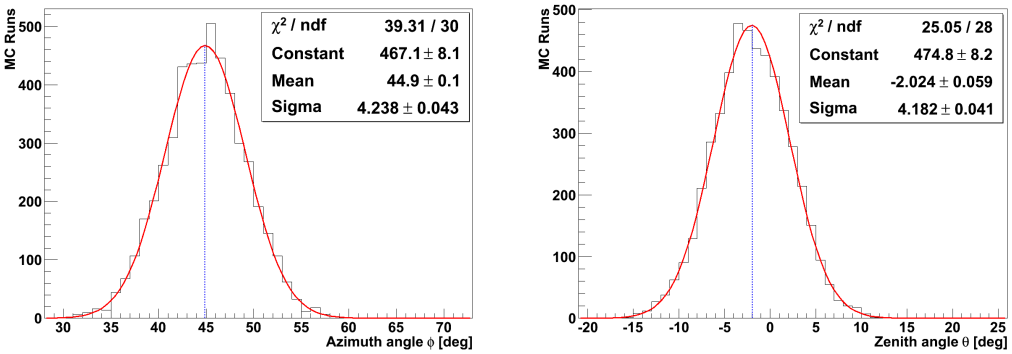

Figure 3.6: Azimuth (left) and zenith angle (right) after 5000 MC runs and one year data taking. The blue line indicates in both cases the true value.

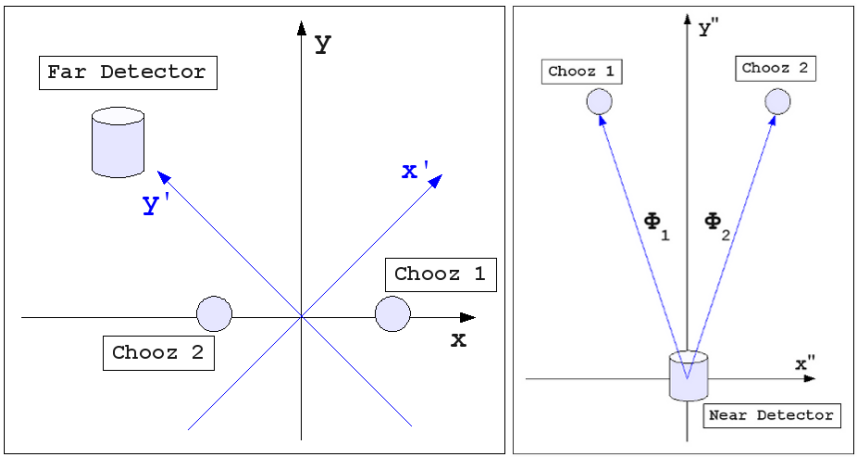

Figure 3.7: **Left:** Coordination transformation $(x, y, z) \longmapsto (x', y', z)$. After transformation the y'-axis is pointing to the far detector.
Right: Geometry of the near detector with separation angles ϕ_1 and ϕ_2.

For 20000 events per year at the far detector this results already after 1/4 year in a 1σ error of only 0.22 cm which is smaller than the Chooz error by a factor of 2. After one year one gets a very exact value with a precision of 0.11 cm.

3.2.4 Measurements with the Near Detector

Due to its smaller distance of only 404 m to the mean of the two reactors the near detector will have roughly seven times more events compared to the far detector. Using equation 3.10 it will be, therefore, possible to resolve the mean azimuth angle $\phi = 45.4°$ and the mean zenith angle $\theta = -5.37°$ after one year with a 1σ precision of 1.4° for both angles.
On the other side the two reactors have a quite large azimuth angle separation $\phi_1 + \phi_2$ of 16.9°. In [90] it was tried to separate the two reactors or, alternatively, to measure the integrated relative reactor output. The applied coordination system is given in figure 3.7 on the right side with $\phi_1 = -\phi_2 = \phi$ and the reactor strength b_1 and b_2 of reactor 1 and 2.

Relative Reactor Strength

In [90] it was demonstrated that the p_x distribution contains the information of the relative reactor strength with

$$\begin{aligned} \overline{p}_x &= (b_1 - b_2)|\vec{p}| \sin\phi, \\ \left\langle p_x^2 - \overline{p}_x^2 \right\rangle &= P^2 + \left[1 - (b_1 - b_2)^2\right] (|\vec{p}| \sin\phi)^2 \end{aligned} \tag{3.14}$$

and, therefore, one can measure $b = b_1 = 1 - b_2$ with

$$b = \frac{1}{2}\left(1 + \frac{\overline{p}_x}{|\vec{p}| \sin\phi}\right), \quad \sigma_b = \frac{P}{|\vec{p}|} \frac{1}{2\sin\phi\sqrt{N}}. \tag{3.15}$$

The reference article used slightly different values for $|\vec{p}|$ and P originating from the CHOOZ result and also applied a separation angle of 30°.[1] Their result was then a precision for b of ±10% at 68% C.L. after one year data taking.
With the values of $|\vec{p}|$ and P calculated by the Double Chooz simulation and the in fact smaller separation angle of 16.9° the result worsens to ±20% at 68% C.L. Both results are in any case not competitive compared to the systematical error of 2% reactor flux uncertainty.

Separation of the two Reactors

In [90] it was shown that it is in general possible to resolve with the near detector the separation angle 2ϕ of both reactors with

$$\cos\phi = \frac{\overline{p}_y}{|\vec{p}|}, \quad \sigma_{\cos\phi} = \frac{P}{|\vec{p}|\sqrt{N}}. \tag{3.16}$$

However, it was already stated in the reference article that assuming a separation angle of 30° the two reactors will be barely separated even after 5 years. The reason for that relatively poor performance is the difficulty to distinguish $\cos\phi = 0.966$ from unity with the given statistical error. Furthermore, the uncertainty of $|\vec{p}|$, which must be known from the far detector geometry, will worsen the result so that a separation of both reactors with the near detector is not possible. Considering the truth near detector location with $\cos\phi = 0.989$ makes a separation even more complicated.

3.3 Background Estimation with Direction Reconstruction

An interesting application of the neutrino directionality is to use it for the estimation of the total background rate. The neutrino events tend to point away from the

[1] Based on earlier plans for the near detector location.

reactors ($|\vec{p}_\nu| > 0$), while background events should be radial isotropic distributed ($|\vec{p}_{\mathrm{BG}}| = 0$).[2]

3.3.1 For-Back Method

This method uses the ratio of forward and backward scattered events to estimate the background to signal ratio and was also applied at the Palo Verde experiment [87]. Again the coordinate system (x', y', z) with y' pointing in the neutrino direction is applied (figure 3.7 on the left side) and ϕ is the separation angle of both reactors. The probability p_{f}^{ν} of a neutrino to be detected in forward direction is given by

$$p_{\mathrm{f}}^{\nu} = \int_0^{\infty} \frac{1}{2\pi\sqrt{P}} \exp\left[\frac{\left(p_{y'} - |\vec{p}| \cdot \cos\phi\right)^2}{2P^2}\right] dp_{y'}. \tag{3.17}$$

and the backward pointing probability $p_{\mathrm{b}}^{\nu} = 1 - p_{\mathrm{f}}^{\nu}$. The forward and backward pointing probability ($p_{\mathrm{f}}^{\mathrm{BG}}$ and $p_{\mathrm{b}}^{\mathrm{BG}}$) of background events is 0.5, as background is expected to come isotropic from all directions.
P can be extracted from the experiment itself. For the study presented here $P = 15.38 \pm 0.13\,\mathrm{cm}$ from simulation is used. The uncertainty of P is very small and can be neglected here. In any case one should not apply $|\vec{p}|$ measured at the experiment for calculating p_{f}^{ν} by equation 3.17 for the use of background estimation as the background had already an influence on the measured value of $|\vec{p}|$ and would, therefore, bias the analysis. $|\vec{p}|$ is, thus, only known from simulation and calculated there to $|\vec{p}| = 1.48 \pm 0.03\,(\mathrm{stat}) \pm 0.30\,(\mathrm{syst})$ assuming a realistic 20% systematic uncertainty of the simulation.
With equation 3.17 one can estimate the probability p_{f}^{ν} to $53.8 \pm 0.8\%$ where the error originates from the uncertainty of $|\vec{p}|$. This analytical calculation is also in agreement with the Monte Carlo simulation result of $53.4 \pm 0.3(\mathrm{stat})\%$.
To clarify how precisely one can extract the total signal rate with that method a Monte Carlo simulation was written:
Using a realistic background to signal ratio of 3% in the **first step** of the simulation it is decided if an event is a neutrino or a background signal. In the **second step** it is determined (using the probabilities just described) if the event is detected in backward or forward direction. After doing that for all events (the number of events is defined by the runtime) one finds N_{f} events in the forward direction and N_{b} events in the backward direction. These two numbers will be observables in the real experiment. Having measured N_{f} and N_{b} one can calculate in the **third step** the number of signals

[2] As one side of the detector might has less overburden than the other there might be a larger muon rate at this side and, therefore, a small anisotropy in the fast neutron background. However, this effect is probably very small and is neglected here.

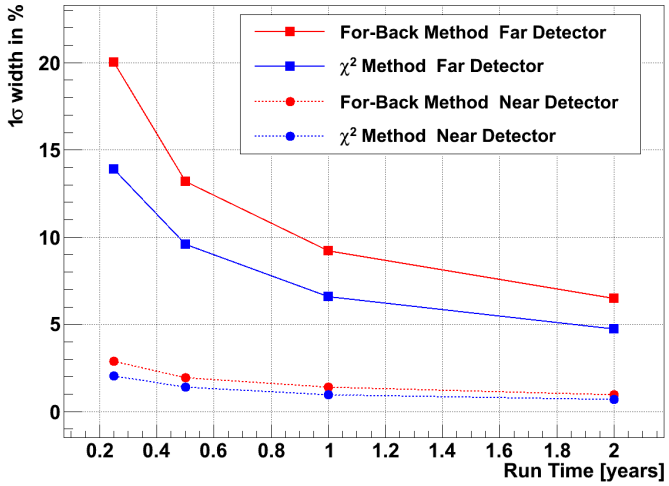

Figure 3.8: 1σ width of the relative residual for the reconstructed number of neutrino events for the two different methods described in the text over the runtime.

(N_ν) and number of background events (N_{BG}) with

$$\begin{aligned} N_\nu &= \frac{p_{\mathrm{b}}^{\mathrm{BG}}}{p} N_{\mathrm{f}} - \frac{p_{\mathrm{f}}^{\mathrm{BG}}}{p} N_{\mathrm{b}} \\ N_{\mathrm{BG}} &= \frac{p_{\mathrm{f}}^{\nu}}{p} N_{\mathrm{b}} - \frac{p_{\mathrm{b}}^{\nu}}{p} N_{\mathrm{f}} \end{aligned} \tag{3.18}$$

with $p = p_{\mathrm{b}}^{\mathrm{BG}} \cdot p_{\mathrm{f}}^{\nu} - p_{\mathrm{f}}^{\mathrm{BG}} \cdot p_{b}^{\nu}$. Doing that for 5000 runs and different runtimes systematical and statistical uncertainties can be estimated. From simulation one ascertains that the reconstructed number of neutrino events is unbiased and has the residual $\left(N_\nu^{\mathrm{reco}} - N_\nu^{\mathrm{true}}\right)/N_\nu^{\mathrm{true}}$ given in figure 3.8 for different runtimes. No systematical error on p_{f}^{ν} was included so far, the limitation comes due the statistical fluctuations. The same analysis can be done for the near detector with a much larger statistic. Even if the near detector geometry with respect to the reactors is slightly different the forward scattering probability stays the same. Executing the Monte Carlo for the near detector one gets the result also shown in figure 3.8. Here the result is much more promising as for the far detector. An estimation of the signal rate with a precision of 1% is possible after 1 year data taking.

Systematical Error The influence of a systematical error in p_{f}^{ν} for the For-Back method is estimated. If one applies a 1σ bias on p_{f}^{ν} (p_{f}^{ν} is assumed to be 53.8% but the true value is 54.6%) the residual is unchanged but biased with 16.9% for all runtimes.

3.3.2 χ^2 Method

The second method to get the Background to Signal Rate with the use of directionality is a χ^2 Method. Using the $\cos\eta$ spectrum of the detected neutron direction with respect to the neutrino direction (figure 3.4) one can fit this spectrum linear and construct from that a PDF for neutrino events. This again can be used as a distinguishing parameter because the PDF for background events is just a line with zero slope (again assuming directional isotropy). From Monte Carlo one gets:

$$\begin{aligned} \mathrm{PDF}_{\mathrm{Signal}} &= 0.093 \cdot \cos\eta + 0.5 \\ \mathrm{PDF}_{\mathrm{BG}} &= \mathrm{const.} \end{aligned} \tag{3.19}$$

Similar to the Monte Carlo Simulation at the For-Back method for each run a $\cos\eta$ histogram is filled using the PDFs of equation 3.19. For each run the result is a $\cos\eta$ histogram which will be an observable at the experiment. Now again using the PDFs of equation 3.19 to fit the histogram one can calculate the reconstructed number of neutrino events.
The result is again unbiased and the residual for the reconstructed number of signals for different runtimes is shown in figure 3.8. As one can see the result is slightly better than the For-Back-Method. For the far detector a relative error on the signal ratio of 6.5% after 2 years can be found which is of course much larger than the needed signal rate precision of less than 1%. However, at the near detector this 1% limit is reached after 1 year data taking. Nevertheless one also has with the χ^2-method the large dependence on a systematical error on $|\vec{p}|$. Again assuming a 20% error on this value bias our result with 11%.
Despite the quite large systematical error, these methods give an independent possibility for background estimation. Especially at the near detector the precision is very promising and should be applied in any case.

3.4 Direction Reconstruction of Geo and Supernova Neutrinos

An interesting application of neutrino direction reconstruction occurs in future large scale experiments using a liquid scintillator. A possible future large scale detector is LENA (Low Energy Neutrino Astronomy) as a detector to search for proton decay, the next galactic supernova, geo neutrinos and solar neutrinos [91]. Present design studies for LENA assume a cylinder with a diameter of 30 m and a length of approximately 100 m filled with 50 kT of Gd loaded or unloaded liquid scintillator. To observe the scintillation light roughly 13.000 PMTs provide a surface coverage of $\sim 30\%$. As the composition of the scintillator is not yet defined the photoelectron efficiency $\mathrm{PEE}_{\mathrm{LENA}}$ is expected to be around $120 - 180\,\mathrm{PE/MeV}$ [91; 92].

One of the main purposes of LENA will be the observation of 1000 geo neutrino events per year by IBD [93; 94]. Beneath the high statistic measurement of the integrated geo neutrino flux and its spectrum also the directional information could be retrieved depending on the possibility of neutrino direction reconstruction as demonstrated in section 3.4.1.
An $8\,M_\odot$ supernova at 10 kpc will produce around 20.000 neutrino events and roughly 8700 of these events will be IBD events [91] resulting in a huge statistic which allows to reconstruct the supernova direction with a good resolution as it will be shown in section 3.4.2.

3.4.1 Direction Reconstruction of Geo Neutrinos

Geo neutrinos born in the radioactive decay of several nuclides in the chains of long-lived radioactive isotopes as ^{238}U and ^{232}Th carry information on the abundances and radiogenic heat sources inside the earth, which are of key importance for understanding the formation and subsequent evolution of our planet [95]. Nevertheless the U and Th abundances and their distribution in the earth is not known, except for a thin layer near the surface, where direct sampling is possible.
KamLAND first claims the observation of geo neutrinos in 2005 [96]. They measured at 90% C.L. between 4.5 and 52.4 geo neutrino events. Despite of the large uncertainties this result was encouraging, as KamLAND demonstrated that geo neutrinos exist at observable scales. In 2010 the Borexino collaboration observed geo neutrinos at the $4.2\,\sigma$-level [97].
Beside measuring only the integrated flux the angular distribution of geo neutrinos would give a great opportunity to set stringent limits on different geological models (e.g. [98]), which give the distribution of radioactive elements throughout the earth [93; 99]. Double Chooz expects only 0.2 events/year due to geo neutrinos. Much larger detectors are needed to observe energy distribution, absolute rate or especially directionality of geo neutrinos.
In [93] calculations for LENA were done assuming a neutron displacement of 1.9 cm. This value originates from CHOOZ, but measured with a relative large error of 0.4 cm. Double Chooz will have the possibility to remeasure this important parameter with a precision of 0.1 cm after 1 year data taking, as demonstrated in section 3.2.3.
However, the result of the study in [93] was not very promising. Assuming the CHOOZ values for the neutron displacement $|\vec{p}|$ and the resolution P (scaled to the PEE of LENA) it was found that even a 50 kt detector as LENA is too small to distinguish between different geophysical models on the basis of directional information alone and the main information will be the total flux and the energy shape. But this calculations were done applying the value of $|\vec{p}|$ measured at the CHOOZ experiment with a quite large error. As shown in section 3.2.3 Double Chooz will remeasure $|\vec{p}|$ precisely and if $|\vec{p}|$ turns out to be significant larger the possibility of direction reconstruction

of geo neutrinos might improve.

3.4.2 Supernova Direction Reconstruction

The supernova SN1987A, which was located in the Large Magellanic Cloud introduced a new method of investigation: Neutrino astronomy. The capabilities of present and future detectors towards detection and the physical outcome of neutrinos from a galactic supernova have been investigated by many authors, e.g. [100; 101; 102; 103]. In particular it is shown in [66; 104] that if the propagation of neutrinos is non-adiabatic in the supernova matter, then they provide us a window to glean into the **θ_{13}-mixing angle**. Since both neutrino and antineutrino fluxes arrive from a supernova, one can in principle also get an idea about the **neutrino mass hierarchy** by observing the difference in the neutrino and antineutrino event rates in the detectors [66]. Comparing the neutrino flux at different detectors one can investigate **earth-matter effects**, which can help in turn to distinguish the mass hierarchies [105]. From the time difference between neutral current and charged current interactions $\Delta t = \langle t \rangle_{NC} - \langle t \rangle_{CC}$ one can yield a sensitive probe for **neutrinos mass** in the tens of eV level [106].
A good pointing accuracy is important for two reasons. First, the MeV-neutrino burst precedes the optical explosion by several hours so that an early warning can be issued to the astronomical community (SNEWS [107]). Secondly, in the absence of any supernova observation in the electromagnetic spectrum a reasonably accurate location in the sky is crucial for determining the earth-crossing path to various detectors since the earth matter effects on supernova neutrino oscillations may hold the key to identify the neutrino mass hierarchy [105].
The best way to locate a supernova by its core-collapse neutrinos is through the $\nu e^- \rightarrow \nu e^-$ elastic scattering in a water Cherenkov detector such as SuperKamiokande [108]. The information of the neutrino direction can be reconstructed by observing the Cherenkov light distribution at the photomultiplier tubes. The pointing accuracy of SuperKamiokande or a future megaton detector is strongly degraded by the inverse beta reactions which are about 30-40 times more frequent than the directional scattering events [109]. It was proposed to add to the water a small amount of gadolinium that would allow to detect neutrons and thus to tag inverse beta reactions [102] which would increase the pointing accuracy from 8° to 3° (95% C.L.) [109].
Other (less sensitive) methods include the time-of-arrival triangulation with several detectors [109; 110], the neutrino-proton elastic scattering [111] and the measurement of the systematic dislocation of neutrons after IBD. Though this last technique offers no event by event pointing possibility the IBD reactions will be the dominant one in large scale scintillator experiments and thus offer large statistics. Assuming a Supernova at the distance of 1 kpc one could expect around 60 supernova neutrino events in both detectors of Double Chooz including target and gamma catcher [112], which is of course to less to observe the direction of the source.

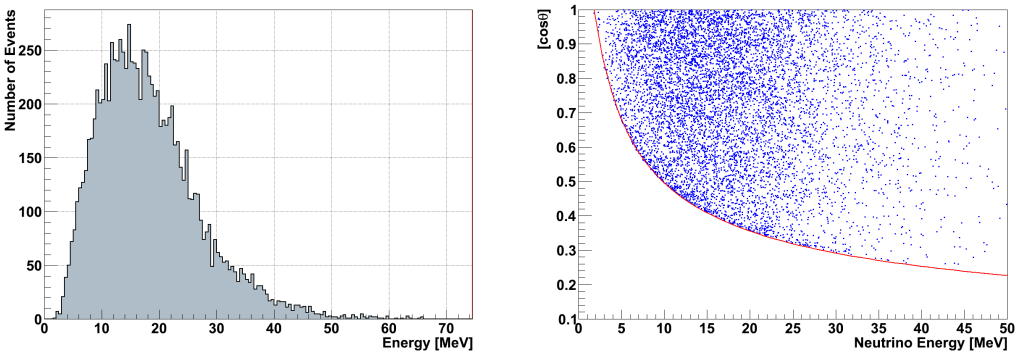

Figure 3.9: **Left:** Energy distribution of $\overline{\nu}_e$ from a supernova.
Right: Simulated $\cos\theta_n$ (blue) and theoretical value of $\cos(\theta_n)_{\max}$ (red) after IBD of supernova neutrinos.

At LENA a very large statistic of roughly $\mathcal{O}(10000)$ neutrino events is expected (depending on the distance and the mass of the star) and it will be demonstrated that the higher neutrino energy with respect to geo- and reactor neutrinos improves the direction reconstruction of supernova neutrinos.
To answer the question which possibility a future large scale (Gd-loaded or unloaded) liquid scintillator has to observe the direction of supernova neutrinos by IBD one has to consider how the two parameters for direction reconstruction namely $|\vec{p}|$ and P change.
Neutron Displacement Modification: To determine the the change of $|\vec{p}|$ due to the larger neutrino energy 10000 IBDs in the target with neutrinos having a supernova neutrino spectrum were simulated using DOGS. A deeper discussion about the expected neutrino spectrum can be found in [66]. In the simulation it is handled as a Maxwell Boltzmann distribution with the temperature $T_{\nu_e} = 5\,\text{MeV}$ [100]. This results in an average energy of about 16 MeV (left side of figure 3.9). The direction of the neutrino beam was in negative z-direction.
As described in [80] the higher neutrino energies have two main influences on the possibility of direction reconstruction. First, the higher neutron energy implies a lower scattering cross section, which in turn results in a larger neutron displacement. Secondly, as one can see from formula 2.11 and in figure 3.9 the maximum angle $\cos(\theta_n)_{\max}$ of the neutron with respect to the neutrino direction directly after IBD increases. While the first effect has a positive influence, the second effect worsens the direction reconstruction.
From simulation with 10000 supernova-neutrinos $|\vec{p}| = 1.95 \pm 0.05(\text{stat})\,\text{cm}$ is determined (compared to 1.48 cm for neutrons of reactor energy). So the positive aspect of the higher neutron energy dominates obviously.

The neutron displacement $|\vec{p}|$ does not change in a loaded or unloaded scintillator. As shown in section 3.1 the full value of $|\vec{p}|$ is reached after at least 10 collisions, so that the increased diffusion time has no influence on this parameter.
Modification of P: So far it is not decided if LENA will be loaded with Gd or not, which has an influence on the directional reconstruction because of two reasons:
First, the diffusion time gets longer (from 25 μs to 180 μs) and, therefore, the width of the neutron cloud grows from 3.4 cm to 5 cm. From simulation it was found that the widening of the neutron cloud due to the larger neutron energy after IBD of supernova neutrinos is negligible (from 3.4 cm to 3.8 cm). Furthermore, as explained in section 2.4 the vertex reconstruction in an unloaded scintillator gets worse: From simulation it was found that the 1σ vertex reconstruction error of neutrons captured on H is 18 cm compared with 13.5 cm for Gd captured neutrons. The positron vertex reconstruction is unchanged with 8 cm. One can analytically calculate P_{l} (loaded) and P_{unl} (unloaded) with

$$P = \sqrt{\sigma_{diff}^2 + \sigma_n^2 + \sigma_{e+}^2} \tag{3.20}$$

and gets P_{l}=15.4 cm and $P_{\mathrm{unl}} = 20,0$ cm for Double Chooz and also for LENA. As the PEE of LENA is expected to be in between 120-180 PE/MeV and, therefore, in the Double Chooz range the effect of a different PEE at LENA was not included.
Finally, to estimate the possibility of direction reconstruction only with IBD events one can assume the supernova to be in z-direction and redo the analysis of section 3.2.2. With

$$\tan\theta = \left(\frac{p_z}{|p_{xy}|}\right). \tag{3.21}$$

one can calculate

$$\Delta\tan\theta = \sqrt{2}\frac{P}{p\cdot\sqrt{N}}. \tag{3.22}$$

This results in a 1σ cone width of 10° for the unloaded and 8° for the Gd-loaded case. That is a promising result as it demonstrates that with large scale scintillator experiments, quite independent of the loaded or unloaded case, a supernova pointing accuracy with the same precision as at SuperKamiokande (using neutrino-electron scattering) can be achieved.

4 Background Studies

Background events can mimic a neutrino event and, therefore, cover the influence of θ_{13} on the observed rate and energy spectrum. The Double Chooz experiment will use the coincidence measurement of a positron and neutron to reject a large part of background. Not a single background event but only two either by chance or by nature correlated background events mimic the neutrino signal. There where made big achievements in the radio-purity of detector materials (scintillator, PMTs and acrylics), cleanliness, experience from previous experiments and, not at last, new simulation techniques improving the signal to background ratio.
This chapter introduces all known sources of background events. Simulations were applied to estimate the rate and energy shape of the background. Furthermore, various rejection techniques and their influence on the neutrino events were analyzed.
Background events can be classified in uncorrelated and correlated background. A correlated background event produces a prompt *and* late event by itself, while an uncorrelated background event is the accidental concurrence of independent background events with a time difference smaller than the time cut.

- Uncorrelated background is on the one side radioactivity from the material in the detector and the surrounding rock but also neutrons produced by muons entering the detector. All these events produce an isolated signal and are, therefore, called singles. If two of such singles fall in the time window with the correct energy deposition they will be interpreted as a neutrino event, called **accidental**. Radio-purity measurements of the detector materials show good results for the single rate and in section 4.1 the accidental rate expected from simulation and the possibilities one has to handle that background will be demonstrated.

- Correlated background events have an event signature similar to the neutrino, a prompt and a late event. These are **cosmogenics** as ^{9}Li and ^{8}He produced by high energetic muons entering the detector and producing cosmogenics in collision with ^{12}C. The cosmogenics will be discussed in section 4.2.
  The next source of correlated background are so called **fast neutrons** produced by muons hitting the rock or steel around the detector and producing neutrons with kinetic energies up to several hundred MeV. These neutrons can enter the

detector and produce a correlated signal similar to the IBD. To characterize that background 30 days of simulated data taking were analyzed during this thesis. In section 4.3 the result is presented.
A last source of correlated background are IBDs taking place not in the target but in the the target acryl and in the gamma catcher. If the neutron enters the target and is captured on Gd such an event will imitate a regular target event. This effect is called Spill In. Vice versa it can happen that a neutron from an IBD in the target leaves the target volume and will, therefore, not be captured on Gd. Such an IBD in the target will never pass the cut on the late event and is lost for analysis. That is called Spill Out. Both effects do not cancel each other. Double Chooz will have a net **Spill In current** which has to be well understood and corrected in the experiment. In section 4.4 a detailed study of that background is presented.[1]

As a short preface on the backgrounds in Double Chooz one can find an illustrative overview in figure 4.1. In the top correlated events fulfilling the condition $NPE_{prompt}>200$, $NPE_{late}>700$ and $\Delta t<200\mu s$ are shown. PE means photoelectrons and NPE denotes number of photoelectrons. The red lines indicate the foreseen energy cuts for a neutrino event with $200<NPE_{prompt}<1700$ ($1\,MeV<E_{prompt}<9\,MeV$) and $1200<NPE_{late}<1900$ ($6\,MeV<E_{prompt}<10\,MeV$).[2] The data correspond to a realistic mixture of neutrino and background events for 10 days of data taking in Double Chooz [113]. Here the focus will be a qualitative point of view, as in the following sections a deeper insight will be given:
In black the neutrino events are visible. In the low-energy part of the positron energy spectrum (at roughly 200-400 PE) they are superimposed by the accidentals (blue color). But also by fast neutrons and spallation neutrons, which happens if two neutrons are captured in the time coincidence, the first on H producing the 400 PE ($\sim$2.2 MeV) peak, the second on Gd with 1500 PE ($\sim$8 MeV). In the middle of the positron energy distribution two ^{9}Li events and two more fast neutron events occur. In the high energy part of the positron spectrum ($\sim$1500 PE) the capture of fast neutrons and spallation neutrons on Gd followed again by a Gd capture dominates.
Fortunately, that figure is not realistic for one reason: It neglects the usage of the inner veto which will be applied in any case. The exact parameters for that cut are not yet defined, most likely a dead time of 500 μs will be applied after an inner veto hit with more than 2500 PE, indicating a muon entering the detector [114]. This cut was applied to the data file. The result can be seen in the bottom of figure 4.1. The

[1] One may argue that this kind of event should not be called background as it is still a detected IBD from another volume. Nevertheless, in this thesis the Spill In is treated as a background because it causes a wrong rate *and* (as it will be shown) also a deformation of the observed energy spectrum. Thus, it is not only an enlargement of the target volume.
[2] At the time of writing the energy cuts are not decided. It depends not only on the observed background rate and spectrum but also on the error in the energy reconstruction.

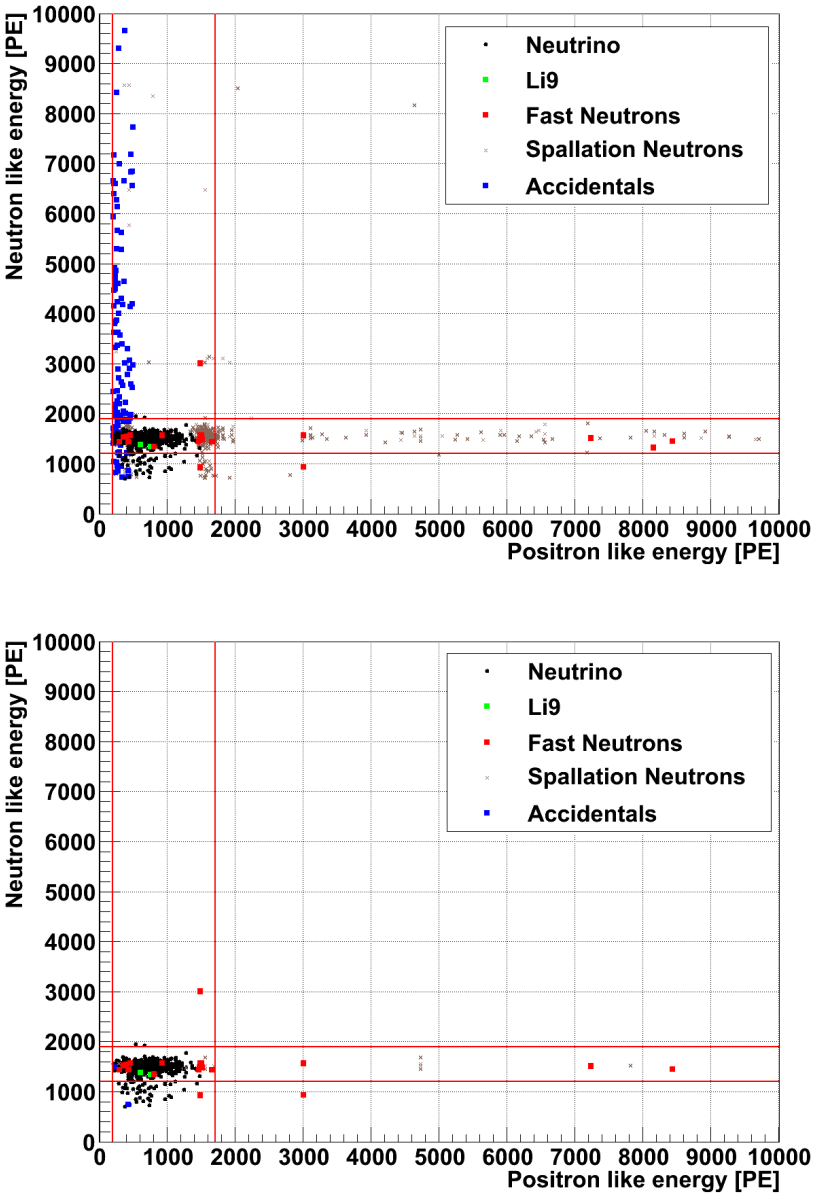

Figure 4.1: Correlation of positron- and neutron-like events produced by simulation for 10 days data taking equivalent.
Top: With cuts $NPE_{\text{prompt}} > 200$, $NPE_{\text{late}} > 700$ and $\Delta T < 200\,\mu\text{s}$. The different particles producing the correlated event are explained in detail in the text.
Bottom: Additional cut applying a dead time of $500\,\mu\text{s}$ after an inner veto Hit with more than 2500 PE.
The red lines indicate the energy cut on neutrino events as explained in the text.

situation has changed notably: The spallation neutrons and accidental events (having mostly the spallation neutrons as late event) have almost disappeared. That is not surprising as the spallation neutrons are created at the same time as the muon travels through the detector and are captured normally before the end of the dead time. It is also not surprising that the ^{9}Li events survive the cut as they have a lifetime of $\sim$0.2 s and are, therefore, not influenced by the dead time. No fast neutron event is rejected. The reason is that fast neutrons were simulated only if the producing muon did not enter the detector (that was done for data memory reasons). In the other case the inner veto cut, optimized for detecting crossing muons, would reject that fast neutrons with a high efficiency as demonstrated for the spallation neutrons.
In the following sections a deeper investigation at the individual backgrounds and the available rejection techniques is presented.

4.1 Accidentals

If an event in the target deposits between $\sim$0.7 and $\sim$9 MeV in the scintillator and this event is accidentally followed within the time coincidence by a 6-10 MeV event, these two totally uncorrelated events will be wrongly identified as a neutrino candidate.

Accidental Prompt Event

The decay of radioactive isotopes in the scintillator and acrylic vessels is one possible source of the prompt event. Contributors are radioactive decays with gamma emission and also beta decays. Alpha decays are less critical as the alpha energy of typically several MeV is quenched down to below 1 MeV in the scintillator.[3] Main contributors are Uranium, Thorium and ^{40}K.
For the radioactive background from outside the scintillator region only gamma emission is important as only high energetic gamma rays can penetrate the detector and reach the active volume, not alphas and betas though. Measurements of the PMT glass have demonstrated the high pureness of the material [118]. Nevertheless, the dominant background contribution is expected from the photomultipliers and their support structure (glass typically has a high concentration of Uranium and Potassium). Due to the shielding in the buffer volume only the highest energetic gamma rays have to be considered, i.e. the 2.6 MeV gamma line from the decay of ^{208}Tl. In figure 4.2 the expected energy distribution based on cleanliness measurements of the accidental prompt event is given.

[3] Following the definition in [115], the quenching process is the loss of scintillation light "attributed to quenching of the primary excitation by the high density of ionized and excited molecules". At the MPIK detailed quenching studies for alphas and electrons were carried out [81; 116] and are planned for protons in the near future [117].

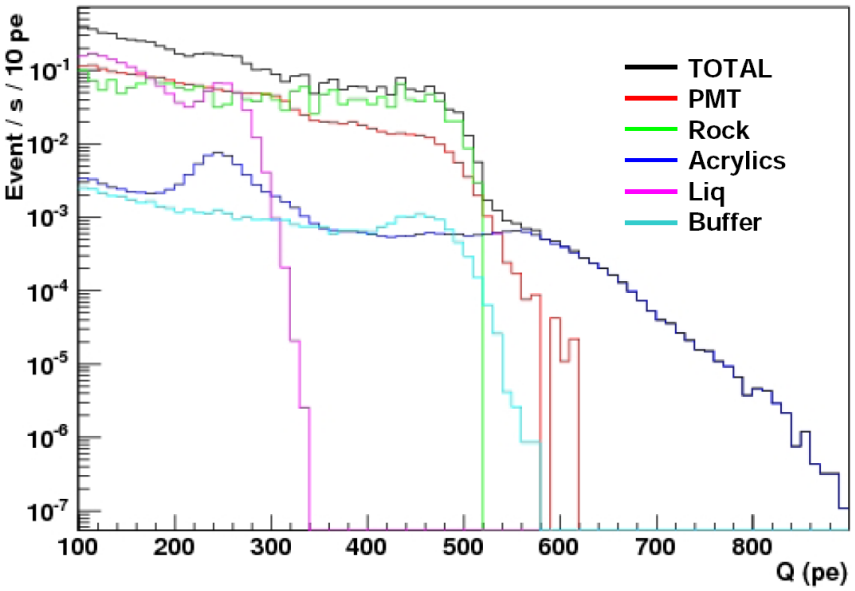

Figure 4.2: Simulated energy spectrum of accidental prompt events [118].

Accidental Late Event

Sources for the accidental late event are captured neutrons produced by cosmic ray muons inside the detector either by spallation or by stopped negative muons that are captured on nuclei. The neutron production rate due to spallation exceeds the rate due to capture of stopped negative muons. In any case as it was demonstrated before, the inner veto is very efficient to detect muons entering the detector and the following deadtime will suppress most of spallation neutrons. As already explained in section 2.4.2 one can, therefore, use these "tagged neutrons" to calibrate the neutron energy scale. An intrinsic neutron source are neutrons produced by (α,n)-reactions and spontaneous fission of heavy elements. As it was calculated in [79] this contribution is negligible.
In the CHOOZ experiment a rate of neutron like events with $(1.25\pm0.06)\cdot10^{-2}$Hz was measured (after all cuts), which was found to be too large to originate only from spallation neutrons. The origin of these energy deposits is still unknown. The radial distribution of the reconstructed vertices, decreasing by two orders of magnitude from the outer wall to the center, suggests an origin outside the detector. The hypothesis has been made that these neutron-like events could be due to Bremsstrahlung photons radiated from cosmic muons which traverse the rock surrounding the detector ("near-miss" muons). A Monte Carlo study was carried out to test this hypothesis [119; 79]. In conclusion, photons from "near-miss" muons explain only 1/10 of the neutron-like energy deposits observed in CHOOZ. It will be an item of study in Double Chooz.

Assuming that the same effect occurs again and scaling the result to the larger Double Chooz target volume a rate of $(2.30\pm0.11)\cdot10^{-2}$Hz is obtained [79]. In the same reference article the aspired upper limit of the accidental rate was given with 1% of the signal rate and one, therefore, gets the constraint to have a prompt event background rate of less than 10 Hz which sets strict limits on the purity of the used materials and the scintillator.

4.1.1 Accidental Rate Measurement at the Experiment

It is an extremely helpful feature of the accidental background that its rate and prompt energy spectrum can be measured at the experiment by shifting the time window of acceptance to a much later time after the prompt event. Due to the uncorrelation the rate stays constant. That was also done in the CHOOZ experiment [120]. So it is not essentially (contrary to other backgrounds as it will be shown later) to determine the accidental rate very precisely by simulation as the experiment itself gives us very good possibilities to determine the accidental rate.

4.1.2 Accidental Estimation from Simulation

To estimate the accidental rate in Double Chooz one can use again the mixed data of all known backgrounds and neutrinos for 10 days data taking. The neutrino events are rejected in this analysis. Figure 4.3 shows the distribution of the produced photoelectrons. The one in red includes all events with more than 200 PE ($\sim$ 1 MeV) without applying any further cut. One can see that below 600 PE ($\sim$ 3 MeV) the single background is dominating. At 1500 PE the neutron capture events from spallation neutrons are pronounced with a production rate of $\sim$ 6000 per day. The nearly flat part in figure 4.3 above 800 PE has its origin mainly from muons entering the detector.
Double Chooz will have the possibility to tag muons entering the detector and, therefore, a deadtime of 500 μs will be applied whenever an energy deposition of more than 2500 PE takes place in the inner veto. The black curve in figure 4.3 shows the impact of that cut on the background. The single rate does not get influenced, while the flat muon contribution is eliminated. Only a few neutron captures survive the inner veto cut, in particular neutrons being captured after the 500 μs. The rates before and after that cut are listed in table 4.1. From this table one can calculate the rate of accidental events R_{Acc} with

$$R_{\mathrm{Acc}} = R_{>200\,\mathrm{PE}} \cdot R_{>1200\,\mathrm{PE}} \cdot \Delta T, \tag{4.1}$$

where $R_{>200\,\mathrm{PE}}$ is the rate of events with more than 200 PE in the prompt event, $R_{>1200\,\mathrm{PE}}$ is the rate of events with more than 1200 PE being the late event and ΔT is the time window. Assuming a time window of 200 μs one gets a rate of **0.04**

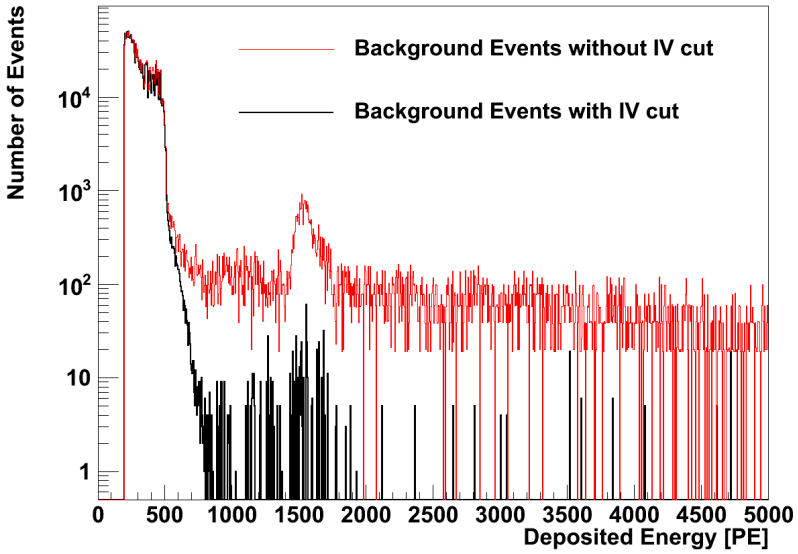

Figure 4.3: Simulated energy deposition in the inner detector of background events after 10 days data taking with and without an inner veto cut.

Energy Cut [PE]	**Background Rate [Hz]**	
	Without IV cut	With IV cut
200 (~ 1 MeV)	2.26	1.98
250 (~ 1.3 MeV)	1.92	1.65
1200 (~ 6 MeV)	0.16	$1.2 \cdot 10^{-3}$
2500 (~ 12.5 MeV)	0.11	$(5.3 \pm 0.3) \cdot 10^{-4}$

Table 4.1: Background rate in Hz for different energy regions. The statistical error is not given if too small.

events/day. **In any case the accidental rate will be larger at the experiment.** In the data set used to estimate the accidental rate only known contributions are included. An unexpected single event source or, as it was observed during the writing of this thesis, a glowing of the PMTs can increase the accidental prompt event rate considerably. The unknown source of neutron like events in the CHOOZ experiment explained before is not included in simulation. Furthermore, simulation of muon induced neutron production has well known uncertainties. Hence, the rate of neutron captures from spallation neutrons can be much higher than obtained from simulation. The neutron rate extrapolated from the CHOOZ experiment is a factor 20 larger than the simulated one, reflecting the existing uncertainty.
Using the prompt event rate of table 4.1 and the neutron rate extrapolated from the CHOOZ experiment the expected number of accidental events per day is 0.8±0.4 (for the error a 50% uncertainty on the prompt event rate was assumed), but will be determined precisely at the experiment as explained in 4.1.1.

4.1.3 Spatial Cut

In the CHOOZ experiment the accidental rate of positron and neutron-like events in a time window of 100 μs was measured to be 3.4 ± 0.15 events/day. A very efficient method to reject accidentals in the CHOOZ experiment was a cut on the positron and neutron-like event distance of 1 m and, therefore, to use the fact that the uncorrelated events in the mean have a large relative distance. Applying the cut $88 \pm 1\%$ of accidental events were rejected at CHOOZ, while $98.4 \pm 0.3\%$ of the neutrino events passed the cut [120].
A Monte Carlo simulation was written during this thesis to estimate the efficiency of a spatial cut for the Double Chooz experiment with a different detector geometry and a better vertex reconstruction compared to CHOOZ:
The late event of accidentals was produced isotropically in the target. The prompt event is expected to concentrate at the gamma catcher wall and decrease from there exponentially. The slope of the exponential curve was estimated from simulation to 443 mm [121]. This information was used for the prompt event production. Furthermore, both the prompt and late event were folded with a Gaussian of 8.5 cm width for the prompt and 13.5 cm width for the late event to simulate the vertex reconstruction error. Finally for each pair of prompt and late event the relative distance was calculated (left side of figure 4.4).[4] The neutrino events were calculated using 1 year of simulated neutrino data and the vertex reconstruction algorithm RecoBAMA.
In the right side of figure 4.4 the efficiency for rejecting accidentals at different cuts and at the same graph the probability for a neutrino event to survive that cut is

[4] It should be remarked, that the spatial distance of accidental prompt and late events can be measured precisely by shifting the window of acceptance as explained in section 4.1.1.

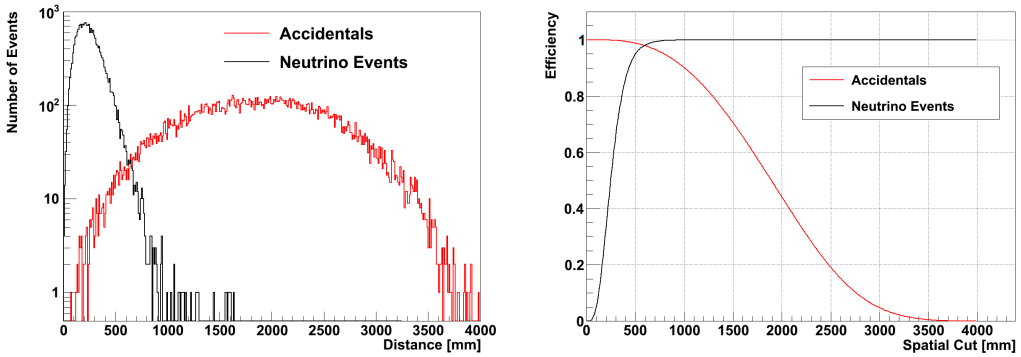

Figure 4.4: **Left:** Simulated distance of prompt and late events for neutrinos (black) and accidentals (red).
Right: Neutrino detection efficiency (black) and accidental rejection efficiency (red) for different spatial cuts.

Cut [mm]	**Rejection Probability** [%]	
	ν	Accidentals
500	4.99±0.15	98.81±0.11
1000	0.101±0.022	90.13±0.61
1500	0.029±0.012	70.49±1.24
2000	0	44.12±1.32

Table 4.2: Rejection probabilities for neutrinos and accidental events at different spatial cuts. The quoted errors are statistical errors for the neutrinos. For the accidentals only the systematical error is calculated as explained in the text.

given. Clearly both distributions are contrary. Increasing the cut-distance one will reject less neutrinos but will weaken the power of the cut to reject accidental events. In table 4.2 one can see the probabilities for different cuts. The number of accidental events were chosen sufficiently high to have no statistical error. The systematical error was calculated by assuming a 20% systematical error on the penetration depth of the singles. The systematical error is then the resulting variation in the rejection probability. Regarding the accidentals the simulation gives a good agreement for the 1 m cut compared to the CHOOZ result. The small difference might be explained by the different detector geometry. As already explained 1.6% of the neutrino events were rejected due to the 1 m cut in the CHOOZ experiment. The quoted systematic error of this cut in the CHOOZ experiment was 0.3% [120]. This simulation for Double Chooz gives a factor 16 smaller probability, which can be explained by the better

vertex reconstruction due to higher light production and PMT coverage of the Double Chooz experiment.
A 1 m spatial cut would reject 90.13±0.61% of the accidental events but only 0.101±0.022% of the neutrino events. The quoted error is only the statistical error of the simulation. It is crucial to know the uncertainty of removing neutrino events by that cut. Without having calibrated data, especially a central neutron and gamma source to determine the vertex reconstruction error, it is not possible to estimate the systematical error on the neutrino rejection probability. Thus, this cut should be only applied if calibrated data are available or the accidental rate is too high.
In any way, if the accidental rate is as low as calculated in the previous section there is no need for such a cut introducing an additional systematic error on the neutrino event number. But as stated before the accidental rate can be much higher than simulated in a Monte Carlo. Furthermore, as it will be shown in chapter 5, even a small accidental rate is a large contributor to the sensitivity of the experiment as the prompt energy of the accidental background is typically in the low energy part of the positron energy spectrum where the largest deformation due to a non-zero θ_{13} is contained. Thus, a small accidental rate is crucial for the experiment and, therefore, the spatial cut could be relevant, if the accidental right is larger than the expected 1-2 events/day.

4.1.4 Pulseshape Analysis for Accidental Reduction

The majority of prompt event vertices of accidental events is found to be in the gamma catcher. As it will be demonstrated especially in section 4.4 one can use the information of the pulseshape to distinguish gamma catcher and target events. In the case of a large accidental rate the pulseshape information could be used to reject accidental events in the gamma catcher. However, at smaller accidental rates one will not use the pulseshape and the relative distance cut as both methods induce an uncertainty for the neutrino sample.

4.1.5 Summary

To summarize the accidental background:

- At the CHOOZ experiment an accidental background rate of 3.4±0.15 events/day was measured [16]. An unexpected high rate of neutron like events was observed, which could so far not be totally explained. Extrapolating this rate to the Double Chooz volume and using the prompt event rate determined from purity measurements and simulation an accidental rate of 0.8±0.4 events/day was calculated. The error is dominated by a supposed 50% error on the prompt event.

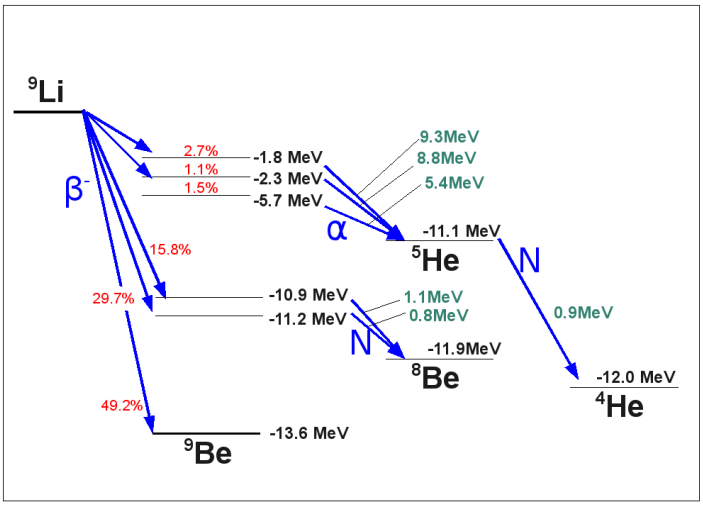

Figure 4.5: Decay channels of ^{9}Li. The blue characters β^{-}, α and N indicate the produced particles. Their energies are green, the probabilities of the different decay channels are red colored.

- The accidental rate can be determined at the experiment by shifting the time window of acceptance to a much later time after the prompt event. The systematic uncertainty should then be well estimated by 10%.
- The accidental rate can be efficiently decreased by the spatial cut. As it will be demonstrated in section 4.4 also the pulseshape information could be used to identify the accidental prompt events emerging to a large part in the gamma catcher. In any case one has to carefully control the influence of these techniques on the neutrino events.

4.2 Cosmogenic ^{9}Li and ^{8}He

Cosmic muons reach the detector with a rate of >5 Hz [122] and some of them may interact with the ^{12}C nuclei in the liquid scintillator and produce long lived radioactive isotopes by electromagnetic or hadronic processes. Details can be found e.g. in [123]. Among them ^{9}Li and ^{8}He (and to a negligible part ^{11}Li) have β-neutron cascade decay modes (for ^{9}Li see figure 4.5) with a very similar energy distribution as the positron signal of neutrino events (figure 4.6). Thus, the decay of ^{9}Li and ^{8}He can mimic both the prompt and late event of the IBD. Furthermore, since both isotopes are relatively long-lived, with half lifes of 0.18 s for ^{9}Li [124] and 0.12 s for ^{8}He [125],

there is no possibility to reject them with a muon veto.
Taking into account measurements at CERN [126] and KamLAND [127] the production ratio of ^{8}He relative to ^{9}Li was determined to $26 \pm 8\%$. Taking furthermore into account that only 12% of ^{8}He decays create a neutron while it is 50.8% for ^{9}Li decay one gets an effective ^{8}He to ^{9}Li ratio of $6 \pm 2\%$. Furthermore, the ^{8}He contribution could be determined by tagging the cascade ^{8}He$\rightarrow^8$Li$\rightarrow^8$Be and will be a method to estimate also the ^{9}Li rate using the ratios described above. Here, for simplicity, it is assumed that cosmogenic background is solely ^{9}Li in this investigation.
In figure 4.6 one can see the deposited energy spectrum of ^{9}Li events together with neutrino IBD events assuming a 2% ^{9}Li to neutrino ratio after four years data taking.[5]
The prompt event of the ^{9}Li mimics the IBD prompt event. But it has significant influence only at the high energy part (>7 MeV) of the positron spectrum. As it will turn out in chapter 5, this feature makes the ^{9}Li less critical for the Double Chooz sensitivity than one would expect from the quite large rate.
In general it would be possible to measure the ^{9}Li rate by analyzing the modification of the positron spectrum above 6 MeV by the ^{9}Li events. That was done to estimate the ^{9}Li rate for CHOOZ as it will be demonstrated in section 4.2.1. But that is non-trivial through the flat component of the fast neutron background[6] and requires a good energy reconstruction capability.
Pulseshape discrimination, often used to distinguish heavier particles from the IBD positrons, does not help here. Due to the quenching most of the visible energy of the prompt event is deposited not by neutrons or alphas but by electrons and thus makes the prompt energy deposition of ^{9}Li indistinguishable from IBD by pulseshape analysis.

4.2.1 Energy Spectrum Analysis during Reactor-Off

Double Chooz highly benefits from having data from the CHOOZ experiment (especially 138 days of reactor-off data). Analysis of the total background rate, a spectral fit to official CHOOZ reactor-off data between 2.8 and 10 MeV and a spectral fit to extended CHOOZ reactor-off data between 2.8 and 30 MeV are in quite good agreement and predict a ^{9}Li rate at Double Chooz of 0.5-1.5 events/day or about 1-2% of the expected signal rate [79]. One of the main problems of that method is the uncertainty of the fast neutron prompt energy spectrum. In the spectral fit a flat distribution for fast neutrons was applied. As it will be demonstrated in section 4.3 this assumption might be inaccurate depending on the used cut to reject fast neutron events.
A possible reactor-off phase during data taking could be used by Double Chooz to redo that analysis.

[5] A 2% ^{9}Li rate was assumed in the Double Chooz proposal [79].
[6] In section 4.3 it will be analyzed if the recoil spectrum is really flat or not.

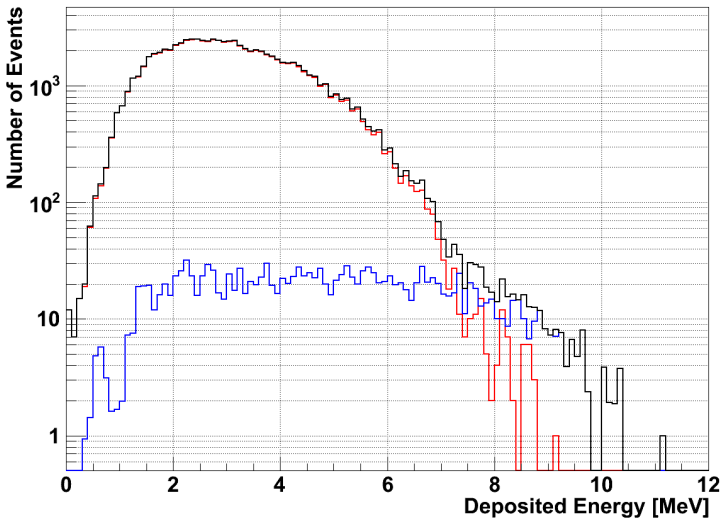

Figure 4.6: Prompt event energy spectrum of neutrino events (red), ^{9}Li events (blue) and both together (black) after 4 years data taking assuming a ^{9}Li ratio of 2%.

4.2.2 Time and Volume Cut after Muons

One possibility to reject ^{9}Li events is to use the fact that ^{9}Li is created and decay in the vicinity of the muon track. KamLAND used this property to reject ^{9}Li by two cuts [128]: 1) A 2 s cut after a showering muons where no clear track can be resolved and 2) A 2 s dead time in a 3 m fiducial volume around the muon track in the non-showering case. Both cuts are not in the same way feasible in Double Chooz. The timecut 1) after a showering muon would work only if the rate of showering muons is not too large. As this point will discussed later in more detail it is only mentioned that most likely only a small fraction of the muons is showering but a large fraction of ^{9}Li is produced by the showering muons.
The cut 2) will not be practical in Double Chooz: A 3 m cut around the track as used in KamLAND would result in a totally blinded detector assuming a muon rate of 5 Hz and a smaller dimensioned cut is critical because of uncertain inefficiencies.
However, the dead time cut 1) would be an interesting possibility in the case the showering rate is not too high. If Double Chooz has collected large statistic one could check if the neutrino-like event rate is larger after showering muons and thus confirming that showering muons are the main source of cosmogenics production. In section 4.2.4 an improved method to check that assumption will be introduced.

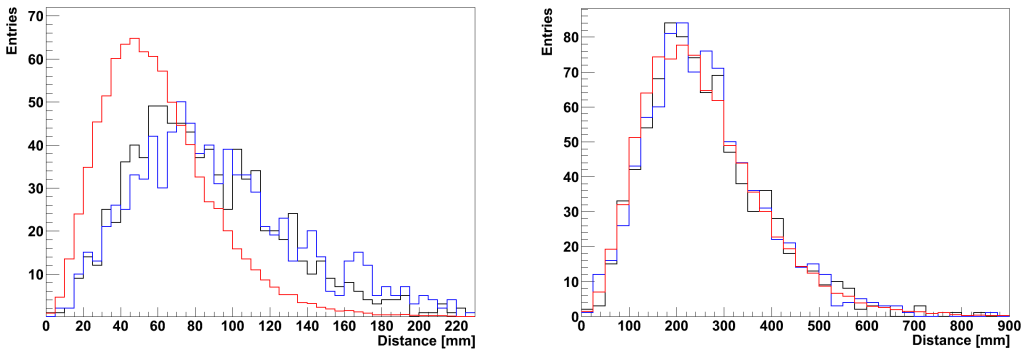

Figure 4.7: True (left) and reconstructed (right) travel distance of neutrons from ^{9}Li decay with 0.8 MeV (black), 1.1 MeV (blue) and neutrons from IBD (red).

4.2.3 Spatial Cut

As one can see from figure 4.5 the neutrons of the ^{9}Li decay have an energy of 0.8 MeV and 1.1 MeV respectively and are expected to travel a wider distance in the scintillator with respect to the keV neutrons of the IBD. That could be used to tag the ^{9}Li events by a spatial cut similar to the one tested for accidental events in section 4.1.3.
To test this idea, 1000 ^{9}Li decays in each of the two ^{9}Li decay branches were produced in the center of the target using the particle generator DCGenSpec [129] (corresponding to roughly 2 years of data taking). Only Gd capture events were analyzed. The true travel distance (without vertex reconstruction) for the two ^{9}Li chains and IBD neutrons is shown in figure 4.7 on the left side. As expected the neutron travel distance increases with the neutron kinetic energy. For 0.8 MeV and 1.1 MeV neutrons it is $\langle\sqrt{r^2}\rangle$=87 mm and 95 mm respectively while IBD neutrons travel only 61 mm on average. But after the reconstruction of the prompt and late event vertex and calculating the neutron radius with that parameters no information is left ($\langle\sqrt{r^2}\rangle$ is 260 mm for all three kinds of neutrons). That is because the value of $\langle\sqrt{r^2}\rangle$ is by far dominated by the vertex reconstruction error. **Therefore, it is not possible to use a spatial cut to distinguish ^{9}Li from IBD events.**

4.2.4 Time since last Muon Method

KamLAND was able to measure the ^{9}Li production rate from the time distribution of the β-neutron event since the last muon having entered the detector [127]. KamLAND was able to apply this method as the overburden of the detector is 2700 m.w.e., resulting in a very small muon flux of 0.2 Hz in the scintillation volume of the detector. Double Chooz at 300 m.w.e. expects a muon flux in the scintillation volume of

roughly 5 Hz, which implies the mean interval of the muons to be 0.2 s, roughly the lifetime of ^{9}Li. In [130] it was demonstrated that it is still possible to determine the ^{9}Li rate even if the muon rate is in the order of the ^{9}Li lifetime. Two methods are presented in the reference article:
First a **Method of least squares**. The general idea is to include the possibility that the ^{9}Li was not created by the last muon but by one of the muons before (weighted with an exponentially decreasing probability). The result is a probability density function $f_{\mathrm{Li}}(t)$ of the ^{9}Li events in terms of the time since last muon

$$f_{\mathrm{Li}}(t) = \frac{1}{\lambda} \exp\left(-t/\lambda\right), \quad \frac{1}{\lambda} = \frac{1}{\tau} + \frac{1}{T} \tag{4.2}$$

where $\tau = 0.257\,s$ is the lifetime of ^{9}Li. T is the average time between two muons in the active volume and at the same time the period between a muon and a neutrino event due to the small neutrino event rate. In Double Chooz the observed distribution of the time since last muon t for all positron-neutron events is a combination of the neutrino events (more precisely: positron-neutron events without a correlation to the muons) and that of the ^{9}Li signal resulting in the equation

$$f(t) = B \cdot \frac{1}{\lambda} \exp\left(-t/\lambda\right) + S \cdot \frac{1}{T} \exp\left(-t/T\right), \tag{4.3}$$

with B and S as the number of ^{9}Li and neutrino events respectively. Equation 4.3 can now be used to fit the observed distribution of the time difference between the last muon and the neutrino like signal (neutrino or ^{9}Li).
The second method (**Method of maximum likelihood**) is based on the same idea but uses an unbinned maximum-likelihood fit with the same probability distribution function. Thus, the log-likelihood function is calculated to

$$\log L = \sum_i \log \left[b \cdot \frac{1}{\lambda} \mathrm{e}^{-t_i/\lambda} + (1-b) \cdot \frac{1}{T} \mathrm{e}^{-t_i/T} \right] \tag{4.4}$$

where t_i is the time of the i-th beta-neutron event since last muon and b is the probability of being a ^{9}Li event.

Monte Carlo Simulation

To test the feasibility of both methods for the ^{9}Li and muon rate expected at Double Chooz a Monte Carlo simulation was written during this thesis.
First a data sample of time differences of neutrino and ^{9}Li events to the last muon were generated in the following way:
In the beginning a decision is made if a neutrino event with probability (1-b) or a ^{9}Li event takes place. If a neutrino event occurs the time after the last muon is determined with the exponentially distributed time difference $\Delta t = \exp(1/T)$ and

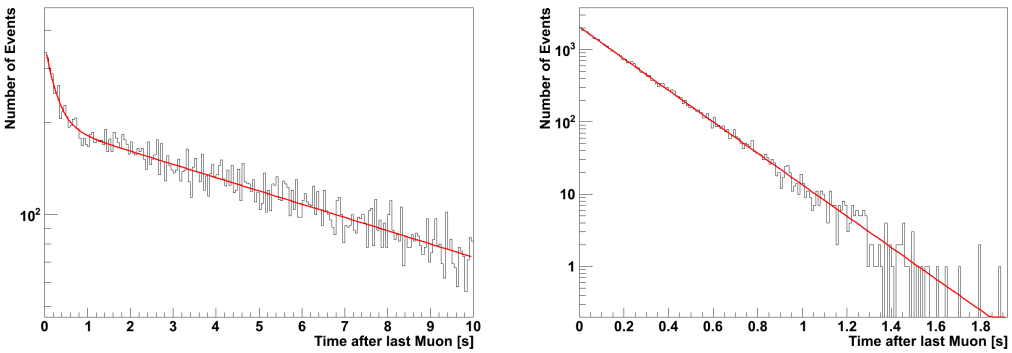

Figure 4.8: Time since last muon distribution after two years data taking in Double Chooz assuming a 2% ^{9}Li probability and 0.1 Hz (left) and 5 Hz (right) muon rate. The χ^2 fit was done with the formula of equation 4.3.

added to the time distribution. If a ^{9}Li event takes place first the lifetime of the ^{9}Li is calculated with $\tau_i = \exp(1/\tau)$ but not yet added to the time distribution. First it is calculated with a Poisson probability distribution how many muons N_μ occurred in between, with $N_\mu = \text{Poisson}(\tau_i/T)$.
Then the time t_μ for each of this muons is calculated uniformly between 0 and τ_i. At last $\Delta t = \tau_i - t_\mu$ ($\equiv$ time since last muon) is added to the time distribution. The time distribution for different muon rates and a runtime of one year (20.000 neutrino events) is illustrated in figure 4.8.

One can use now both methods described above to extract the background to signal ratio. The χ^2-method was performed using the data analysis package ROOT [131] while for the likelihood analysis MINUIT [132] was used. Each run consists of creating a data sample and a fit with one of the two methods and was repeated 500 times to investigate the potential bias and the precision of the fit. The result of different muon rates and for the two most likely cases b=1% and b=2% is plotted in figure 4.9. The Maximum-Likelihood method has the smaller bias and better precision compared to the χ^2-method. That is conform with the result in [130]. **Using the likelihood method and the most probable muon rate of 5 Hz one should be able to extract the ^{9}Li rate nearly unbiased with a relative precision of 66% after one year data taking and 45% after two years, which is a promising result as the uncertainty of the ^{9}Li rate is so far estimated to 50% [79].**

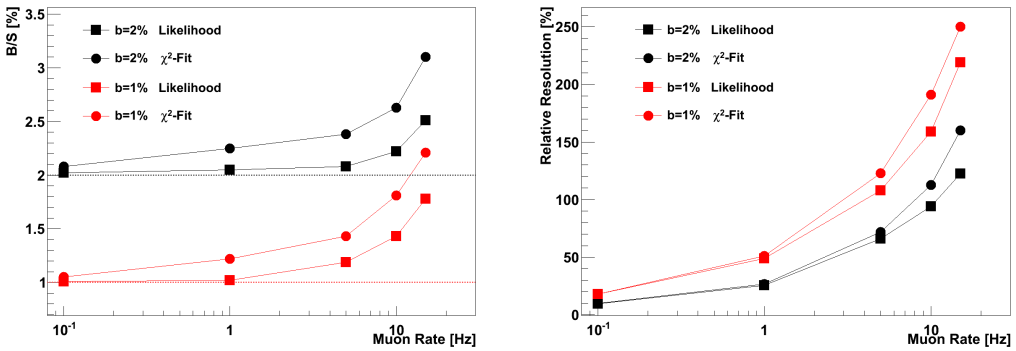

Figure 4.9: **Left:** Background to Signal ratio for b=1% and b=2% and different muon rates after one year data taking using both methods described in the text.
Right: Relative resolution of both methods as a function of the muon rate. The relative resolution is defined as the statistical error obtained from the fit normalized to the true input value of b. Both figures correspond to one year of data taking.

Time since last Muon Method assuming an effective Muon Rate

The main limitation of this analysis method originates from the high muon rate. So far it was assumed that each muon entering the active volume of the detector has the same probability of producing radioactive isotopes, which is actually not the case. Most of the cosmogenics are produced due to the photonuclear reaction when a high energetic gamma interacts with a ^{12}C. But the dominant gamma production is from the Bremsstrahlung of muons shower particles and not from the Bremsstrahlung of the muon itself [123]. That is illustrated in figure 4.10. In [123] it was found that the dominant gamma energy for the production of cosmogenics is in the Δ-peak of 400 MeV (left side of figure 4.10), where the gamma production due to secondary particles Bremsstrahlung is nearly 100 times larger than the gamma production by the muon itself (right side of figure 4.10). Showering muons have, therefore, a much larger cross section for ^{9}Li production compared to non-showering muons.
During this thesis the idea was developed to apply the analysis described above only to the showering muons, as they will occur with a much lower frequency and would allow a very high precision using the method described above.
Also to answer the question what is the fraction of showering muons at Double Chooz the Tübingen group performed extensive muon studies. At low energies from 100 MeV to 100 GeV the muon energy loss is dominated by atomic ionization and the muons are minimally ionizing particles. At higher energies, radiative processes such

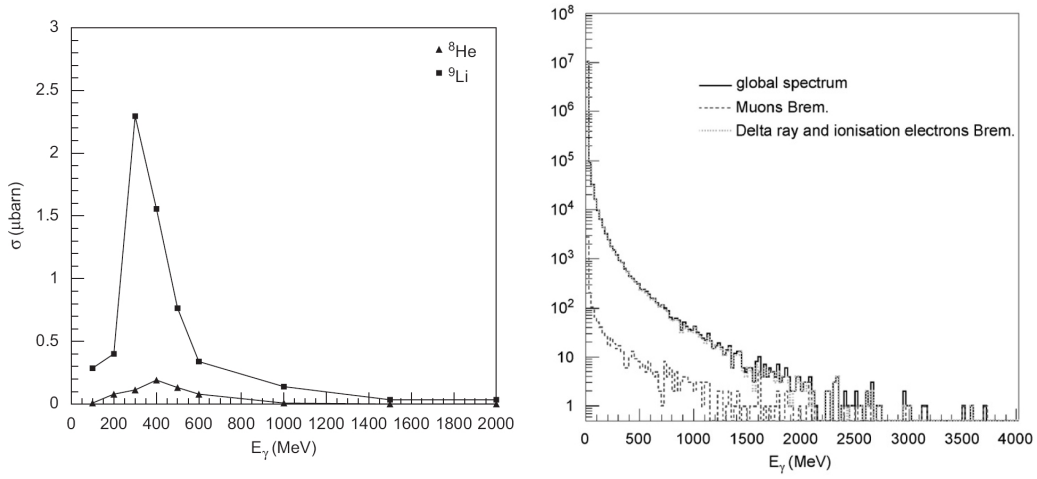

Figure 4.10: **Left:** Simulated cross-section of ^{9}Li and ^{8}He production from interaction of gammas through 1 m of ^{12}C.
Right: Simulated gamma spectra produced by Bremsstrahlung process from interactions of muons with energy of 10 GeV through 10 m of rock [123].

as e^{+}-e^{-}pair production, Bremsstrahlung, and photonuclear interactions become important, resulting in a huge energy loss with large fluctuations, known as showering. The critical energy where ionization energy loss is equal to the average radiative energy loss is about 1 TeV. The fraction of muons entering the detector having an energy of more than 1 TeV is roughly $5{\cdot}10^{-3}$ [133]. Assuming a total muon rate of 5 Hz will result in a rate of showering muons of roughly 25 mHz. **With such a low rate one could extract the ^{9}Li rate with a relative precision of 5% after 1 year data taking.**
However, the central question is if Double Chooz can resolve showering muons. In [134] it is demonstrated that in SuperKamiokande showering muons could be separated from non-showering. A non-showering muon has a constant dE/dx along the muon track (∼4 MeV/10 cm) while that number is much higher and not constant along the track for showering muons, illustrated in figure 4.11. However, that was possible for the SuperKamiokande experiment and it must be demonstrated that this is also feasible for the Double Chooz experiment with a smaller detector size and a poorer direction resolution for muons.

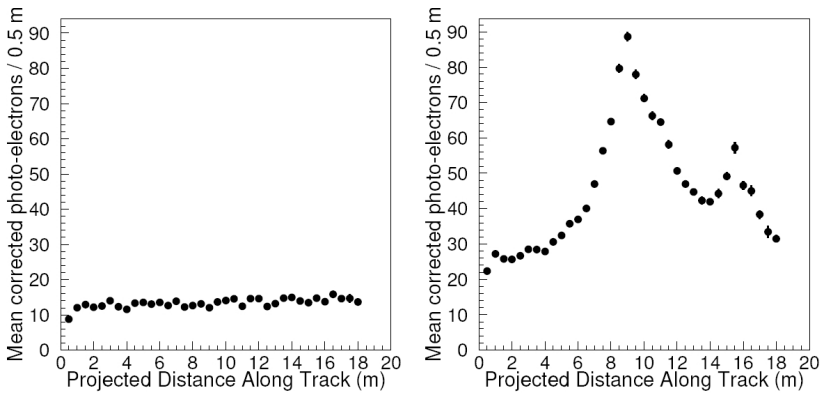

Figure 4.11: **Left:** Approximately flat dL/dX distribution of a normal ionizing muon of energy 20 GeV in the SuperKamiokande detector.
Right: dE/dx distribution of a showering muon of energy 10 TeV [134].

4.2.5 Summary

To summarize the ^{9}Li background:

- It was demonstrated that the cosmogenic background (especially ^{9}Li) is difficult to distinguish from a neutrino event. Neither the pulseshape nor the spatial cut can be used for that background. Simulations of the ^{9}Li production rate are difficult because of the given theoretical uncertainties in the ^{9}Li production cross section and the needed computing time to simulate especially showering muons.

- A very valuable information is in any case the extrapolation of the reactor-off period in the CHOOZ experiment resulting in 0.5-1.5 events/day.

- The time-since-last-muon method could be a helpful tool for an independent result if the muon rate in the inner detector is not significantly larger than 5 Hz. Assuming a 5 Hz muon rate the ^{9}Li contribution can be determined in the far detector with an uncertainty of 66% after one year data taking.

4.3 Fast Neutrons

Fast neutrons are produced by cosmic muon interaction with nuclei. While neutrons produced in the detector can be tagged by the muon interaction in the inner and outer veto, muons also can produce neutrons in the surrounding rock. These fast neutrons

can hardly be identified by the veto systems and mimic a neutrino signal.
Fast neutrons are produced in the following processes [135]:

1. Muon interaction with nuclei via a virtual photon producing a nuclear disintegration. This process is usually referred to as "muon spallation" and is the main source of theoretical uncertainty.

2. Muon elastic scattering with neutrons bound in nuclei.

3. Photonuclear reactions associated with electromagnetic showers generated by muons.

4. Secondary neutron production following any of the above processes.

5. Stopping and captured muons, resulting in highly excited isotopes emitting one or more neutrons.

While the last process is relatively well understood, the others are still poorly known. Although the total neutron yield has been, to some extent, experimentally measured [136; 137], theoretical models are not consistent with each other and with data [135]. In addition the few measurements of neutron energy spectrum are not well reproduced by theoretical calculations and simulations [138]. Interpretation of experimental data is complicated by the fact that the neutron energy spectrum depends upon the muon spectrum that, in turn, is a non-trivial function of the depth at which the measurement was carried on. So one has to be aware of the fact that the result of simulation presented in this section might has large uncertainties especially in the fast neutron yield, multiplicity and energy spectrum.
In section 4.3.1 some important properties of the fast neutron background are given and in section 4.3.2 the influence of different cuts on the fast neutron rate is demonstrated. In section 4.3.3 it is considered how one can crosscheck the simulation with experimental data. In section 4.3.4 it will be discussed if pulseshape analysis can be used to identify fast neutron events.

4.3.1 Characteristics of the Fast Neutron Background

Fast neutrons produced outside the detector may enter the active volume and slowed down by multiple scattering in the scintillator. Figure 4.12 shows the general possibilities of fast neutrons to mimic a neutrino event. The recoil protons may generate the prompt signal which might be in the allowed energy window for positron events. After being slowed down to thermal energies the neutron can be captured and produce the late event signature. Such an event type is called **RN event (Recoil-Neutron event)** which corresponds to coincidence 1 and 2 in figure 4.12. Another possibility to produce a correlated event is due to the fact that more than one neutron can be

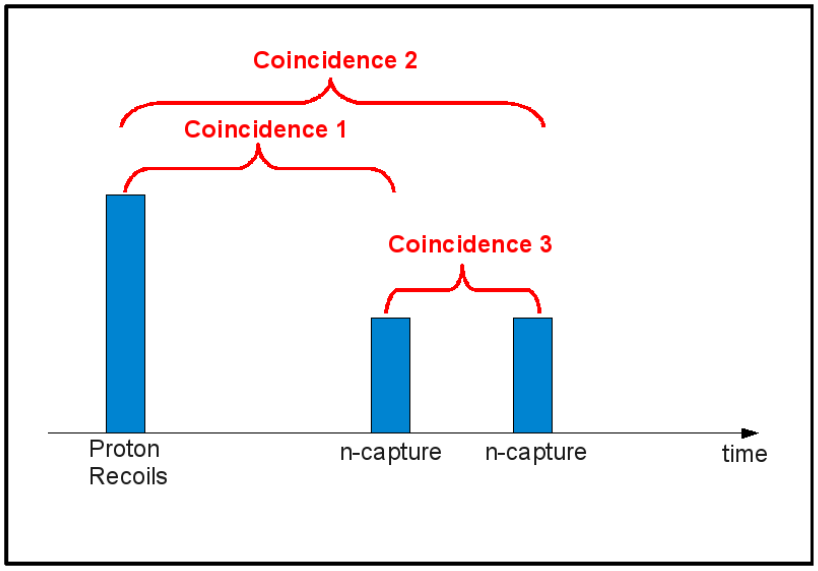

Figure 4.12: Possibilities of a fast neutron event to produce a correlated event. All three coincidences may fulfill the neutrino candidate criteria.

captured in the detector. This might happen due to two or more muons producing a fast neutron at the same time or due to multiple neutron production by one muon or the fast neutron itself. Even if the proton recoil peak itself is too small or too large for being a prompt event the neutron captures itself can produce a neutrino like prompt event. Such an event is called **fake-event** [139] illustrated as coincidence 3 in figure 4.12.
The total correlated background at CHOOZ experiment was quoted with $1.01 \pm 0.04(\text{stat}) \pm 0.1(\text{syst})$ events/day [120] and fast neutrons were considered as main contributor to correlated background [79]. For Double Chooz a lower fast neutron rate is expected due to the improved detector design. Using steal instead of sand increases the neutron path length by about one attenuation length. From that one can predict a factor 3 decrease, leading to roughly 0.3 events/day [79].
The group of the TU in Munich tried to reproduce these numbers by simulation applying the same cuts as the CHOOZ experiment [140]. First 31 hours of data taking in the CHOOZ experiment were simulated and one correlated event was observed resulting in 0.8 events/day, which is in good agreement with the CHOOZ result. After having validated the Monte Carlo 43 hours of data taking for the Double Chooz experiment were simulated with an overburden of 100 m.w.e. and then scaled to the actual overburden of 300 m.w.e.. Again one event was observed. That leads to 0.15 events/day at the far site.

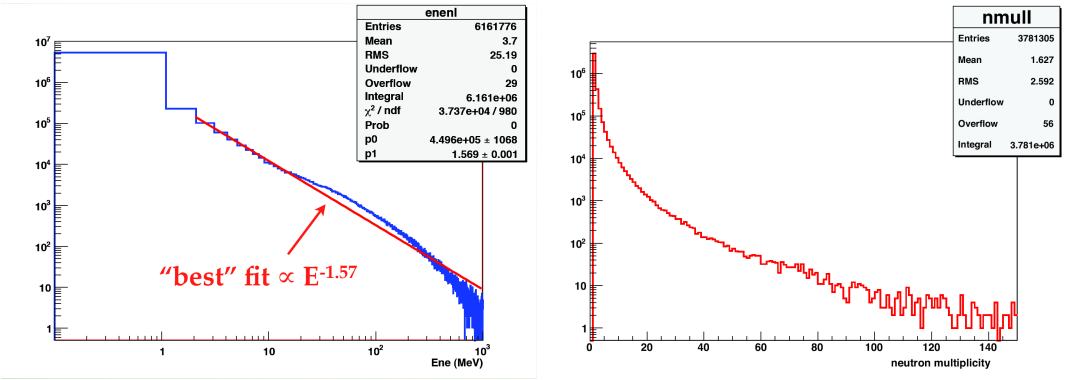

Figure 4.13: **Left:** Simulated energy distribution of fast neutrons behind the shielding.
Right: Simulated neutron multiplicity behind the shielding [139].

The Munich simulation is in good agreement with CHOOZ result even though it lacks statistic. Therefore, a new data set production was performed at the IPHC in Strasbourg and the APC in Paris and analyzed during this thesis. Here muons were produced in a 120×120 meter surface 12 meters above the detector using a realistic energy and angle dependence and propagated through the rock using MUSIC (a simulation package for muon transport through matter [141])[142].
30 days of Double Chooz data taking were simulated. Only the energy and multiplicity distribution of neutrons entering the detector, while the muon does not, were stored. That is because fast neutrons of muons entering the detector would be removed by the inner veto deadtime. These neutron files were taken as the input for the DCGLG4sim code simulating the propagation and light production of the neutrons through the scintillator. The result were ∼6 million neutrons simulated after the shielding. Out of these only a small fraction actually reaches the detector scintillation volume. The initial energy and multiplicity distribution of simulated fast neutron events is shown in figure 4.13.

Is the observed Fast Neutron Energy Spectrum flat?

It is crucial to know the prompt energy spectrum of the fast neutrons for two reasons: First, to subtract the fast neutron background correctly from the neutrino spectrum. Second, if one wants to extract the ^{9}Li rate from the high energy part of the energy spectrum (as explained in section 4.2.1) one has to know the shape of the fast neutron spectrum in that area. So far the fast neutron spectrum was assumed to be flat [79; 143]. Simulations were used to check this assumption.
In figure 4.14 on the left side one can see the produced photoelectrons of fast neutron events versus their kinetic energy. Most of the fast neutrons produce only a

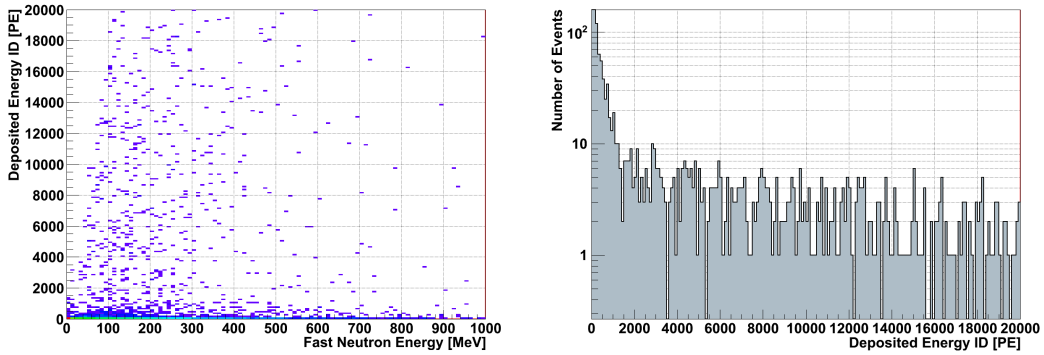

Figure 4.14: **Left:** Deposited energy of the fast neutron recoils in the inner detector (target and gamma catcher) over the kinetic energy of the fast neutron.
Right: Deposited energy of the fast neutron recoils in the inner detector. Both figures do not have the condition of a subsequent late event.

few photoelectrons despite their large kinetic energy. These are mostly fast neutrons depositing energy only in a small part of the scintillation volume. Above $\sim 2000\,\mathrm{PE}$ one can see a weak but existing correlation between the fast neutron kinetic energy and its photoelectron production.
From that correlation of fast neutron energy and PE production one can understand that the fast neutron distribution decreasing with energy in figure 4.13 results also in a decreasing (and not flat) distribution of the produced photoelectrons above $\sim 2000\,\mathrm{PE}$ shown in figure 4.14 on the right side (below $2000\,\mathrm{PE}$ one can find again the fast neutrons crossing only a small part of the inner detector and thus producing less light).
However, still the photoelectron distribution is not realistic as so far no cut for a subsequent Gadolinium capture event was applied. Using that cut for the fast neutron distribution of figure 4.14 on the right side the result is shown in figure 4.15. 107 events occurred in the observed energy region up to $20000\,\mathrm{PE}$ ($\sim$100 MeV). The exponential fit indicates a very small slope of $-1.8 \cdot 10^{-5}(\pm 1.9 \cdot 10^{-5})1/\mathrm{PE}$, which is close to a flat distribution.
But even if one assumes that in a good approximation the RN coincidences produce a flat prompt energy distribution the fake coincidences will deform the flat distribution at 2.2 and 8 MeV (H and Gd capture). It will be demonstrated that depending on the applied cut the fake events dominate the RN-contribution.
One has to conclude that without an exact knowledge of the n-n contribution the assumption of a flat fast neutron distribution might be wrong.

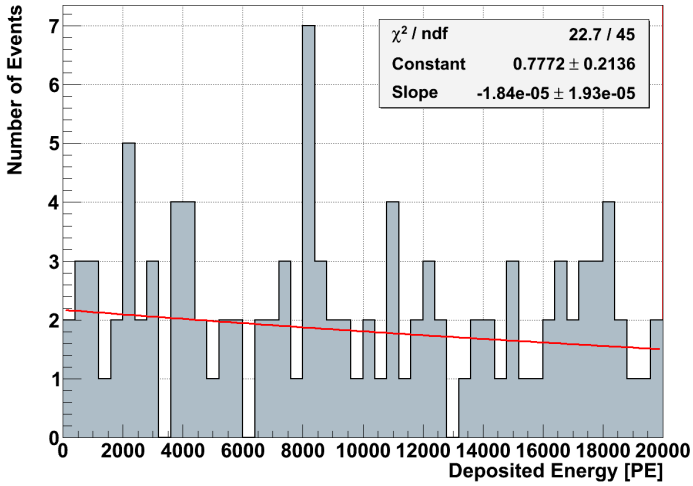

Figure 4.15: Simulated energy deposition of fast neutron recoils in target and gamma catcher with an Gd capture following in a time window of 200μs (RN-events) fitted with an exponential function.

In figure 4.16 one can see the prompt and late energy of correlated events satisfying the condition: $\mathrm{NPE_{prompt}} > 200$, $\mathrm{NPE_{late}} > 700$ and $\Delta T < 200\,\mu$s resulting in 371 correlated events after 30 days. Not all of these correlated events would be counted as neutrino events. 168 events fulfill the neutrino event condition $190 < \mathrm{NPE_{prompt}} < 1700$ ($1\,\mathrm{MeV} < \mathrm{E_{prompt}} < 9\,\mathrm{MeV}$) and $1200 < \mathrm{NPE_{late}} < 1900$ ($6\,\mathrm{MeV} < \mathrm{E_{late}} < 10\,\mathrm{MeV}$). **This would result in a neutrino-like event rate of 5.6±0.4(stat) events/day.** There is a clustering of events at (450 PE,1500 PE) and (1500 PE,1500 PE). These events are fake events due to the coincidence of two captured neutrons. ∼93% of all neutrino-like events in this simulation are fake events. As the observed fast neutron rate would be roughly 10% of the expected neutrino signal one has to introduce further cuts.

4.3.2 Cuts for the Fast Neutron Background

Inner Veto Cut

An obvious cut is to include the inner veto. Optimized to observe muons crossing the detector the inner veto is also able to detect in some cases fast neutrons even if they produce considerable less light compared to muons. If one introduces a further cut rejecting correlated events if together with the prompt event an inner veto energy deposition with more than 50 PE occurred, 85% of the RN-events vanish. The fake

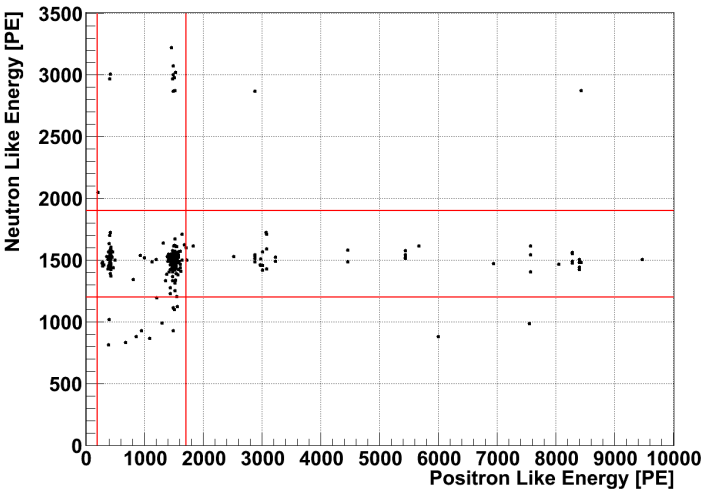

Figure 4.16: Correlated events due to fast neutrons after 30 days data taking. The red lines indicate the energy cuts for the prompt and late event.

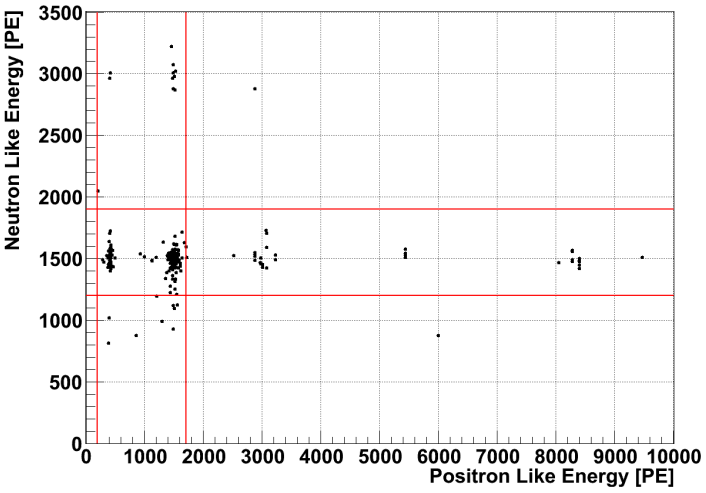

Figure 4.17: Correlated events due to fast neutrons after 30 days data taking with the inner veto cut explained in the text.

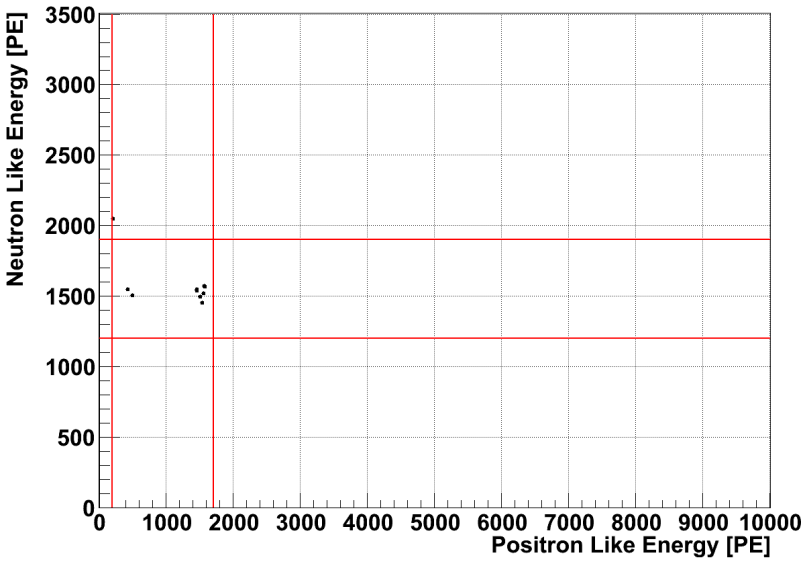

Figure 4.18: Correlated events due to fast neutrons after 30 days data taking with the recoil and the inner veto cut.

events get of course not influenced by that cut.
Depending on the rate of inner veto events with more than 50 PE that cut can have an influence on the neutrino events but as this rate can be directly measured at the experiment the influence should be under control and an inner veto hit during the prompt event will be a strong indication for a fast neutron event. 161 neutrino like events survived that cut (figure 4.17) and, therefore, **the remaining neutrino candidate rate is 5.4±0.4(stat) events/day.**

Proton Recoil Cut

To further reduce the fake events there is the possibility to search for the often huge energy deposition of the recoil protons before the correlated event. This possibility was first proposed and tested for Double Chooz in [139]. It is searched for an energy deposition >2500 PE (∼12 MeV) in the inner detector in a time window of 200 μs before the correlated event (no positron events are expected to produce such a large energy deposition). If there is such an energy deposition (together with the inner veto cut described before) the correlated event is rejected. RN-events are, therefore, not affected by that cut. Due to the used method also prompt events having more than 2500 PE were rejected but these events would in any case not counted as neutrino candidates. Only 9 neutrino like events survived that cut (figure 4.18) and only

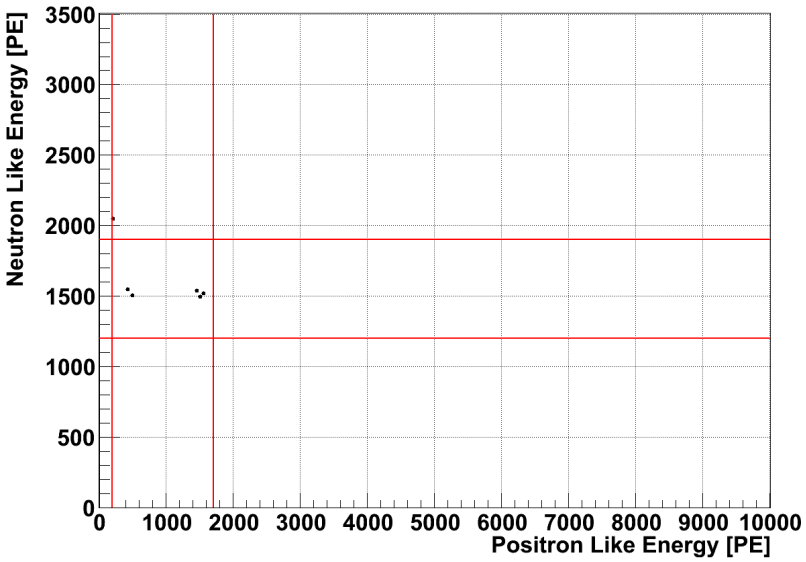

Figure 4.19: Correlated events due to fast neutrons after 30 days data taking with neutron multiplicity cut.

one of the remaining events was due to a RN-event, the rest were fake coincidences. **After applying both cuts the resulting neutrino like event rate would be $0.3 \pm 0.1\,(\text{stat})$ events/day.**
To estimate the probability p_{recoil} of that cut to reject a neutrino event one has to calculate the probability of an energy deposition with more than 2500 PE (without an inner veto hit triggering the muon dead time) in a time window of 200 μs. That is:

$$p_{\text{recoil}} = R_{>2500,\text{no IV}} \cdot \Delta T. \tag{4.5}$$

As shown in table 4.1 on page 59 the expected rate $R_{>2500,\text{no IV}}$ from simulation is $5.3(\pm 0.3) \cdot 10^{-4}$ Hz leading to a probability of rejecting a neutrino event of $2.7 \cdot 10^{-7}$ % and, therefore, negligible. In any case $R_{>2500,\text{no IV}}$ is a measurable value at the experiment and if it is as small as in the simulation this cut could be crucial for the fast neutron rejection.

Neutron Multiplicity Method

In the CHOOZ experiment the neutron multiplicity cut rejected correlated events if an energy deposition with more than 1.3 MeV occurred along with the neutrino like event, to reject fast neutron events [16; 120]. To test the efficiency of such a cut

Used Cut	Neutrino-like rate [events/day]	Fraction of n-n Coinc. [%]
No cut	5.6±0.4(stat)±5.6(syst)	93
+IV cut	5.4±0.4(stat)±5.4(syst)	99
+Recoil Cut	0.3±0.1(stat)±0.3(syst)	89
+n-multipl. cut	0.2±0.1(stat)±0.2(syst)	80

Table 4.3: Summary of the influence of various cuts on the fast neutron background rate. A systematic error of 100% was assumed.

for fast neutron events in Double Chooz a slightly modified cut was applied to the simulation (together with the inner veto and proton recoil cut). A correlated fast neutron event is rejected if in a time window of 200 μs before or after the correlated event a third event with more than 1200 PE (a neutron capture on Gd) occurred. Only 5 of 9 fast neutron events survived that cut **leading to a fast neutron rate of 0.2±0.1(stat) events/day.**
To estimate the influence of that cut on neutrino events one has to calculate the probability of an event for depositing >1200 PE in the inner detector 200 μs before or after the correlated event (as it was similarly done in [120]). That is

$$p_{\mathrm{nm}} \approx 2 \cdot R_{>1200\,\mathrm{PE,noIV}} \cdot \Delta T. \tag{4.6}$$

With table 4.1 one can calculate that this probability is with $2.4 \cdot 10^{-5}$% absolutely negligible.
In table 4.3 a summary of all cuts and the resulting fast neutron rate is given.

The very low neutrino rejection probabilities are caused by the extremely low single rates above 2500 PE (for the proton recoil cut) and above 1200 PE (for the multiplicity cut). As stated before in section 4.1.2 these rates are based on simulations and might be considerably larger in the experiment. However, the inner veto cut (for RN-events) and the proton recoil cut (for fake events) remain as powerful cuts for the fast neutron background, while the multiplicity cut should only be applied if the measured single rate above 1200 PE is not too large and the probability to reject a neutrino event is sufficiently small (<0.1%).

4.3.3 Comparing Simulation with Experiment

Aforementioned the simulation of the muon produced neutron flux has considerable uncertainties in the energy and multiplicity distribution. But both are crucial values for the correct estimation of the fast neutron background in a simulation. If e.g.

the neutron multiplicity is overestimated by the simulation one will observe less fake coincidences in the experiment. If the neutron energy distribution is different the total amount of neutrons entering the target volume will change considerably.
One, therefore, has to cross check the simulation with experimental data as good as possible. That is only feasible to some extent as neutrino like fast neutron events have very often a signature which can not distinguished from other background or neutrino events. However, it will be a helpful test to search for clear fast neutron candidates. These are not too large inner veto hits indicating fast neutrons entering the detector followed by energy depositions of several 100 PE in the inner detector as good hints for proton recoils. That PE distribution can then be compared with the simulated one in figure 4.14. Furthermore, one can search for subsequent neutron captures and determine if neutron multiplicity is similar to the simulated one. For such a study one needs a large statistic of several month. Thus, the knowledge of the fast neutron background will improve with time.

4.3.4 Pulseshape Analysis

Pulseshape analysis means analysis of the time distribution of the produced light of a particle in scintillator. From that one can get valuable information of the particle type or the volume of light production. Pulseshape analysis is widely used at scintillator experiments like GERDA [144] or Borexino [145].
First it will be demonstrated in which way the pulseshape contains information on the particle type. Then the Late Light method, a special kind of pulseshape analysis, will be explained before focusing on the application of distinguishing fast neutron from neutrino events with the help of Late Light analysis.

Pulseshape

The time distribution of light production (that is the pulseshape) caused by a particle interacting in the liquid scintillator depends on its energy deposition per unit path length (dE/dx) and thus on the particle mass and charge (figure 4.20). This allows the discrimination of different particles with pulseshape analysis. The pulseshape $f(t)$ of the photon emission process in liquid scintillator can be described by the sum of several exponentials:

$$f(t) = \sum_i \frac{N_i}{\tau_i} \exp\left(-t/\tau_i\right) \tag{4.7}$$

where τ_i is the decay time constant of the exponential function i and N_i its normalized weight. The exponential function with the shortest decay time constant ($i = 1$) is usually called the fast component, the other exponential functions are the so called slow components. If N_1 is smaller for one event that event is called slower than the other with a larger N_1. The parameters N_i and τ_i for electrons and alphas were

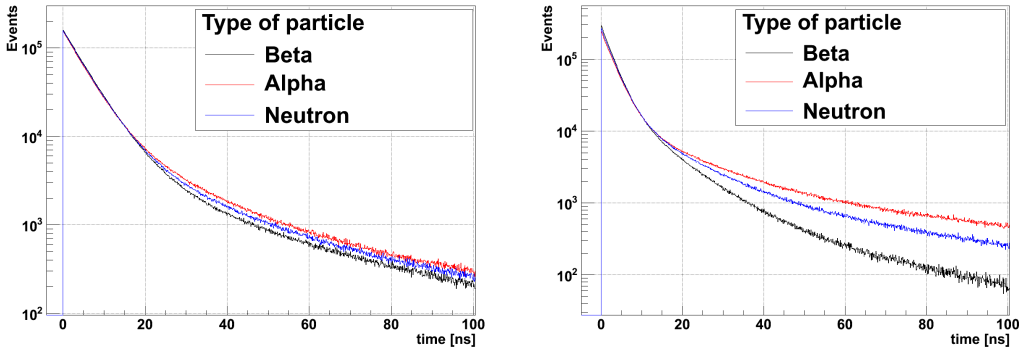

Figure 4.20: Simulated pulseshape of electrons, alphas and neutrons in the gamma catcher (left) and target (right) scintillator.

measured at the MPIK [146].
Furthermore, not only particles can be distinguished by their individual pulseshape but also the volume of light production. In general a particle producing light in the gamma catcher will be slower than the same particle having deposited its energy in the target volume, due to the Gd in the target region. More details can be found in [147; 148].
Neutrons generate scintillation light only indirectly by elastic scattering with free protons and inelastic scattering with carbon, where amongst others gammas, protons and α-particles are produced. The dominant light production comes from the elastic produced protons. The pulseshape of protons is due to the lower mass faster compared to alpha particles and slower than the beta pulseshape. While not measured yet for the Double Chooz scintillator the pulseshape of the protons (and, thus, the one for the fast neutrons) will be between the measured beta and alpha pulseshape. In figure 4.21 one can see the simulated pulse shape curve of neutrons and electrons in the target and gamma catcher volume.

Method of Late Light Analysis

One possibility to distinguish particles or the volume of the light production is the so called **Late Light analysis** which was first used and tested for Double Chooz in this thesis. To get the Late Light ratio of an event one first has to reconstruct the vertex of the event in order to correct for the time of flight for each PMT. That was done with the vertex reconstruction algorithm RecoBAMA. After that one can sum up the time of flight corrected FADC output of each of the 390 PMTs. The

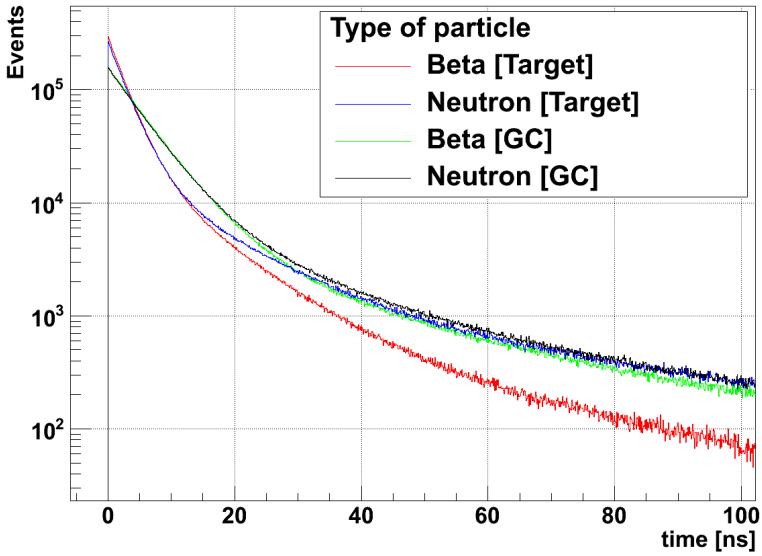

Figure 4.21: Simulated pulseshape of neutrons and electrons in the target and gamma catcher scintillator.

result is the reconstructed pulseshape of the event. Now one can calculate the ratio of light arriving a certain time (Late Light time) after the maximum and the total light. That is the Late Light ratio (LLR). In optimization studies it was found that the separation of events for different particles and volumes is best for a Late Light time of 10 ns [147]. Errors in vertex reconstruction and PMT characteristics (late pulses and transit time spread) can introduce a broadening of the pulseshape.

Results of Late Light Analysis for Fast Neutron Events

In figure 4.22 one can see the LLR of fast neutron recoils for neutron energies of 10, 20 and 30 MeV. Only neutrino like prompt energy depositions are included, that is a prompt energy between 1 and 9 MeV. As there is obviously no energy dependence in the LLR one can concentrate in the following on 10 MeV neutrons.
In figure 4.23 one can see the LLR of simulated neutrino events with the prompt energy deposition taken place in the target and fast neutron events with 10 MeV kinetic energy in the target and gamma catcher. The neutrinos and fast neutrons produced in the target tend to have a deviation from Gaussian distribution at higher LLRs. That is because parts of the produced gammas travel in the gamma catcher and, therefore, produce light with the gamma catcher pulseshape. The same is true for the fast neutrons in the gamma catcher. Part of the produced gammas or the

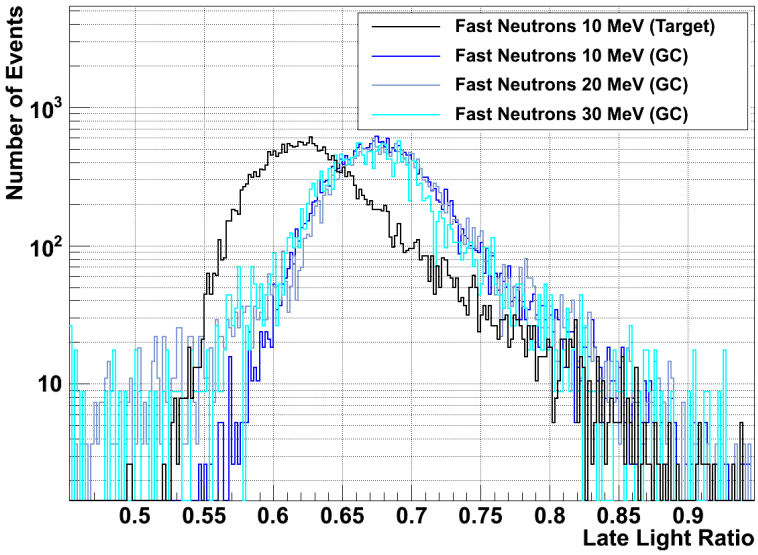

Figure 4.22: LLR of simulated fast neutrons with a neutrino like energy deposition in the prompt event as explained in the text.

neutron itself reach the target and create a smaller LLR. This and the fact that there is no clear separation of the three distributions will it make difficult to identify an event as a fast neutron with the Late Light method.
However, even if pulseshape analysis is not very helpful in identifying particles like accidentals, cosmogenics or fast neutrons it is helpful for another kind of background, the so called Spill In current as it will be demonstrated in the following section 4.4.

4.3.5 Summary

To summarize the fast neutron background:

- In simulation the fast neutron rate depends strongly on applied cuts. The proton-recoil cut together with the inner veto-cut presented in this thesis are feasible tools to reject that background. In simulation both cuts combined reduced the fast neutron rate from 5.6±0.4 to 0.3±0.1 events/day. Both cuts have the advantage that the influence on the neutrino events can be well estimated.

- The simulation of muon induced neutron production has large uncertainties. Therefore, possibilities were presented to crosscheck the simulation with the experimental result.

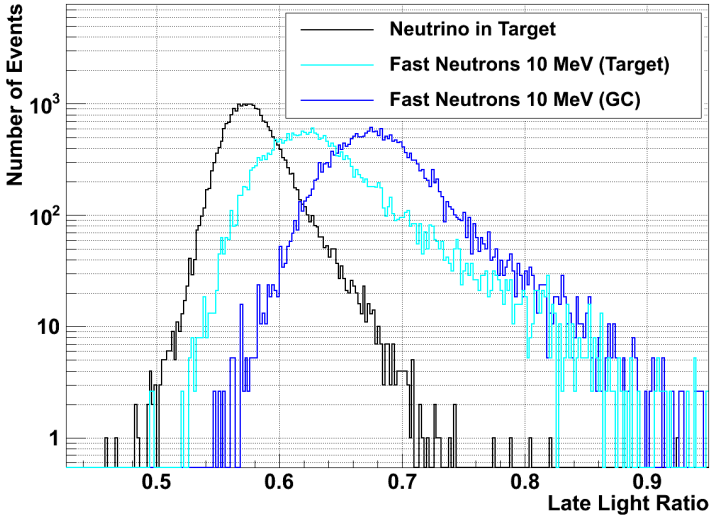

Figure 4.23: Simulated reconstructed LLR of neutrino events in the target and fast neutron events in target and gamma catcher with 10 MeV kinetic energy.

- Pulseshape analysis turned out to be not appropriate to reject fast neutron events as the separation power of fast neutron and neutrino events is to weak.

4.4 Spill In and Spill Out

It was demonstrated in section 3.1 that after IBD the neutron travels several cm before being captured and, therefore, there is the possibility for a neutron produced in the gamma catcher or the target acryl to reach the target and being captured on Gd. Both the prompt and the late event may now fulfill the energy cuts and, thus, an actual non-target event is counted for a target event. Such an event is called Spill In. On the other hand neutrons produced by IBD in the target can leave the target volume and enter the gamma catcher. Such a Spill Out event will never be observed as the late event energy cut is adjusted for Gd capture events. Figure 4.24 illustrates this behavior.
In the CHOOZ experiment the Spill In effect accounted for 4% and the Spill Out for 2% of the events. The quoted error was 40% (from Monte Carlo simulation) inducing an additional 1% uncertainty of the total number of neutrino events [79].
In case of comparing the neutrino flux of two identical detectors the Spill In and Spill Out effect vanishes, which is not the case for other kinds of background. But as the

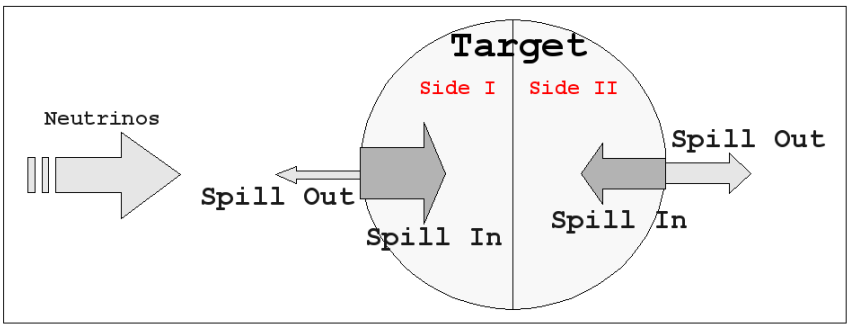

Figure 4.24: Sketch of Spill In and Spill Out and of their dependency from the neutrino directionality discussed in section 4.4.4. Top view of the target volume.

far detector operates at least 1.5 years without the near detector the Spill In and Spill Out effect is critical for the sensitivity of the experiment.
In section 4.4.1 it will be shown which Spill In and Spill Out ratio is predicted by simulation and in section 4.4.2 the possibility is considered to tune the simulation with calibration results. In section 4.4.3 it will be demonstrated that the different time distribution of Spill In events compared to regular target events gives the possibility to estimate the Spill In rate. In section 4.4.4 it is shown that the Spill In current produces an inhomogeneity in the neutrino event vertices. In the following sections 4.4.5 and 4.4.6 it is pointed out that pulseshape analysis can be used to measure the Spill In rate and finally in section 4.4.7 it is demonstrated how Spill In events will deform the observed PE spectrum of neutrino events

4.4.1 Spill In and Spill Out Rate from Simulation

Total Spill In and Spill Out Rate

To analyze the general behavior of Spill In and Spill Out events $5 \cdot 10^5$ IBD events isotropically distributed in target and gamma catcher were analyzed using NuGen2 and the DOGS package based on GEANT4 for simulation of the particle transport in scintillator.
In table 4.4 the amount of Spill In and Spill Out events is listed. From that one can calculate that **8.48±0.08(stat)% of all neutron capture events in the target are due to Spill In while 2.57±0.04(stat)% of the neutrons produced in target leave that volume due to Spill Out. Both effects lead to 6.46±0.09(stat)% more Gd-capture events than expected (Spill In current).**
Spill In and Spill Out does not cancel each other. The fact that there is a Spill In excess can be explained by the larger gamma catcher volume. Furthermore, it is shown

	Total IBD in T and GC	IBD in T	Spill In	Spill Out
Number of Events	500.000	143.326	12.942	3.683

Table 4.4: Total number of Spill In and Spill Out events without any time or energy cut. The statistic corresponds to roughly 6 years data taking in the Double Chooz far detector.

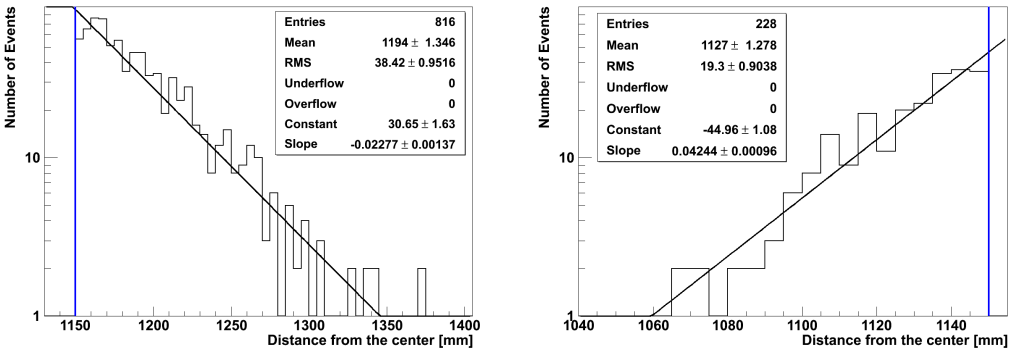

Figure 4.25: Distance of the IBD vertex to the central z-axis for Spill In (left) and Spill Out events (right) from simulation. Both distributions are fitted with an exponential function. The blue vertical lines indicate the position of the target acryl.

in figure 4.25 that the skin depth parameter[7] of Spill Out events is only 23.6 mm due to the higher neutron capture cross section in the Gd-doped target scintillator while it is 43.9 mm for Spill In events.
As stated before, there are also Spill In neutrons from IBD in the target-acryl reaching the target volume. From simulation 12.07±0.32(stat)% of all Spill In events are neutrons produced in the acryl.

Spill In and Spill Out Rate for different Time Cuts

Figure 4.26 on the left side shows the time distribution of target events and of Spill In events from the gamma catcher volume and the target acryl (all these events were captured on Gd). While the exponential time constant of target events is 26.3 μs, acryl neutrons need already 34.9 μs and neutrons from the gamma catcher even 125.8 μs for being captured on Gd in the target. The reason is that neutrons from the acryl

[7] The slope of the exponential in figure 4.25.

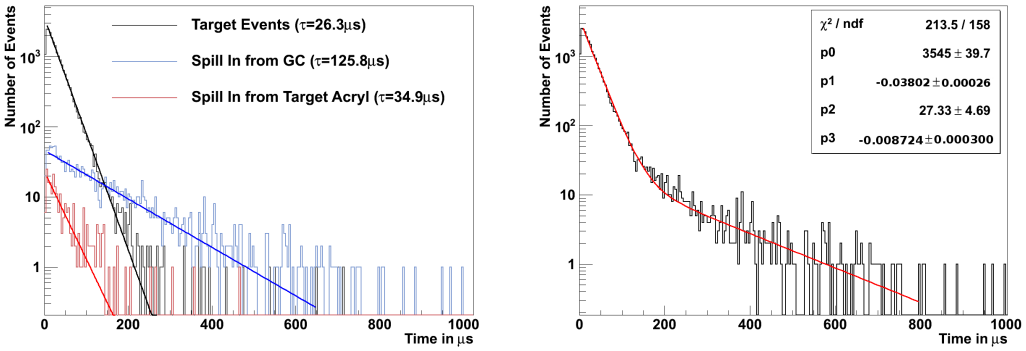

Figure 4.26: **Left:** Target events (IBD in Target) and Spill In events (IBD in gamma catcher and acryl) with a subsequent Gd capture.
Right: ΔT of all events with a Gd capture in the late event fitted with the sum of two exponentials. This distribution will be an observable in the experiment.

and even more from the gamma catcher have a systematically larger travel distance and, therefore, need more time to be captured in the target. **The deformation of the time distribution will be an observable in the experiment** (figure 4.26 on the right side). In the section 4.4.3 that will be used to estimate the Spill In ratio independent from simulation.
As a consequence of the different neutron capture times Spill In events are in a different way influenced by the time cut than the regular IBD in the target. This is illustrated in figure 4.27. Setting the time cut to $\Delta T = 100\,\mu$s results in a loss of 2.2% of all regular events while already 41.8% of the Spill In events vanish. If the timecut is $\Delta T = 200\,\mu$s nearly no regular events are lost ($<$0.3%) while still 17.5% of all Spill In events are rejected. Because the influence of the time cut evolves equal for Spill Out and regular events the total Spill In current decreases with a declining timecut. In Double Chooz the used ΔT is not yet defined but will be between $100\mu s$ and $200\mu s$. For $200\mu s$ the Spill In current reduces to 4.67±0.08(stat)% and for $100\mu s$ to 2.96±0.08(stat)%, which is an argument to use a smaller time constant. However, this value is not yet the final Spill In current ratio as no cut on the prompt event energy was applied so far. In section 4.4.7 that will be done and the final Spill In current calculated.

Monte Carlo Performance Evaluation

The question how precise is the Monte Carlo simulation is not easy to answer as there is so far no possibility to compare their result with real data. The GEANT4

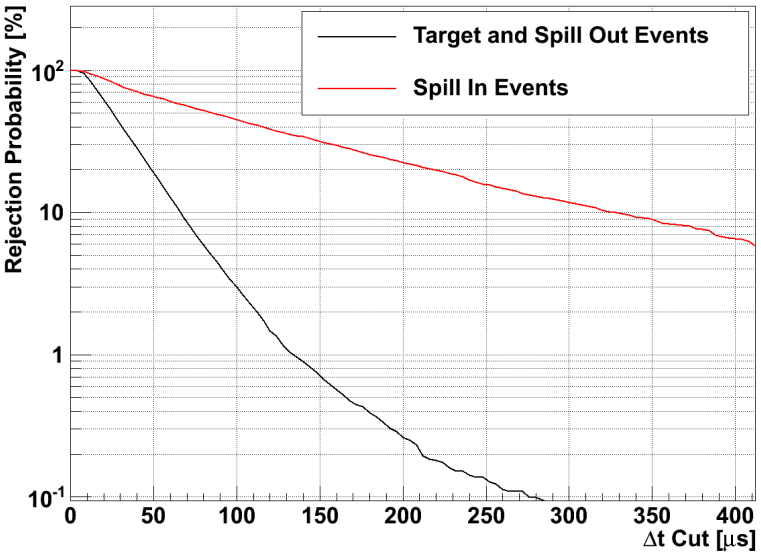

Figure 4.27: Rejection probability at different time cuts of target, Spill In and Spill Out events.

simulation package was originally developed to describe the passage of high energetic particles through matter, but it also offers additional packages allowing in general the usage in the thermal regime. Nevertheless, the correct treatment of neutron thermalizing and diffusion is crucial for the Spill In and Spill Out effect. In this energy regime the GEANT4 transport code has a lack of treatment of the atomic bonds. More precisely in GEANT4 the hydrogen atoms (which are the most important collision partners of thermalizing and diffusing neutrons) are considered as a free gas. However, in condensed matter atoms are linked by chemical bonds with energies in the eV regime. That is why, when a neutron has reached these low energies the chemical binding energy can not be neglected anymore during the collision with an atom of the scintillator medium [149].
To check the influence of that effect on the Spill In and Spill Out there were two studies performed, one with DCGLG4sim and one with TRIPOLI4 [150] which includes CH_2 bonds and additionally the presence of C_6H_6 benzene rings [149]. Both studies simulated neutrons with a fixed energy of 20 keV, not neutrons with the energy distribution resulting from IBD. In simulations, numerous observables, linked to neutron physics could be studied under different treatments of the chemical bond. The result using GEANT4 was a Spill In current of 5.35% and, therefore, quite similar to the one from default Double Chooz simulation, having in mind that the energy distribution in

the study of section 4.4.1 is not sharp but has the realistic energy distribution given from the IBD. The TRIPOLI4 simulation using a free gas model (like GEANT4) resulted in a Spill In current of 6.04%. That relative difference of 13% in both codes using in principle the same model gives an important hint on the systematic error of the simulation.
However, the Spill In current reduces to 4.20% when taking the chemical bonds into account and thus is relative reduced by 29% due to the more realistic model. The reason for that reduction of the Spill In current is an increase of the mean kinetic energy of the diffusing neutrons due to the molecular bonds and because of the $1/v$ cross-section of the neutron capture processes also an increase of the mean free path. Now a non intuitive effect happens: Even if the travel distance of the neutrons is increased, the direct distance between the production of the neutron and its capture decreases. The consequence is a smaller skin-depth and, therefore, a reduced Spill In current.
As a consequence of that study one should have in mind that the GEANT4 result of this work may overestimates the true unknown value. Nevertheless, one should be careful just to correct the result with the relative change of 29% from the TRIPOLI4 code using the improved chemical bond model instead of the free atom model as there were also quite large difference in the default TRIPOLI4 and GEANT4 result. One should rather take that result to have an valuable impression of the systematic error of the Spill In current estimation from simulation. **The systematic uncertainty should be well estimated with a 30% relative error.** As told before Chooz claimed a 40% systematic error on the Spill In uncertainty, the smaller value of Double Chooz accommodates the improved and better understood uncertainties in the simulation. In chapter 5 the influence of this systematic error on the sensitivity of the Double Chooz experiment will be demonstrated.

4.4.2 Tuning the Monte Carlo with Calibration

Double Chooz will use various calibration sources at different points of the detector. Already at very early stages of the data taking the guide tube will give the possibility to position different calibration sources in the gamma catcher close to the target acryl. This will also be used to check how many neutrons from a neutron source (e.g. AmBe) close to the target acryl reach the target volume. But that number will not provide directly the Spill In probability, as the energy of these neutrons is in the MeV range and, thus, much more neutrons will enter the detector than with keV energy. But one can crosscheck a simulation also using MeV neutrons and obtain a first impression how accurate the Spill In effect is described by the simulation.
Nevertheless, the limiting factor of using the calibration is the high energy of the neutrons. It is a test of the MeV neutron simulation (where GEANT4 is known to work well) but unfortunately not a test of the critical and less understood keV→eV

region. Therefore, even if the calibration and simulation will show a good agreement this will not influence considerably the systematical uncertainty in the Spill In ratio and other possibilities to obtain the Spill In ratio are important.

4.4.3 Spill In Rate Reconstruction from the Time Distribution

As already explained regular target events show a different ΔT distribution than Spill In events and that will be an observable in the experiment (right side of figure 4.26). So naturally one can ask the question if one can get the Spill In rate by analyzing the ΔT distribution. As it is distinguishable from figure 4.26 on the left side this will be only possible for Spill In events from the gamma catcher with a much larger time constant than regular target events. Even with large statistic it will not be possible to resolve Spill In events from the acryl as their time constant is too close to the time constant of regular events (34.9μs compared to 26.3μs). Nevertheless, it would be very helpful to obtain the number of Spill In events from the gamma catcher volume as they are the majority of Spill In events and one can add the acryl events whose fraction is quite well known from simulation.
To test that possibility a Monte Carlo simulation was written during this thesis where in a first step a ΔT distribution is filled by target and Spill In events from the gamma catcher using the two different time constants. In a second step this distribution is fitted by a sum of two exponentials where only the time constant of the target events is fixed (that value will be well known by calibration). From that fit the Spill In ratio is calculated. These steps are repeated 1000 times for different number of events to estimate the systematic and statistical error of the method. The true Spill In ratio was assumed to be 5%.
As one can see in figure 4.28 the result is very promising although up to roughly two years the result of the fit is biased to smaller Spill In ratios. The reason is that the fit tends to overestimate the ratio of the dominant target events. After 1/4 year data taking the result will be biased by 1.5% and has a relative statistical error of 25%. This is already better than the uncertainty of the simulation. **With one year data taking one get a slightly biased Spill In ratio of 4.7% (the true value was 5% in simulation), a relative statistical error of 12% and, therefore, an error smaller than from simulation.** The situation gets much better if one has 1 year data with the near detector resulting in over 100.000 events and one observes an unbiased Spill In ratio result with a relative error of only 4%.
So, that method is very promising although a complication might be the presence of background. Nevertheless, the rate should be quite low and not influence that method strongly. **This method is in any case independent from simulation and calibration and could, thus, be applied already after 1/4 year data taking.**

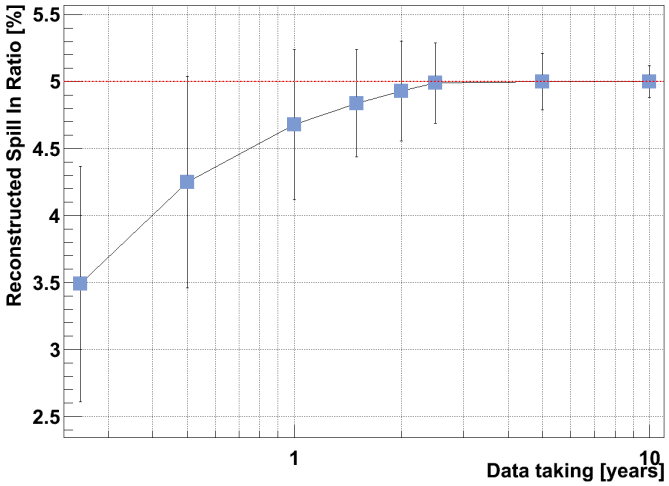

Figure 4.28: Reconstructed Spill In ratio for different event numbers. The red line indicates the true Spill In ratio of 5%. The given errors are statistical.

4.4.4 Spatial Anisotropy due to Spill In and Spill Out

The Spill In current produces a spatial anisotropy of the observed neutrino events in the target. There will be systematically more observed neutrino events in the side of the detector facing the reactor (Side I) than in the other side (Side II) as illustrated in figure 4.24. That is because after IBD neutrons have the information of neutrino direction and are strictly emitted in forward hemisphere with respect to neutrino incoming direction. This effect was already explained in chapter 3 and used there to detect the neutrino direction.
In the $5{\cdot}10^5$ simulated neutrino events there was a clear anisotropy observable. In Side I 7404 Spill In events occurred while only 1418 Spill Out events were observed resulting in a Spill In current of 5986 (8.35%). In Side II one observes 5538 Spill In events but 2265 Spill Out Events and so only a Spill In current of 3318 (4.63%). However, due to a realistic timecut of $200\mu s$ and a 1 MeV cut on the prompt event this effect will reduce to 5.77% more events in Side I and 2.82% in Side II.
If one wants to observe this effect in experiment the statistical fluctuation in both sides must be smaller than 1%. The 1σ fluctuation of one side is just given by $\sqrt{n/4}$ and, therefore, ~ 5.000 events or 1/4 year data taking should be sufficient to observe this effect at the 3σ level.

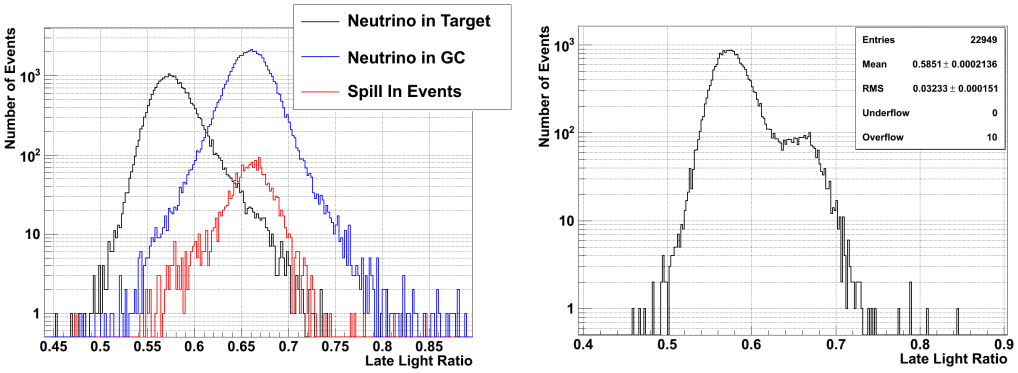

Figure 4.29: **Left:** LLR of simulated IBD events in the target (black), gamma catcher events (blue) and Spill In events (red).
Right: LLR of all prompt events with a subsequent following Gd capture. This simulated distribution is an observable at experiment.

4.4.5 Pulseshape Analysis for Spill In Events

In section 4.3.4 the method of pulseshape analysis was introduced to identify fast neutron events. Now that method will be applied to separate Spill In events from regular neutrino events in the target. Because of the Gd in the target the pulseshape of beta events in the gamma catcher is slower as one can see in figure 4.21. In figure 4.29 the LLR of regular events, gamma catcher events and Spill In events is shown. All three types of events have not a simple Gaussian structure. That is because parts or all of the photons e.g. produced in the target might deposit their energy in the gamma catcher volume. The same is possible for gamma catcher photons producing light in the target volume and so adopting the LLR fingerprint of that volume. **As a result it is not possible to apply a cut to separate Spill In events from regular neutrino events based on the LLR (table 4.5)**. But anyway one can use the pulseshape analysis for two other applications: **First**, to get a very clean Spill In sample which can be used for other studies. **Second**, two assume that the simulation describes the shape of the LLR correct and so to be able to fit the whole LLR-spectrum to extract the Spill In ratio.

1) Generation of a pure Sample Using figure 4.29 on the left side one can calculate the probability to accept a real neutrino event in the target and a Spill In event for different LLR. In figure 4.30 on the left side and table 4.5 the result is shown. As one can see the efficiency to separate Spill In events is very small. If less than 0.5% of all neutrino events should be lost only 23.1±1.1(stat)% of the Spill In

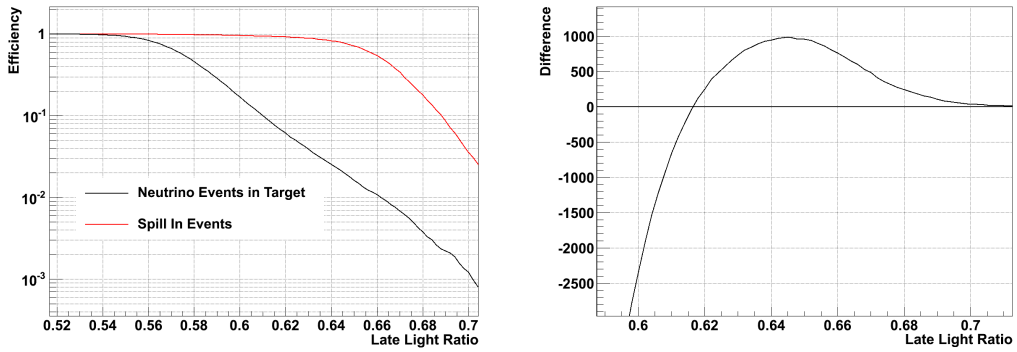

Figure 4.30: **Left:** Efficiency to accept a neutrino event in the target and a Spill In event for different LLR.
Right: Difference of Spill In events to neutrino events in target for different LLR for the used data sample.

LL Cut	**Efficiency [%] for**	
	ν	Spill In
0.6	17.02±0.26	96.13±2.30
0.65	1.62±0.08	71.72±1.95
0.66	1.08±0.07	54.40±1.63
0.67	0.69±0.05	34.59±1.35
0.68	0.38±0.04	17.85±0.97
0.69	0.22±0.03	8.63±0.67
0.7	0.12±0.02	3.60±0.43

Table 4.5: Acceptance probability for target and Spill In events for different LLR.

events are rejected. One can ask another question. Applying which LLR cut the data sample contains the most Spill In events compared to target events. More precisely, at which LLR is the largest difference of Spill In and target events. The result is shown in figure 4.30 on the right side. Using a LLR cut of 0.645 one has 478 neutrino events but 1459 Spill In events resulting in a good pureness of 75±2(stat)% Spill In events combined with a large statistic. This filtered datasample can then be used to probe other Spill In characteristics like energy spectrum, ΔT distribution and vertex anisotropy.

2) Calculation of the Spill In Ratio On the other side one can try to fit the Late Light spectrum of prompt events followed by a Gd-capture (figure 4.29 on the right side). All these events are possible neutrino candidates and, thus, this spectrum will be an observable in the experiment. Clearly the double peak structure of the target and Spill In events is visible. To analyze the Spill In fraction the important part of the target event spectrum is the right side which is not well described by a Gaussian (χ^2/dof=1.6, compared to a χ^2/dof of 0.7 for the left side) because of gammas depositing parts of their energy in the gamma catcher volume. This side is better described by an exponential (χ^2/dof=1.1). In figure 4.31 one can see the result of a fit of nearly 23.000 Gd capture events (roughly one year data) with a sum of an exponential (for the target events) and a Gaussian (for the Spill In events). The only parameter fixed was the mean of the Spill In Gaussian estimated by fitting all gamma catcher events, which will be a well known observable in the experiment due to the huge amount of gamma catcher events. The fit gives a good χ^2/dof of 1.0. In the fitted data set one gets a Spill In ratio of 8.0±0.3% (error from the fit) compared with the true value in the simulation of 7.8%. The lower value of the true Spill In current compared to the number presented in chapter 4.4.1 is due to the fact that for analysis a cut of 100 PE for the prompt event was used. That was done to have a realistic as possible LLR distribution.
This method provides an estimation of the Spill In ratio mostly independent from simulation. As stated before simulation was done with a statistic of 1 year data taking in Double Chooz but should in principal also yield good results in an earlier stage of the experiment.

4.4.6 Combined Pulseshape and Vertex Analysis

Using the vertex information of a prompt event with a subsequent Gd capture event has the advantage that one can apply a spatial cut on the event distance from the target acryl. The vertex reconstruction error around the acryl is 8.5 cm and for the following analysis only events are contained which are reconstructed in the whole gamma catcher or in the target not farther from the target acryl than the 8.5 cm reconstruction error. Thus, 84% of all target events are rejected while only 13% of

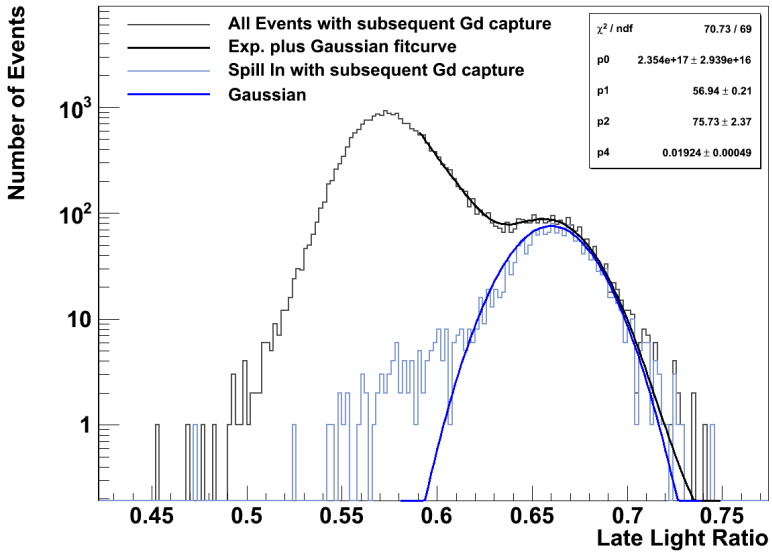

Figure 4.31: Fit of all Gd capture events with a sum of an exponential and a Gaussian function to estimate the Spill In fraction.

the Spill In events vanish due to that cut. So one obtains a much better Spill In to target event ratio.

1) Generation of a pure sample After having applied this spatial cut one can repeat the task to produce an as pure as possible Spill In sample by using the LLR. From figure 4.32 one finds that at a LLR cut of 0.635 is the maximum in the difference between Spill In and target events. In the used datasample one obtains 1467 Spill In events and only 244 target Events resulting in a pureness of 86±2(stat)% combined with a good statistic.

2) Calculation of the Spill In Ratio The idea is now to fit as before all Gd events observed in the fiducial volume with an exponential and a Gaussian curve to obtain detailed information about the Spill In LLR distribution. That was done in figure 4.33 on the left side. From the fit one gets a Spill In ratio in the fiducial volume of 28.2±1.1% , the true value is 29.9%. One can use now the sigma of the Gaussian curve to fit again the Late Light distribution of *all* observed Gd capture events. The result can be seen in figure 4.33 on the right side. From the fit one calculates now a Spill In ratio of 7.8±0.3% while the true value is indeed 7.8%.
Compared with the result in chapter 4.4.5 using no vertex information for the fit of

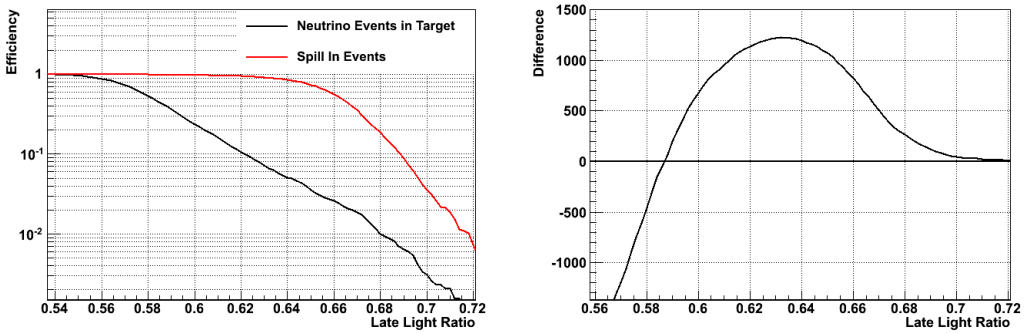

Figure 4.32: **Left:** Efficiency to accept a neutrino event in the target and a Spill In event for different LLR.
Right: Difference of Spill In events to neutrino events in target for different LLR.

the LLR of all Gd capture events one has here an even better result.
One can conclude that this method to achieve the sigma of the Gaussian Spill In distribution by the fit of the LLR of events only in the volume of the spatial cut and afterward using that sigma for the fit of all events with a subsequent Gd capture gives promising results. The systematical error should not be larger than 20%. That is because only few estimates based on simulations are necessary. If e.g. the LLR distribution of the Spill In events is not well described by a Gaussian that will introduce a systematical error. However, the fit parameters can all be extracted from the observed Late Light distribution.

An other Pulseshape Method: PSDD

The PSDD (**P**ulse **S**hape **D**iscrimination by **D**ario) is another sophisticated pulse-shape method to decide in which volume an event took place [151]. It compares the measured pulseshape spectrum of an event with an average target and an average gamma catcher event and decides then applying a Kolmogorov-Smirnov test in which volume the event took place. This method has the disadvantage to be more dependent on well calibrated data as it directly influences the volume decision. The LLR method does not need any calibrated data.
In the moment of writing this thesis the PSDD-method is not finished. It will be in any case advantageous to use two quite independent pulseshape instruments to check the correlation of both methods.

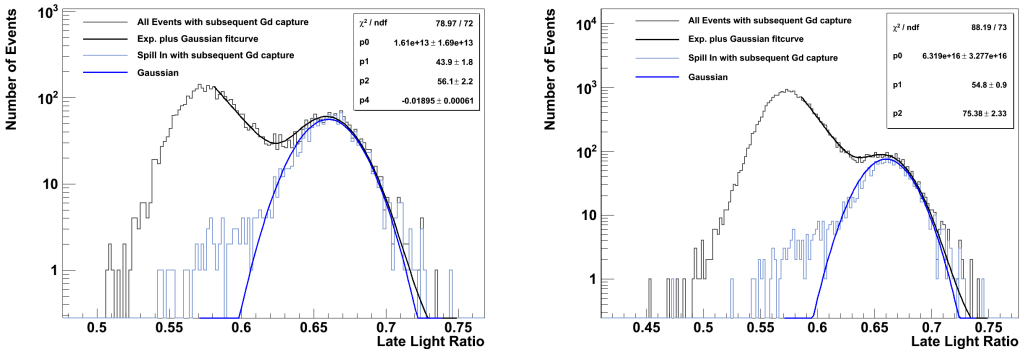

Figure 4.33: Fit of the LLR of IBD prompt events followed by a Gd capture with (left) and without (right) the spatial cut. The fit on the right side uses information (the σ) of the fit on the left side as explained in the text.

4.4.7 Deformation of the Positron Spectrum due to Spill In and Spill Out

As Spill In and Spill Out occur for IBDs close to the target acryl, it is to expect that their prompt event spectrum looks different to the mean spectrum of all events in the target. Therefore, it is not possible just to subtract the Spill In current from the whole positron spectrum by means of a simple normalization factor. That deformation is because of three reasons:

1. The gammas of Spill In and Spill Out events have a higher probability to enter the buffer volume and, thus, to produce no light resulting in a decrease of the observed PE spectrum.

2. Spill In and Spill Out events are closer to the PMTs at their side and thus events where the gammas are not lost in the buffer produce even more light than the mean target events.

3. Events from an IBD in target acryl (12% of all Spill In events) are expected to produce 1 MeV visible light due to annihilation gammas of the positron while the kinetic energy deposited in the non-scintillating acryl is lost for light production.

So in total one expects a quite complicated spectrum which is shown in figure 4.34. To be as realistic as possible the histograms are filled with reconstructed photoelectrons (after applying RoSS and RecoPulse) as it will be observed at experiment. All expected effects 1)-3) can be identified in the figure, especially the 1 MeV ($\sim$ 140

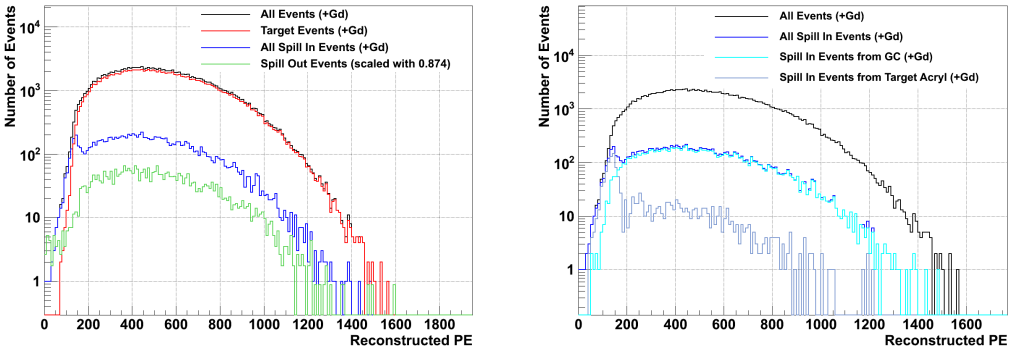

Figure 4.34: **Left:** Different types of events followed by a Gd capture. Spill Out events are scaled with the Gd capture probability.
Right: Distribution of Spill In events.

reconstructed PE) energy deposition of the acryl events. To see what is the total influence of the Spill In and Spill Out effect the ratio

$$\frac{\text{Gd capture events}}{\text{Gd capture events and IBD in target} + \text{Spill Out events} \cdot 0.874} \tag{4.8}$$

was calculated using the spectra of figure 4.34. **That is the percentage of more events per energy bin due to Spill In current.** Spill Out events are multiplied with the Gd capture probability. The result is given in figure 4.35. Clearly one can distinguish at 50-200 PE (0.4 MeV-1.5 MeV) the influence of the Spill In events from the acryl and at >1200 PE (>8.5 MeV) the effect resulting from the vicinity of the Spill In and Spill Out events to the PMTs. But also in between a non linear deformation of the spectrum occurs due to the loss of some gamma energy in the buffer volume. Moreover there is an influence of the time cut on the deformation. As already shown in figure 4.26 the Spill In events from the acryl are not as strong influenced by the time cut as the Spill In events from the gamma catcher. Therefore, the strong deformation below 250 PE stays quite constant after applying a timecut, which is also shown in figure 4.35.
So the influence of the Spill In and Spill Out is not only a larger event number but also a significant deformation of the visible energy spectrum depending on the applied cuts.
Obviously also an energy cut on the prompt event will have an influence on the Spill In current as especially the acryl events have quite low energy depositions. In figure 4.36 the resulting Spill In current depending on the used energy cut for the prompt event is shown. The MeV-scale on the x-axis is calculated from the reconstructed NPE and is thus realistic. One can see that there is at ∼1 MeV a clear decrease in

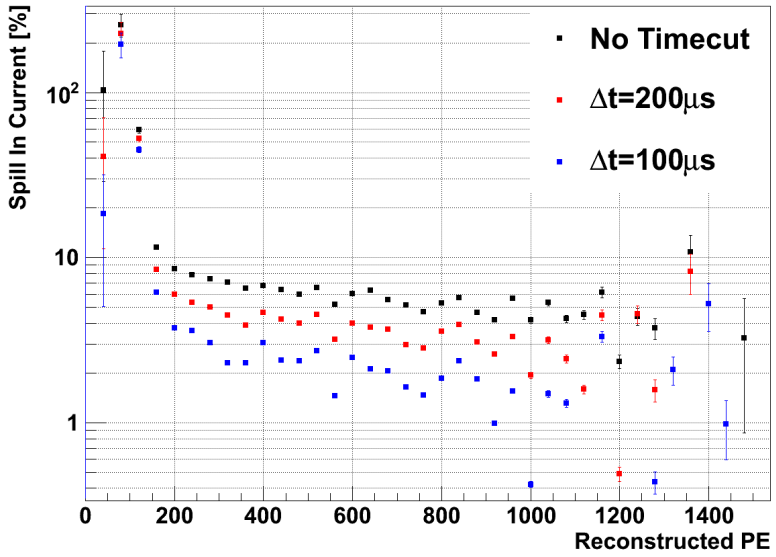

Figure 4.35: Energy dependent deformation of the pure (no Spill In and Spill Out) energy spectrum due to the Spill In current.

the Spill In current. That is due the Spill In events from the acryl having (as said before) only an energy deposition of the positron annihilation energy of 1 MeV while the kinetic energy of the positron is lost in the acryl.
From that figure one observes for an energy cut at 0.8 MeV and a timecut of 200(100) μs a Spill In current of 4.6(2.9)%. For a cut at 1 MeV these numbers reduce to 4.3(2.6)%. At 1.2 MeV one still has a Spill In current of 4.1(2.4)%. The statistical error from the simulation can be neglected compared with the systematical error of 30%.
That influence of the prompt energy cut is to have in mind when the used energy cuts are discussed in the collaboration.

4.4.8 Summary

To summarize the Spill In current background:

- Depending on the cut the Spill In current to signal ratio is between 2-5% and, therefore, similar to the sum of all other backgrounds. Assuming a 30% uncertainty of the simulation this results in an additional normalization uncertainty of 0.5-1.5% and is of nearly the same magnitude as the reactor flux uncertainty.

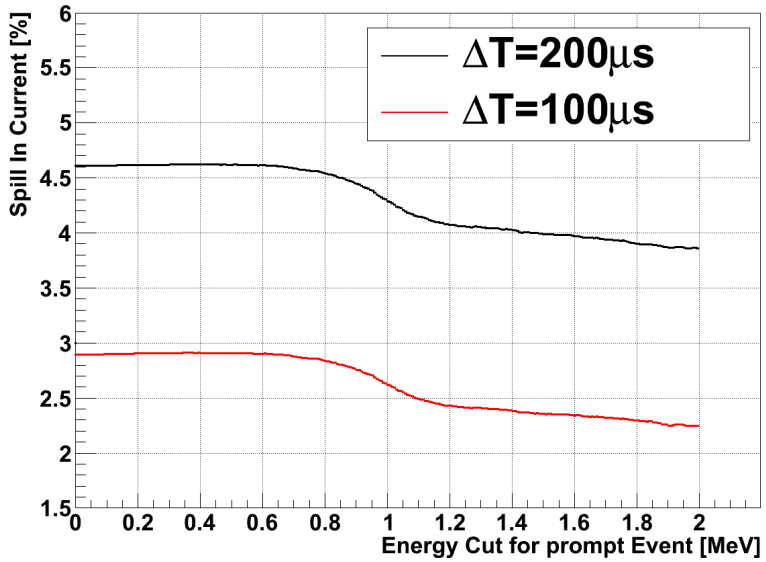

Figure 4.36: Total Spill In current in % depending on the used energy cut in MeV for two different time cuts.

- As the near detector will observe the same Spill In current effects that background will vanish in the Phase-II of the experiment.
- The Spill In current causes not only a systematical normalization error but also a deformation of the positron energy spectrum. This effect is important to have in mind if that background is subtracted from the positron spectrum.
- The Spill In current has large uncertainties in the simulation. Thus, in this thesis various possibilities were presented to obtain the Spill In current ratio. Using the combined pulseshape and vertex information and analyzing the time distribution give the possibility to crosscheck the simulation and reach a combined sensitivity of 10% after one year taking data.

4.5 Background Summary

To close the chapter the most important results are summarized. If the simulation result, especially of the single rate, is close to the numbers of the experiment, Double Chooz will have a very good background to signal ratio. Assuming an accidental rate of 0.8 ± 0.4 events/day, a fast neutron rate of 0.3 ± 0.1 events/day and a ^{9}Li rate of 1.5 ± 0.4 events/day it results in roughly 2.6 ± 0.6 background events/day. Assuming

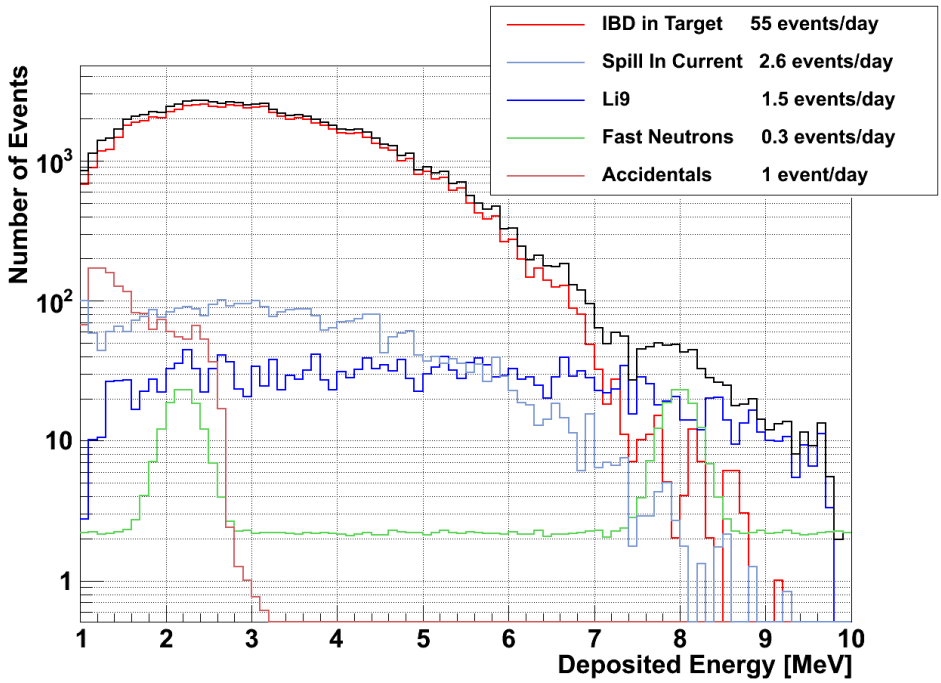

Figure 4.37: Energy deposition of IBDs in the target and of all background events assuming realistic rates. For the fast neutrons a flat RN-event spectrum was assumed as motivated in section 4.3.1 but a 50% contribution of fake events was included.

a neutrino rate of 55 events/day this means a background to signal ratio of roughly 5%. Additionally the Spill In current will contribute with 1-3 events/day. In figure 4.37 the expected prompt energy deposition of these background events is given.

5 Data Analysis and Sensitivity

In this chapter it is demonstrated how a nonzero θ_{13} is extracted from the data or either way a new upper limit of that value is established. The influence of the various systematic errors on the sensitivity is given.[1]
Hence, first the data analysis of past reactor experiments is reviewed in section 5.1. In section 5.2 the used χ^2-pull analysis is explained and the optimal number of energy bins for the data analysis is discussed. In section 5.3 the influence of reactor, detector and analysis induced systematics on the sensitivity is given. In section 5.4 the influence of the various backgrounds, discussed in the previous chapter, on the sensitivity is analyzed.

5.1 Data Analysis at previous Reactor Experiments

As Double Chooz is not the first experiment using a reactor and a scintillation detector for the search of θ_{13} it is obvious to reconsider the analysis strategy of earlier experiments, especially CHOOZ and Palo Verde.

5.1.1 CHOOZ Experiment

The CHOOZ experiment [16] compared the measured positron spectrum X_i with the expected spectrum $\overline{X_i}$ (i is the energy bin) and found no evidence for a nonzero mixing angle with an 82% probability using a Kolmogorov-Smirnov test (figure 5.1 on the left side). Then to establish an upper limit of θ_{13} three kinds of analysis (Method A,B and C) were performed with different sensitivities and dependencies on statistical and systematical errors.
Method A uses all available information of the experiment comparing the measured positron spectra of each reactor with the predicted one merging the reactor information, the neutrino spectrum model and the detector response. Method A has, therefore, the largest dependence on the correct determination of the integrated neutrino flux, number of target protons, detection efficiencies and neutrino cross section.

[1] In general the sensitivity is defined as the average upper limit one would get from an ensemble of experiments with the expected systematics and no oscillations [152].

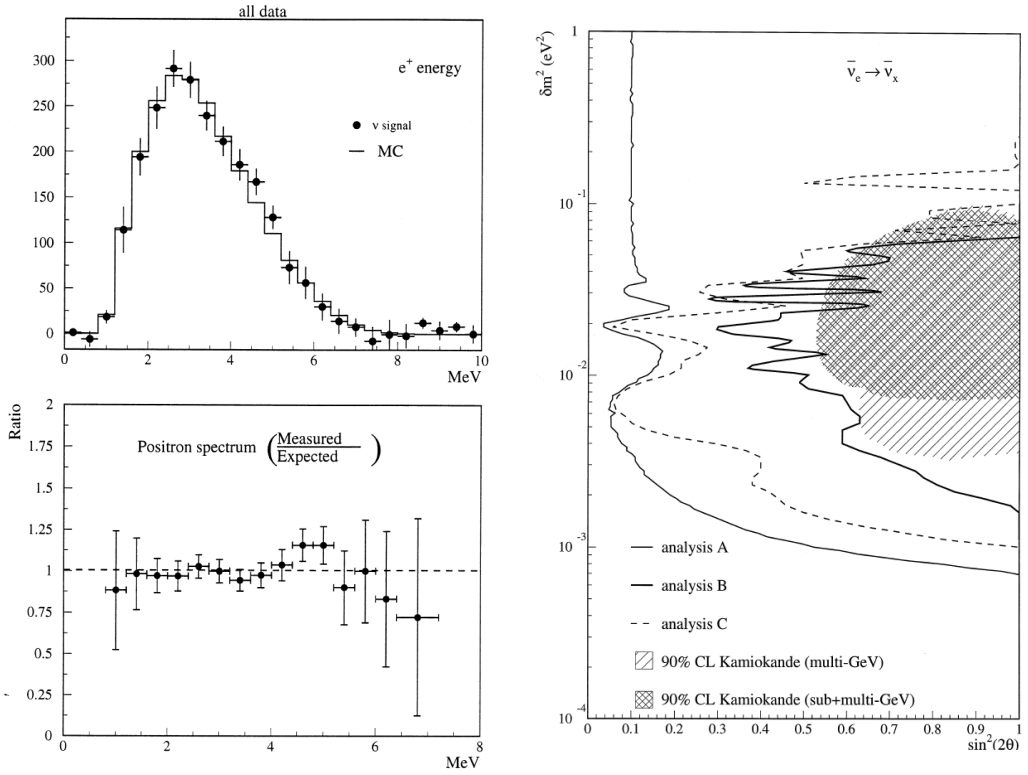

Figure 5.1: **Left:** (Above) Expected positron spectrum for the case $\theta_{13} = 0$, superimposed on the measured positron spectrum obtained from the subtraction of reactor-ON and reactor-OFF spectra.
(Below) Measured versus expected ratio. The errors shown are statistical.
Right: Exclusion plots at 90% C.L. obtained from the analysis methods A,B and C [16].

CHOOZ benefited from obtaining data from each reactor separately due to maintenance work. Therefore, CHOOZ measured the positron yield of both reactors using 7 energy bins resulting in a 14-element vector

$$X = \left(X_1\left(E_1\right), ..., X_1\left(E_7\right), X_2\left(E_1\right), ..., X_2\left(E_7\right)\right), \tag{5.1}$$

with $X_1\left(E_i\right)$ and $X_2\left(E_i\right)$ as the yield contribution in energy bin i of reactor 1 and reactor 2 respectively. As neutrino yields corresponding to the same energy bin are extracted for both reactors simultaneously these components are not independent leading to off-diagonal elements in the 14×14 covariance matrix

$$V_{ij} = \delta_{i,j}\left(\sigma_i^2 + \tilde{\sigma}_i^2\right) + \left(\delta_{i,j-7} + \delta_{i,j+7}\right)\sigma_{12}^{(i)} \quad \text{with } \left(i, j = 1, ..., 14\right), \tag{5.2}$$

where σ_i are the statistical errors associated with the yield array in equation 5.1, $\tilde{\sigma}_i$ are the corresponding systematical uncertainties, and $\sigma_{12}^{(i)}$ are the statistical covariances of the reactor 1 and 2 yield contributions to the i-th energy bin. For more details the reader is referred to [16].
This leads to finding the minimum of

$$\begin{aligned}\chi^2_{\mathrm{A}}(\theta, \Delta m^2, \alpha, g) = &\sum_{i=1}^{14}\sum_{j=1}^{14}\left(X_i - \alpha\overline{X}\left(gE_i, L_i, \theta, \Delta m^2\right)\right) V_{ij}^{-1}\left(X_j - \alpha\overline{X}\left(gE_j, L_j, \theta, \Delta m^2\right)\right) \\ &+ \left(\frac{\alpha - 1}{\sigma_\alpha}\right)^2 + \left(\frac{g-1}{\sigma_g}\right)^2\end{aligned} \tag{5.3}$$

with α being the absolute normalization constant, g the energy-scale calibration factor, $L_{i,j} = L_1$ for $i, j \leq 7$ and $L_{i,j} = L_2$ for $i, j > 7$ the distances of the two reactors to the detector.
Method B compares only the ratio $R(E_i) = X_1(E_i)/X_2(E_i)$ of the measured positron spectra of reactor 1 and 2 with the expected value $\overline{R}$. This method is almost completely independent of the correct determination of the integrated neutrino flux and is mostly affected by statistical errors due to the small oscillation effect considering the very small relative reactor distance. This leads to the χ^2 function

$$\chi^2_{\mathrm{B}} = \sum_{i=1}^{7}\left(\frac{R(E_i) - \overline{R}(E_i, \theta, \Delta m^2)}{\delta R(E_i)}\right)^2, \tag{5.4}$$

and $\delta R(E_i)$ is the statistical uncertainty on the measured ratio.
Method C is mathematically similar to analysis A but is a pure Shape analysis,

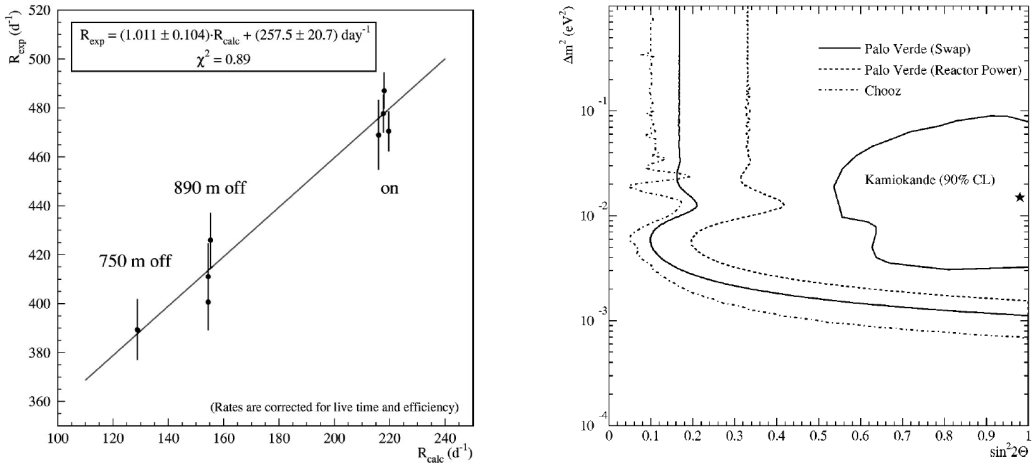

Figure 5.2: **Left:** R_{exp} for different data taking periods at Palo Verde plotted vs the expected neutrino interaction rate R_{calc} for the no oscillation case. The errors shown are statistical.
Right: Exclusion plots at 90% C.L. obtained with the Swap and the Reactor Power method at Palo Verde explained in the text [87].

therefore, α is as a free parameter ($\sigma_\alpha = \infty$) in 5.3 and

$$\chi^2_{\text{C}}(\theta, \Delta m^2, \alpha, g) = \sum_{i=1}^{14}\sum_{j=1}^{14}\left(X_i - \alpha\overline{X}\left(gE_i, L_i, \theta, \Delta m^2\right)\right) V_{ij}^{-1}\left(X_j - \alpha\overline{X}\left(gE_j, L_j, \theta, \Delta m^2\right)\right) + \left(\frac{g-1}{\sigma_g}\right)^2 . \tag{5.5}$$

To test a particular oscillation hypothesis $(\Delta m^2, \sin^2 2\theta_{13})$ against the parameters of the best fit, the **Unified Approach** [152] was used. The resulting exclusion plots for the three kinds of analysis are shown in figure 5.1 on the right side.
As Method A uses all available information it gives the best limit on θ_{13} and leads with $\Delta m^2_{31} = 2.5 \cdot 10^{-3}\,\text{eV}$ to the CHOOZ-limit of $\sin^2(2\theta_{13}) < 0.15$.

5.1.2 Palo Verde Experiment

The competitive Palo Verde Experiment [87] used two reactors with 890 m and 750 m distance as neutrino source and finished data taking in 2000. The segmented detector consisted of 66 acrylic cells filled with 11.34 tons of Gd-loaded liquid scintillator [86]. As in CHOOZ the neutrino flux was detected through the correlated positron and

neutron signal. In figure 5.2 on the left side the experimental rate R_{exp} (corrected for efficiency and deadtime but including the background) against the signal rate R_{calc} expected under the assumption of no oscillation is shown for different data-taking periods. If the data were consistent with no oscillations and the background rate were constant over time the points should lie on a straight line with unity slope. The y-intercept is equal to the rate of background events scaled by the ratio of the background to neutrino detection efficiency. In fact data were consistent with the no-oscillation hypothesis. A linear fit to these data gave a slope of 1.011 ± 0.104(stat.) and a y-intercept of 257.5 ± 20.7(stat.) 1/day with a χ^2 of 0.89.
To test data for the oscillation hypothesis throughout the $\Delta m^2_{31} - \sin^2(2\theta_{13})$ plane two different analysis methods were performed: The Reactor Power and the so called Swap Method.
Reactor Power Method: A χ^2-pull analysis using the reactor power changes (left side of figure 5.2) was carried out with

$$\chi^2_{\text{RP}} = \sum_{i=1}^{8} \frac{\left(R^i_{\text{exp}} - \text{BG} - \alpha R^i_{\text{calc}}\right)^2}{\sigma_i^2} + \frac{(\alpha - 1)^2}{\sigma^2_{\text{syst}}}, \tag{5.6}$$

where i runs over the 8 data taking periods, R^i_{exp} is the observed rate for period i, BG is the constant background rate, $R^i_{\text{calc}}\left(\Delta m^2_{31}, \theta_{13}\right)$ is the calculated rate for period i and the pull α accounts for possible global normalization effects due to systematic uncertainties. Finally, σ_i^2 denotes the statistical uncertainty of run period i, while $\sigma_{\text{syst}} = 0.061$ is the systematic uncertainty discussed in more detail in [87] .
Swap Method: The basic idea of the Swap Method [138] was to reduce the background rate by applying positron cuts to the delayed event and vice versa neutron cuts to the prompt event. The main background source at the Palo Verde experiment were accidentals and neutron-neutron correlated events due to muon spallation and fast neutrons. The rate-difference $N_1 - N_2$, with N_1 being the event rate with the normal cut and N_2 the rate after having applied the Swap cut, is mostly free of that backgrounds as they have identical prompt and late event-signatures. About 20% of the neutrino signals were canceled as determined from simulation (the systematic uncertainty of that number was not presented in the reference paper [87]). The dominating remaining background rate $(1-\epsilon_1)B_{\text{pn}}$ are the proton-neutron correlated events due to fast neutrons. Similar to the Reactor Power analysis a χ^2-pull analysis was carried out with

$$\chi^2_{\text{SM}} = \sum_{i=1}^{8} \frac{\left(N_{1,i} - N_{2,i} - (1-\epsilon_1)\, B_{\text{pn}} - \alpha\left(R^{1,i}_{\text{calc}} - R^{2,i}_{\text{calc}}\right)\right)^2}{\sigma_i^2} + \frac{(\alpha - 1)^2}{\sigma^2_{\text{syst}}}, \tag{5.7}$$

where σ_{syst} for the swap-method was estimated to 0.053.
The results of both types of analysis are shown in figure 5.2 on the right side together

with Method A of the CHOOZ experiment. Using the Swap Method and with $\Delta m^2_{31} = 2.5 \cdot 10^{-3}\,\text{eV}$ the Palo Verde limit is $\sin^2(2\theta_{13}) < 0.24$.

5.2 Data Analysis at Double Chooz

As details of the χ^2-analysis are beyond the scope of this thesis, only the basic principle of the Double Chooz analysis strategy is given. For more details the reader is referred to e.g. [153; 154].

5.2.1 χ^2-Pull Analysis

The analysis methods presented above were well motivated for the particular experiment: The Swap Method of Palo Verde rejected nearly all occurring background in the remaining data which was useful in that experiment with a background to signal ratio of more than 10% [86]. On the other side as explained before this analysis rejected roughly 20% of neutrino events. That number had to be well known from simulation and introduced an additional systematical error.
The usage of the separated reactor spectrum in CHOOZ had the advantage of additional information in the resulting data but requires a very exact knowledge of relative fissile isotope composition and relative reactor power.
In Double Chooz a good background to signal ratio is combined with a relatively large event rate. In such a case an analysis strategy introducing as less as possible new systematic errors seems to be the most appropriate strategy. As it was proposed in [79] a χ^2-pull analysis comparing the expected positron spectrum $T_i^d(\theta_{13})$ with the observed one O_i^d (where i denotes the compared energy bin and d the particular detector) will be used to extract the value of θ_{13} with the largest likelihood. All systematics will be handled as pulls in the χ^2 function which so gets the form:

$$\begin{aligned}\chi^2 =& \sum_{d=1}^{N_d}\sum_{i=1}^{N_b}\frac{\left[O_i^d - T_i^d - \wp_i^d\right]^2}{\left(\sigma^d_{\text{stat},i}\right)^2} + \frac{\alpha_{\text{n}}^2}{\sigma_{\text{n}}^2} + \frac{\alpha_{\text{cal}}^2}{\sigma_{\text{cal}}^2} + \sum_{R=1,2}\left(\frac{\alpha_{\text{react},R}}{\sigma_{\text{react}}}\right)^2 + \sum_{I=1}^{N_{\text{iso}}}\left(\frac{\alpha^I_{\text{iso}}}{\sigma_{\text{iso}}}\right)^2 \\ &+ \sum_{d=1}^{N_d}\left[\left(\frac{\alpha_{\text{n}}^d}{\sigma_{\text{n}}^d}\right)^2 + \sum_{b=1}^{2}\left(\frac{\eta_b^d}{\sigma^d_{\text{bg},b}}\right)^2 + \left(\frac{\eta^d_{\text{fn}}}{\sigma_{\text{fn}}}\right)^2 + \left(\frac{\eta^{\text{rel}}_{\text{fn}}}{\sigma^{\text{rel}}_{\text{fn}}}\right)^2\right]\end{aligned} \tag{5.8}$$

with

$$\begin{aligned}\wp_i^d =& T_i^d\left(\alpha_{\text{n}} + \alpha_{\text{n}}^d\right) - \sum_{I=1}^{N_{\text{iso}}} T^d_{i,I}\alpha^I_{\text{iso}} - \sum_{R=1,2} T^d_{i,R}\alpha^R_{\text{react}} + \alpha_{\text{cal}}M_i^d \\ &+ \sum_{b=1,2}\left(\eta_b^d B^d_{b,i}\right) + \eta^d_{\text{fn}}\left(P_i^d + F_i^d\right) + \eta^{\text{rel}}_{\text{fn}}\left(\lambda P_i^d - \mu F_i^d\right).\end{aligned}$$

Absolute Normalization	α_{n}	σ_{n}
Relative Normalization	α_{n}^{d}	σ_{n}^{d}
Reactor Power	α_{react}	σ_{react}
Energy Scale	α_{cal}	σ_{cal}
Isotope Fraction	α_{iso}	σ_{iso}

Table 5.1: Overview of pulls and systematic errors used in equation 5.8.

Some notations and remarks:

1. The pulls α and the corresponding systematical errors σ are listed in table 5.1.

2. N_b is the number of used energy bins and N_d the number of detectors. $\sigma_{\mathrm{stat},i}^{d}$ is the statistical error of bin i and detector d. The choice of the number of used bins N_b for analysis is non-trivial. This will be discussed in more detail in section 5.2.2.

3. As it was demonstrated in section 4.3 the fast neutron energy distribution is not purely flat but has two Gaussian peaks in the prompt energy spectrum. To include that uncertainty $\eta_{\mathrm{fn}}^{\mathrm{rel}}$ with error $\sigma_{\mathrm{fn}}^{\mathrm{rel}}$ as the pull on the uncertainty of the proton-neutron (pn) to neutron-neutron (nn) ratio of fast neutron events with amplitudes F_i (pn-component) and P_i (nn-component) were introduced here. η_{fn}^{d} is the pull on the total fast neutron rate at detector d with the uncertainty σ_{fn}. λ and μ are normalization constants including the relative distribution of the pn- and nn-component to the total fast neutron rate.
η_{b}^{d} are the pulls for the cosmogenic and accidental background rate at detector d.

4. There is the normalization $T_i^d = \sum_{R=1,2} T_{i,R}^d$ and $T_i^d = \sum_{I=1}^{N_{\mathrm{iso}}} T_{i,I}^d$ of the expected energy spectrum T_i^d.

5. α_{cal} is the variation of T_i^d if there is an incorrectness in the energy calibration with
$$T_i^d = \int_{E_i(1+\alpha_{\mathrm{cal}})}^{(E_i+\Delta E_i)(1+\alpha_{\mathrm{cal}})} f\left(E\right) dE. \tag{5.9}$$

It should be remarked that there is no fundamental difference in calculating the minimum of the χ^2-function with a covariance method similar to equation 5.3 and with the pull method in equation 5.8. Both methods would give the same minimum [155]. Nevertheless there are two convincing arguments to use the χ^2-pull method rather than the covariance method:
First, the minimization of equation 5.3 implies the inversion of a $N \times N$ matrix, with

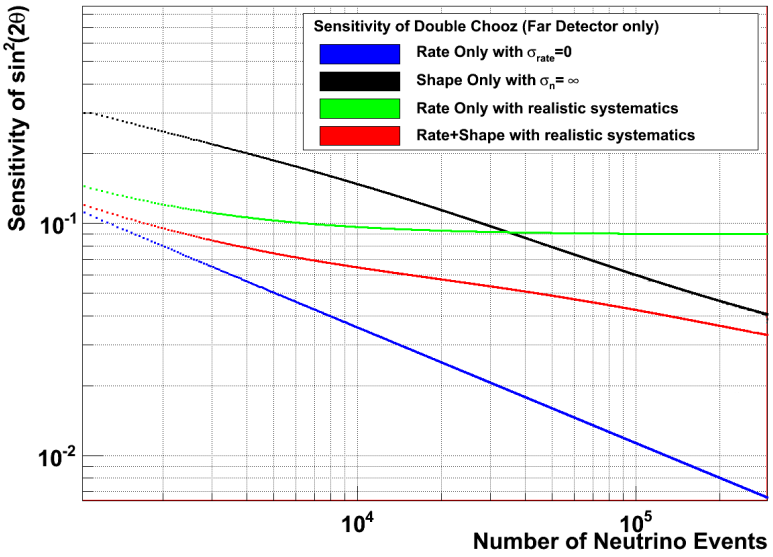

Figure 5.3: Sensitivity of Double Chooz for different kinds of analysis methods vs the observed number of events (far detector only). 10^4 events correspond to roughly 200 days of taking data.

N being the number of energy bins whereas the solution of the χ^2-pull minimization is analytically possible and requires only the inversion of a $K \times K$ matrix which is beneficial, as in most cases $K < N$.
The **second** advantage is that the final decomposition in terms of pulls of systematics allows to trace the individual contribution of each systematic to the χ^2 and, therefore, to reveal anomalously large residuals. That is important for the understanding of the result and advantageous compared to the covariance method where after minimization no information of the influence of different systematics is left.

5.2.2 Rate and Shape Analysis

Rate versus Shape Analysis

There exists two somehow extreme possibilities of comparing the observed with the calculated energy spectrum. The **Rate-Only analysis** uses only one energy bin for minimization in equation 5.8. No information about the shape of the energy spectrum is included. The other extreme is a **Shape-Only analysis**. In that case the error on absolute normalization has no influence on the minimization process ($\sigma_n = \infty$).
An illustrative overview of the performance of different analysis methods is shown in

figure 5.3. The sensitivity of Double Chooz using only the far detector is plotted for different event numbers. That analysis was done with a sensitivity-program using a χ^2-pull function similar to equation 5.8 [156].
In blue color a Rate-Only analysis assuming no error in the absolute number of neutrino events is plotted. All systematic errors in table 5.1 were set to 0 as they all introduce an error on the absolute rate ($\sigma_{\text{rate}} \equiv \sum \sigma_i = 0$). Therefore, the blue distribution is limited only by statistical fluctuations.
In black a Shape-Only analysis is drawn ($\sigma_{\text{n}} = \infty$, the other sensitivities have realistic uncertainties given later in table 5.2). In green again a Rate-Only and in red a Rate+Shape analysis both with now realistic rate uncertainties σ_{rate}. The Shape-Only and the Rate+Shape analysis were carried out using 20 energy bins. Some remarks to the result in figure 5.3:

1. Up to roughly $3.5 \cdot 10^4$ neutrino events (1.5-2 years) the **Rate-Only analysis** with realistic systematics gives a smaller sensitivity than the Shape-Only analysis. However, already at $\sim 10^4$ events (200 days) the Rate-Only analysis reaches its limit due to the systematic errors in the neutrino event rate.

2. The **Shape-Only analysis** is at the beginning mostly restricted by statistical fluctuations but approaches to the Rate+Shape analysis in the limit of large event numbers.

3. The **Rate+Shape analysis** will be the used one in Double Chooz. Obviously at the very first months of data taking ($2 - 3 \cdot 10^3$ events) the most information is contained in the pure rate of the neutrino events. The Rate+Shape curve is close to the two Rate-Only curves and considerably better than the Shape-Only curve. But with increasing event numbers ($> 10^4$ events) the Rate+Shape limit approaches to the Shape-Only analysis. The most information is now in the shape of the energy spectrum. The information of the total rate gets less important due to relatively large systematic uncertainties in the total rate.

Number of Energy Bins in the χ^2 Minimization

Another important detail is the question how many bins of the positron energy spectrum should be used in the Rate+Shape analysis. Figure 5.4 can give here an instructive answer. Shown is the sensitivity of Double Chooz after 3 month data taking using only the far detector and applying realistic sensitivities vs the number of used equally sized energy bins. Only the fast neutron rate is chosen slightly higher than expected from simulation (1 event per day instead of 0.3) for illustrative reasons. Clearly one can distinguish the large improvement to go from $1 \rightarrow 2$ bins. The reason is that in the two-bin case one uses information of a nonzero θ_{13} in the low energy bin while the high energy bin includes information of the total rate and is mostly unaffected by θ_{13} (see figure 1.2 on page 10). The next large improvement in the sensitivity is to go

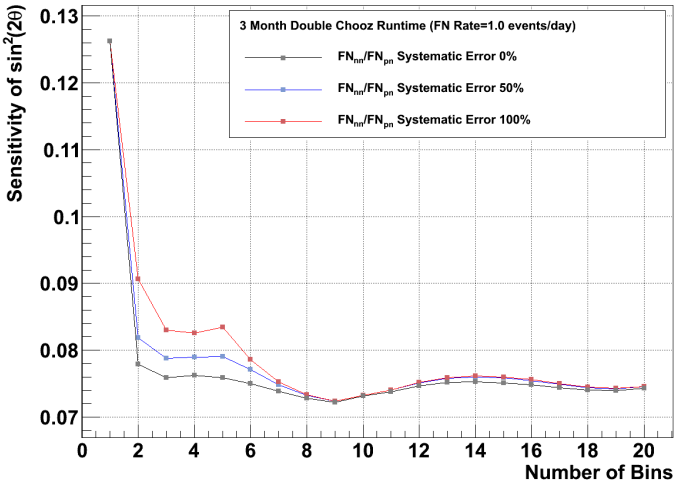

Figure 5.4: Influence of the number of energy bins in the Rate+Shape analysis on the sensitivity of Double Chooz after 3 month data taking, where the prompt energy range of 1-10 MeV is divided up into equally sized energy bins.

from $5 \rightarrow 6$ energy bins. Now the information of the background shape is included. With increasing bin numbers the sensitivity stays now more or less constant.
But there is another reason using more than e.g. 2 energy bins in data-analysis. That is also shown in figure 5.4. The sensitivity at >8 bins is mostly unaffected by a large uncertainty in the neutron-neutron to proton-neutron ratio uncertainty $\sigma_{\mathrm{n}}^{\mathrm{rel}}$. As expected the Rate-Only analysis is influenced not at all while the two-bin analysis is affected strongly. The reason for that is that assuming a large uncertainty in the relative height of the two Gaussian peaks is affecting only a few bins of a 20-bin-Rate+Shape analysis. The same but smaller effect would occur with the lower fast neutron rate of 0.3 events/day. This result clearly favors the usage of many bins (>8) for the Rate+Shape analysis.

Error Description	Uncertainty	
	Correlated	Uncorrelated
Reactor		
Isotope Fraction	1.5%	
Reactor Power	2.0%	
Solid angle		0.07%
Detector		
Detection Cross Section	0.1%	
Target Mass		0.2%
Target free H fraction	0.5%	
Analysis		
e^+ identification Cut		0.1%
n identification Cut		0.2%
n capture on Gd		0.3%
ΔT Cut		0.1%
Total error Phase-I	**2.6%**	
Total error Phase-II	**0.5%**	

Table 5.2: List of correlated and uncorrelated systematic errors among the near and far detector [153]. Background systematics are not given here.

5.3 Reactor, Detector and Analysis induced Systematics

5.3.1 List of Systematics

Systematic errors can be classified into four categories: Reactor, detector, background and data analysis induced uncertainties. Before concentrating in section 5.4 on the influence of background events in this section a brief description of the three other systematic uncertainties is provided, given in table 5.2.

Reactor Uncertainties: The dominant reactor induced uncertainty comes from the limited knowledge of the physical processes producing $\overline{\nu}_e$ in the nuclear reactors resulting in a 2% uncertainty on the absolute core power. The evolution with time of the reactor fuel composition and isotope fraction, the so called burn-up effect [157], introduces an additional error of 1.5%. Furthermore, the near detector is affected by finite size and solid angle effects up to a level of 0.1%.

Detector Uncertainties: The basic principle of the two-detector concept is the cancellation of reactor and correlated-detector uncertainties. Correlated detector uncertainties are the $\overline{\nu}_e$-cross section quoted with 0.1% and the free H fraction in the

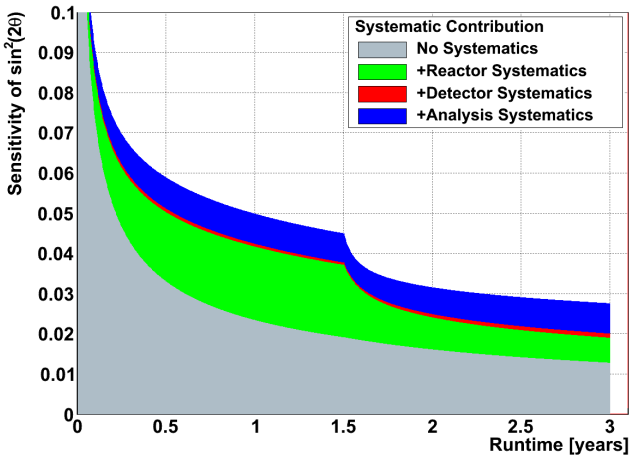

Figure 5.5: Influence of the systematic errors described in section 5.3 on the sensitivity for different runtimes of Double Chooz. After 1.5 years the near detector is assumed to start data taking. No background is included.

target with 0.5%. An uncorrelated detector uncertainty is the relative target mass with 0.2%.

Analysis induced Uncertainties The used cuts in particle identification will introduce uncorrelated systematical errors. The most basic cuts are the energy cut on the positron (0.1%), the neutron (0.2%) and the ΔT cut (0.1%). Furthermore, there is an uncertainty in the fraction of neutrons being captured on Gd (0.3%).

This results in a total systematical error for the period without the near detector (Phase-I) of 2.6% and for the two detector period (Phase-II) of 0.5%.

5.3.2 Influence on the Sensitivity

To test the individual contribution of each type of systematic a Shape+Rate analysis using 20 energy bins was applied and the different systematics of table 5.2 were used for the calculation of the sensitivity. The reactor power σ_{react} and isotope uncertainty σ_{iso} are set to the values in table 5.2. The other correlated and uncorrelated errors of table 5.2 are included in σ_{n} and σ_{n}^{d} respectively. The energy calibration error σ_{cal} was set to 0.5% [153]. No uncertainty due to background was included so far.

In figure 5.5 the influence of the three types of background (reactor, detector and analysis uncertainties) is illustrated, assuming the near detector to start data taking after 1.5 years.

Some remarks to figure 5.5 are given below:

- In the first weeks of data taking the influence of the statistical error (gray curve) dominates clearly the sensitivity. After roughly 0.5 years the systematic errors are of similar size. If there would be no correlated systematic errors the near detector data would contain no information and thus there is no improvement in the sensitivity after 1.5 years in the gray distribution.
- The dominating systematical errors in Phase-I are the reactor uncertainties (green curve) as they are the largest contributor to the total error. After the near detector starts data taking their influence decrease but does not vanish totally as still the information of the Phase-I period is contained in the data.
- The analysis induced errors (blue curve) dominate the sensitivity especially after 1.5 years as they are treated as uncorrelated and, therefore, not influenced by the near detector.
- The detector systematics (red curve) play a minor role in both phases of data taking as they are relatively small.

5.4 Influence of Background on the Sensitivity

After having analyzed the different backgrounds occurring in Double Chooz in chapter 4, one can now determine their influence on the sensitivity again using the sensitivity-program [156].

5.4.1 Accidentals

As explained in section 4.1 it is a very helpful feature of the accidental background that one can measure the rate and shape accurately in the experiment itself. Therefore, in this sensitivity studies a rate uncertainty of only 10% was assumed.
In figure 5.6 one can see the influence on the sensitivity of the accidental background for different rates. The gray colored distribution includes no background but the expected systematical errors from the reactor, detector and analysis cuts explained in the last section. For the near detector a ten times higher single rate was assumed which should be realistic and is mainly a result of a higher muon induced neutron rate [79]. No other background was applied in this analysis. In figure 5.6 the result is illustrated. Table 5.3 shows the relative change of the sensitivity for different accidental rates for a short runtime (1/4 year) and right before the near detector starts data taking (1.5 years). Thus, it is obvious that a clean detector and a good shielding is important. At the short runtime the influence of the accidental background is relatively small as statistical fluctuations and total rate uncertainties dominate. At

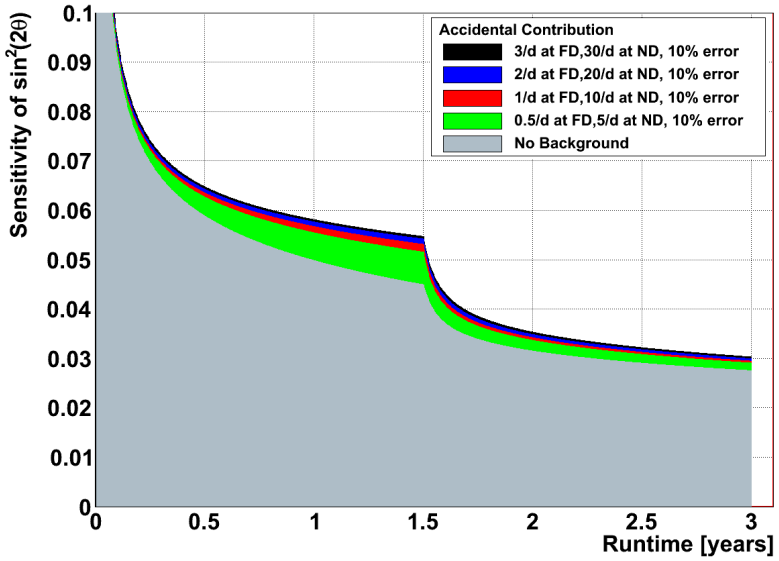

Figure 5.6: Influence of accidental background on the sensitivity for different accidental rates.

Accidental Rate	1/4 year data taking		1.5 years data taking	
[events/day]	Sensitivity	Rel. Change	Sensitivity	Rel. Change
0.00	0.0699	0%	0.0450	0%
0.5±0.05	0.0723	3.4%	0.0516	14.6%
1±0.1	0.0729	4.3%	0.0531	18.0%
2±0.2	0.0736	5.3%	0.0542	20.4%
3±0.3	0.0743	6.3%	0.0547	21.6%

Table 5.3: Change of the Double Chooz sensitivity due to different rates of accidental background after 1/4 and 1.5 years of data taking.

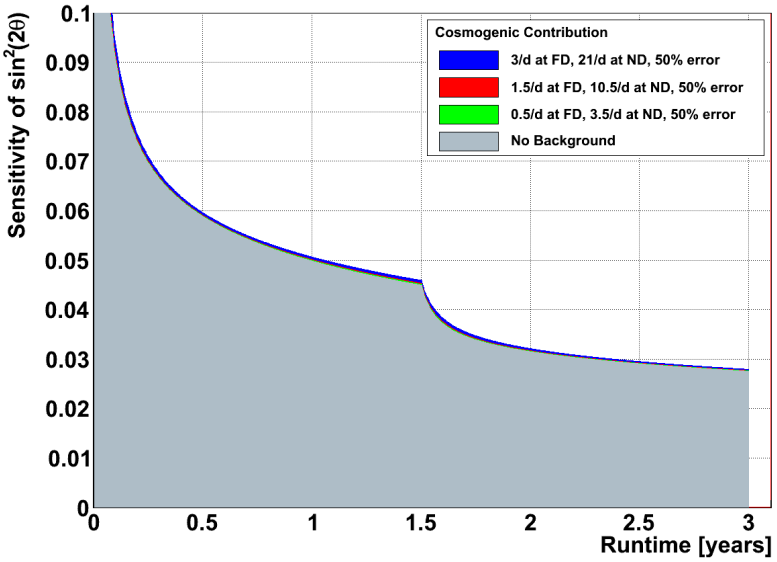

Figure 5.7: Influence of cosmogenic background on the sensitivity for different cosmogenic rates.

later stages the contribution of the accidental uncertainty to the total systematic error becomes sizeable. Therefore, it is obvious that a low accidental rate is crucial for the experiment.

5.4.2 Cosmogenics

According to Monte Carlo studies and extrapolation from the CHOOZ result the cosmogenic background (mainly ^{9}Li) will be the one with the largest absolute rate (beside Spill In current). Naively one would, therefore, expect that the cosmogenic background gives the largest contribution to the sensitivity. But that is not the case as one can see in figure 5.7. It will be demonstrated in section 5.4.5 that only in the first weeks, when the sensitivity is mostly influenced by the rate uncertainty, the cosmogenics are a large contributor to the sensitivity. Later, when the shape gets more and more important (as pointed out in section 5.2.2) the cosmogenic background gets less important and only with an unrealistic high ^{9}Li rate of 3 events/day there would be a notable degradation on the sensitivity. The reason is that the ^{9}Li events are mostly dominant in the high energetic part of the positron spectrum.
As shown in section 4.2 the most accurate determination of the ^{9}Li rate comes from the extrapolation of CHOOZ reactor-off data, resulting in a systematic error of 50%. For the near detector a 7-times larger cosmogenic rate was assumed [79]. The result

Cosmogenic Rate	1/4 year data taking		1.5 years data taking	
[events/day]	Sensitivity	Rel. Change	Sensitivity	Rel. Change
0.00	0.0699	0%	0.0450	0%
0.5±0.25	0.0700	0.1%	0.0452	0.4%
1.5±0.75	0.0703	0.6%	0.0454	0.9%
3±1.5	0.0712	1.9%	0.0460	2.2%

Table 5.4: Change of the Double Chooz sensitivity due to different rates of cosmogenic background after 1/4 and 1.5 years of data taking.

is given in figure 5.7. In table 5.4 the influence of different cosmogenic rates on the sensitivity is shown. The relative influence of the cosmogenic background on the sensitivity is larger at a later runtime, as it was already observed for the accidental background. The reason is again that in the first time of experiment statistical errors dominate. Systematical errors have, therefore, only a relatively small influence. At later time when the shape information gets more important the relative influence of background events increase.

5.4.3 Fast Neutrons

The fast neutron background was intensely studied in section 4.3. It was demonstrated that from simulation the rate is 0.3 events/day (applying the IV-cut and the proton-recoil-cut) with a statistical error of 30%. Furthermore, one does not expect a purely flat energy distribution from proton-neutron events but also two Gaussian peaks at 2.2 and 8 MeV from neutron-neutron (fake) events with fraction r_{nn}. This result was included in the equation 5.8 and in the sensitivity-program [156]. For the following study $r_{\mathrm{nn}} = 0.5$ was assumed. The absolute fast neutron rate and relative contribution of neutron-neutron events are expected to have a large uncertainty, as it is difficult to simulate muon induced neutron production yields. Although one will have during the running experiment some possibilities to cross-check the simulation (see section 4.3.3) the systematical error will stay large. For the absolute rate σ_{fn} and the relative secondary neutron contribution $\sigma_{\mathrm{fn}}^{\mathrm{rel}}$ of equation 5.8 an error of 100% was assumed. For the near detector a 6-times larger absolute fast neutron rate was applied [79].
The result for different fast neutron rates can be seen in figure 5.8. Remarkable is the difference in the sensitivity between a purely flat energy distribution ($r_{\mathrm{nn}} = 0$) and a distribution including the neutron-neutron event contribution ($r_{\mathrm{nn}} = 0.5$) which are the green and red distributions. Naively one would expect that an additional uncertainty would worsen the sensitivity. But that is obviously not the case. The reason is that as a consequence of the Gaussian contribution the 8 MeV region gets populated

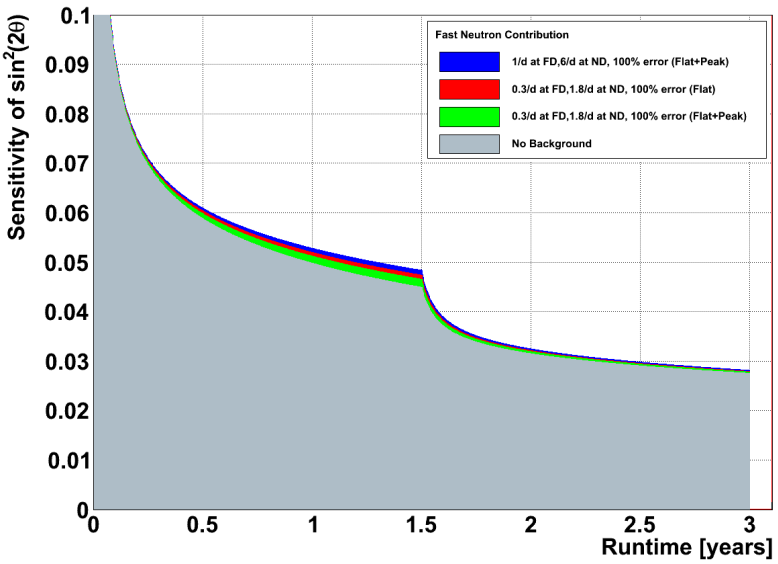

Figure 5.8: Influence of fast neutron background on the sensitivity for different rates.

(where nearly no information of θ_{13} is contained) while the lower energetic part gets depopulated of fast neutron events. As a natural result increasing the relative probability of the 2.2 MeV peak relative to the 8 MeV peak worsens the sensitivity (not shown here). In table 5.5 one can see the result as presented in the tables before. Again one observes the effect that the relative contribution of fast neutron background gets obviously more important with increasing runtime of experiment. The reason is the same as before: The statistical error decreases while the energy shape, much influenced by fast neutrons, gets more important than the pure rate.

Fast Neutron Rate	1/4 year data taking		1.5 years data taking	
[events/day]	Sensitivity	Rel. Change	Sensitivity	Rel. Change
0.00	0.0699	0%	0.0450	0%
0.33±0.33(F+P)	0.0705	0.9%	0.0466	3.6%
0.33±0.33(F)	0.0709	1.4%	0.0474	5.3%
1±1	0.0713	2.0%	0.0484	7.6%

Table 5.5: Change of the Double Chooz sensitivity due to different rates of fast neutron background after 1/4 and 1.5 years of data taking.

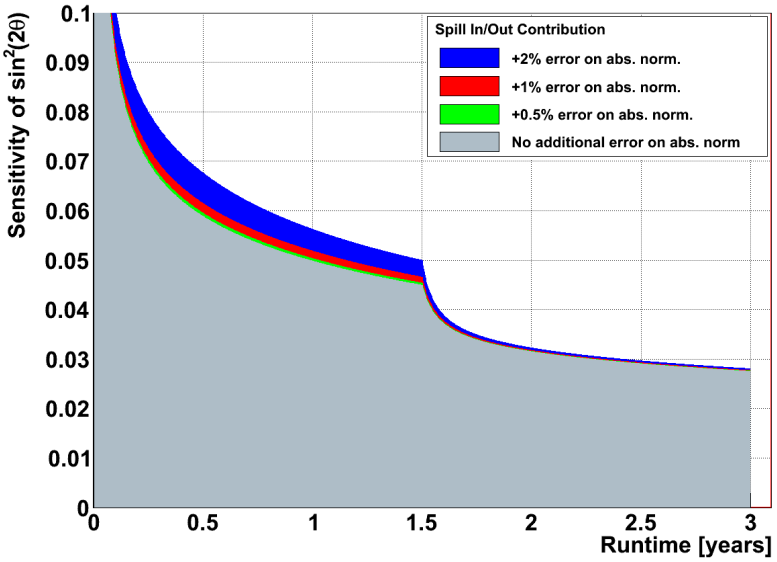

Figure 5.9: Influence of Spill In and Spill Out background on the sensitivity.

5.4.4 Spill In and Spill Out

In section 4.4 it was found by simulation of $5 \cdot 10^5$ IBDs in the target and gamma catcher volume that depending on the time and energy cut one has due to Spill In current 2-5% more neutrino-like events. It was furthermore demonstrated that the systematic uncertainty of Spill In events in simulation is relatively large due to difficulties in simulation to handle low energetic neutrons. Additionally it was demonstrated that not only an increase of detected neutrino events takes place but also a considerably deformation of the observed positron spectrum.
The deformation of the positron spectrum by Spill In current is so far not included in the sensitivity-program used to calculate the influence of different backgrounds on the sensitivity. Therefore, only the influence of an uncertainty on the total event number is given. This is equivalent with an uncertainty of the correlated absolute normalization α_n in equation 5.8, as Spill In current is expected to be the same in near and far detector.
If a timecut ΔT of 200 μs and an energy cut on the prompt event of 0.8 MeV is applied, a Spill In current of 4.6% was calculated (section 4.4). Assuming a 30% uncertainty on Spill In current, the contribution to the uncertainty of the absolute normalization is 1.4%. Figure 5.9 shows the influence of applying different absolute normalization errors to the value of α_n. One can distinguish that after entering the phase with two detectors the absolute normalization error nearly vanishes as expected.

Add. Error abs. Norm.	1/4 year data taking		1.5 years data taking	
[%]	Sensitivity	Rel. Change	Sensitivity	Rel. Change
0.0	0.0699	0%	0.0450	0%
0.5	0.0706	1.0%	0.0454	1.0%
1	0.0728	4.2%	0.0466	3.6%
2	0.0800	14.7%	0.0500	11.1%

Table 5.6: Change of the Double Chooz sensitivity due to different additional errors on the absolute normalization due to Spill In current after 1/4 and 1.5 years of data taking.

Some remarks are given below:

- In table 5.6 the change of the relative distribution of Spill In current is given. It would be crucial to keep the additional error on the absolute normalization below 1%. As one can not change the absolute value of the Spill In current a good understanding of this effect and, hence, a reduction of the systematic uncertainty is important. Using e.g. the methods introduced in section 4.4, after 1 year of data taking the systematic uncertainty can be reduced to 10% compared to 30%, which reduces the contribution for the total systematic uncertainty to below 0.5% and improves the sensitivity considerably.

- Because the Spill In current influence was treated here only as an error on the absolute normalization it is not surprising that the relative contribution gets smaller with the runtime (contrary to other background described before).

- However, as the spectrum deformation of the Spill In current was not included, the real relative contribution of the Spill In current will stay large or even grow relatively compared to the other backgrounds with the runtime. On the other side, the total rate of Spill In current might be overestimated. That was the result of comparing a more realistic bond-atom simulation with a free-atom model, which is the default in DOGS (section 4.4.1). That effect might be up to 30%. As the spectrum deformation and the possible overestimation do not cancel each other the next step must be the integration of the spectrum deformation in the sensitivity-program [156] to correctly determine the Spill In current contribution to the sensitivity of Double Chooz.

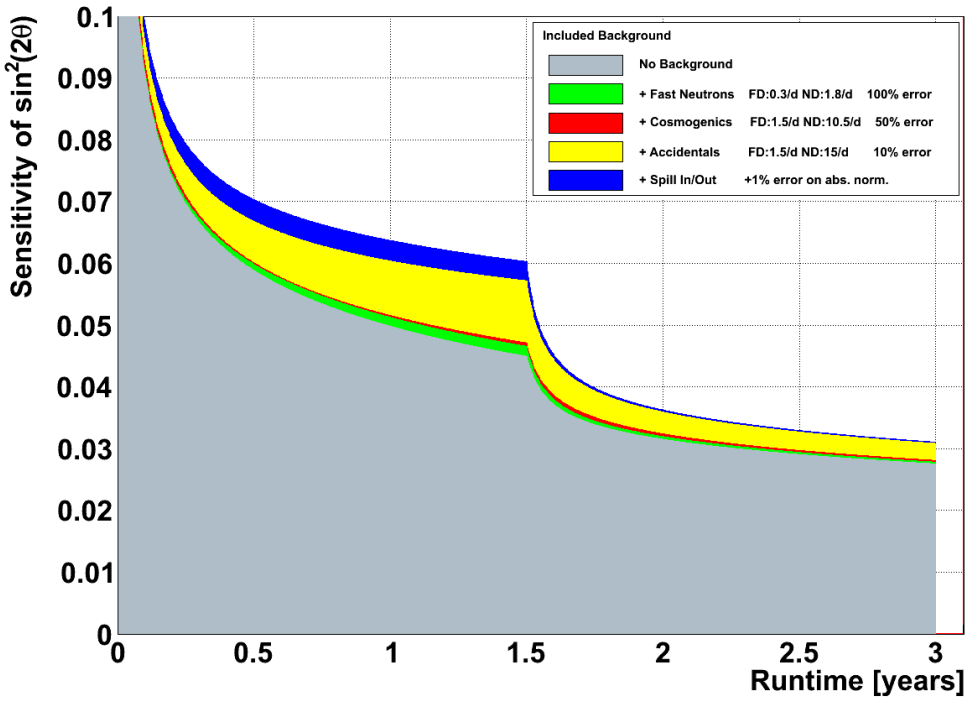

Figure 5.10: Expected sensitivity of Double Chooz for realistic systematic uncertainties and the different background contributions. The Spill In current can be a 0.5-1.4% effect on the absolute normalization, depending on applied cuts. For simplicity 1% is shown.

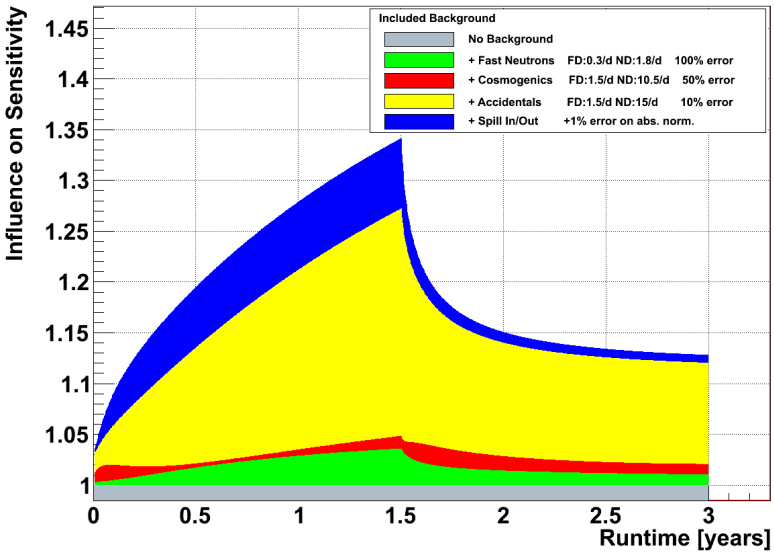

Figure 5.11: Relative influence of the different backgrounds on the sensitivity of Double Chooz.

5.4.5 Global Effect of Background

To close this chapter, the influence of different backgrounds on the sensitivity of Double Chooz is summarized. Therefore, realistic rates and uncertainties for the backgrounds and the no-background systematics are used (the last ones listed in table 5.2). In figure 5.10 one can see the result over the runtime of Double Chooz assuming again the near detector to start data taking 1.5 years after the far detector. In figure 5.11 the relative contribution of backgrounds to the sensitivity is shown.
One can see from figure 5.10 that the limit of CHOOZ ($\sin^2(2\theta_{13}) = 0.15$) is reached already after **one month** of good data taking. Here background plays not the dominant role (<8% decline in the sensitivity due to background) because the total rate contribution of the background is of the same order as statistical rate uncertainty with roughly 3%.
After **three month** the sensitivity will reach $\sin^2(2\theta_{13}) = 0.08$, approximately half of the old limit. The contribution of background is now important as the shape of the spectrum starts to contain information. More precisely, background worsen the sensitivity by now nearly 14%.
After **1.5 years**, right before the start of the near detector the situation has changed. The sensitivity has reached $\sin^2(2\theta_{13}) = 0.06$ while now nearly 32% of the sensitivity limit are build up by background uncertainties. Cosmogenics get relative unimportant

as they leave the low energy part mostly unaffected. Fast neutrons, Spill In current and most of all accidentals limit now the sensitivity strongly due to deformation of the positron spectrum and the large normalization error.
After **three years** data taking (including 1.5 years with the near detector) the sensitivity of $\sin^2(2\theta_{13}) \approx 0.03$ is reached. The relative importance of background events has decreased to a 12% contribution as the relative error of background decrease due to the near detector, the main contributors are now remaining reactor uncertainties of Phase-I and uncorrelated uncertainties of the analysis cuts (figure 5.5).

6 Conclusion

In this thesis detailed studies of the potential of neutrino direction reconstruction have been presented. Already after one year of taking data Double Chooz will be able to resolve the direction of the two reactors with the far detector with a precision of 4.2°. A successful measurement of the reactor direction will be an important test for the detector. Furthermore, it has been demonstrated that Double Chooz will be able to measure the neutron displacement vector with unreached precision and thus will clarify the general possibility of future large volume scintillator experiments to resolve the direction of geo- and supernova neutrinos.
Detailed analysis of all expected sources of backgrounds have been carried out. Predictions for the accidental background based on simulations have been turned out to be uncertain because of the intrinsic difficulties of the simulation to reproduce the muon induced neutron production. However, it is possible to estimate the accidental rate quite precisely with the experiment itself by shifting the coincidence window. Furthermore, it has been demonstrated that the spatial cut between the prompt and late event is an efficient method to reject accidental events. The accidental background has a large influence on the sensitivity of Double Chooz. Depending on the observed accidental rate the application of the spatial cut or even a pulseshape analysis could be appropriate.
This thesis has clarified that it is difficult to set adequate cuts for the ^{9}Li background. Nevertheless the "time since last muon method" turned out to be an efficient tool to determine the ^{9}Li contribution if the muon rate in the inner detector is not too high. Despite an expected rate of 1-2 events/day it has been shown that the ^{9}Li background has a relative small influence on the sensitivity. This has been explained by the fact that ^{9}Li deforms primarily the high energy part of the positron energy spectrum where little information on θ_{13} is contained in a rate+shape analysis.
Various cuts for the fast neutron background and their influence on the neutrino events have been investigated. This thesis has demonstrated that the combined inner veto and proton recoil cuts reject the fast neutron background very efficiently. According to simulations this background can be reduced from 5.6 to 0.3 events/day when both cuts are combined. As the simulation of muon induced processes has quite large uncertainties the possibilities of comparing simulation and experiment have been analyzed. Furthermore, it has turned out that pulseshape analysis is not appropriate for fast neutron events.
Detailed studies have been dedicated to the Spill In current. It causes 2-5% more

neutrino events depending on the applied cuts. The systematic uncertainty has been estimated to 30% which entails an additional systematic normalization uncertainty of $\sim 1\%$. It has been shown that this uncertainty considerably degrades the sensitivity of the experiment during the first phase of the experiment. As soon as the near detector starts taking data, the influence of the Spill In current will nearly disappear. Because calibration and simulation are not able to determine the Spill In current adequately, it has been demonstrated that especially a combined pulseshape and vertex analysis can be used to determine the Spill In rate. An alternative method is the fit of the ΔT spectrum. Both methods combined reduce the uncertainty from 30% to 10% after one year and, hence, improve the sensitivity of Double Chooz significantly. It has been stated that by applying more stringent time and energy cuts the total Spill In current can be reduced by 2%. Finally it has been shown that the Spill In current acts not only as an uncertainty on the total rate but also causes a deformation of the observed positron spectrum. This influence has to be considered in upcoming sensitivity studies.
In summary, the Double Chooz experiment profits from its sophisticated detector design and the purity of the used materials. This thesis has been demonstrated that despite all naturally given uncertainties Double Chooz can reach the CHOOZ limit of $\sin^2 2\theta_{13} = 0.15$ after a few months of taking data. Already in the first phase of the experiment with only using the far detector Double Chooz will achieve a sensitivity of $\sin^2 2\theta_{13} = 0.06$ after 1.5 years. A combined data taking of the near and far detector will bring the sensitivity to $\sin^2 2\theta_{13} = 0.03$ after 3 years totally, which will be the new benchmark value for the last unknown neutrino oscillation angle.

A PMT Calibration and Simulation

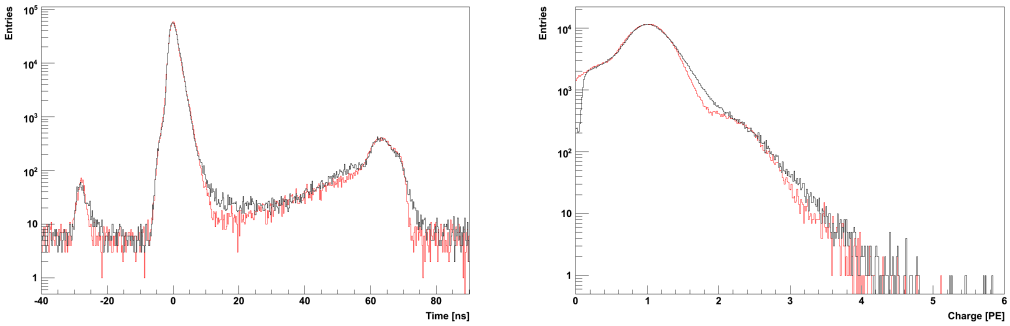

Figure A.1: Simulated (red) and measured (black) time (left) and charge (right) spectrum.

The 390 PMTs in the inner detector observe light produced by particles in the scintillator. These PMTs have to be well tested and calibrated before installation. The qualification tests are shortly summarized in section A.1. Detailed characteristics of afterpulses were performed described in section A.2. The correct implementation of the charge and time response of PMTs in the Double Chooz simulation was done during this PhD as demonstrated in section A.3.

A.1 Calibration of the Inner Detector PMTs

In order to validate specifications and preselect inner detector PMTs before installation at the experiment detailed characterizations of the PMT behavior have been performed. 474 PMTs (half of all PMTs, while the second half were tested in Japan) were tested in the Faraday lab at the MPIK mounted in a 5×6 racking system allowing to test 30 PMTs simultaneously. For each PMT important characteristics like the optimal high voltage, single-photoelectron (SPE) intensity time and charge response, linearity of the integrated charge at increasing light intensity, sensitivity, dark and afterpulse rate and a search for flashers have been investigated. The results

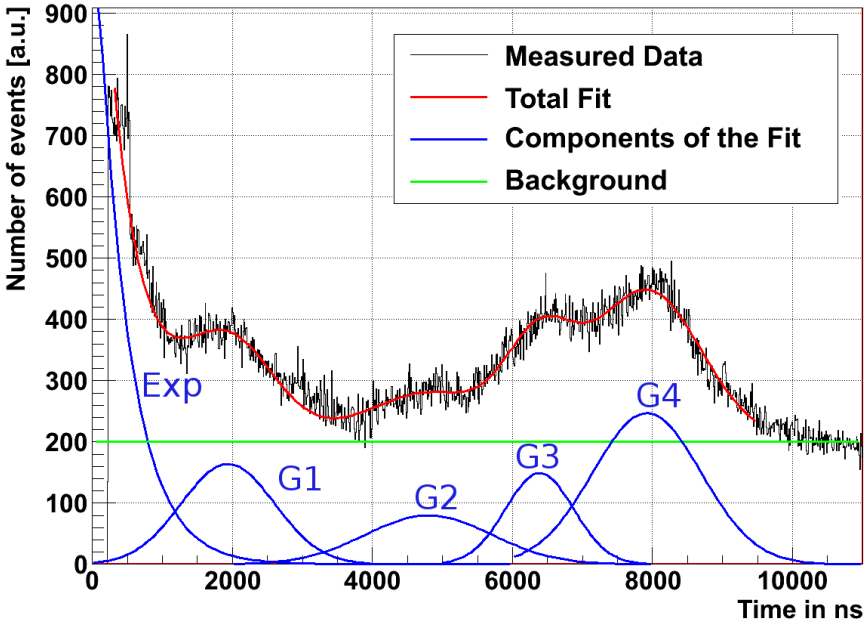

Figure A.2: Measured time distribution of afterpulses (black). The regular pulse is at t=0ns. The red curve is the fit of the measured data using an exponential and 4 Gaussian curves indicated in blue color. Additionally a green background curve was added to the fit function.

of that work are summarized in a paper [20] and two diploma theses [158; 159] and will, therefore, not repeated here.

A.2 Afterpulse Measurements

The origin of afterpulses in a PMT is mainly ionization of residual gas in the PMT by the electron cloud of a regular pulse. The positive charged ion is then accelerated to the photocathode and emits one or more electrons producing a secondary pulse some μs after the regular one. If many of these afterpulses occur at the same time in the detector e.g. after a large energy deposition of a muon they might activate a trigger signal. To estimate this probability it is crucial to know the charge and time distribution of afterpulses and their probability. Therefore, combined charge and time measurements of afterpulses were performed during this thesis.

Fit curve	Parameters
Exponential (Exp)	$c = 1150$, $\tau = 454\,\text{ns}$
Gaussian 1 (G1)	$c = 164$, $\mu = 1936$, $\sigma = 665$
Gaussian 2 (G1)	$c = 80$, $\mu = 4804$, $\sigma = 901$
Gaussian 3 (G1)	$c = 149$, $\mu = 6387$, $\sigma = 487$
Gaussian 4 (G1)	$c = 247$, $\mu = 7919$, $\sigma = 775$

Table A.1: Parameters for the different fit curves describing the afterpulse distribution in figure A.2.

The probability of the afterpulses was measured to roughly 5% in SPE-intensity but varying depending on the analyzed PMT with roughly ±2%. The measured time distribution of the afterpulses can be seen in figure A.2 in the black curve. This distribution was then fitted with an exponential, 4 Gaussian and one constant curve. While the origin of the exponential is not totally resolved the Gaussian curves correspond to different molecules and atoms ionized by electrons. The constant curve includes the noise of the PMT. The fit values can be found in table A.1 Fore more details the reader is referred to [22; 160].

A.3 Simulation of the Charge and Time Response

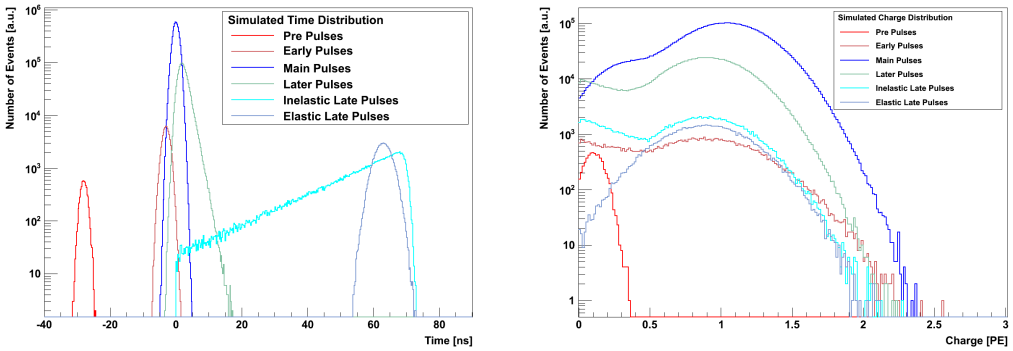

Figure A.3: Simulated time (left) and charge (right) spectrum of SPE intensity.

Figure A.1 shows transit time and charge spectrum of the inner detector PMT using laser light with SPE intensity. In figure A.4 one can see the combined charge over time spectrum. There three kinds of pulses can be distinguished as indicated

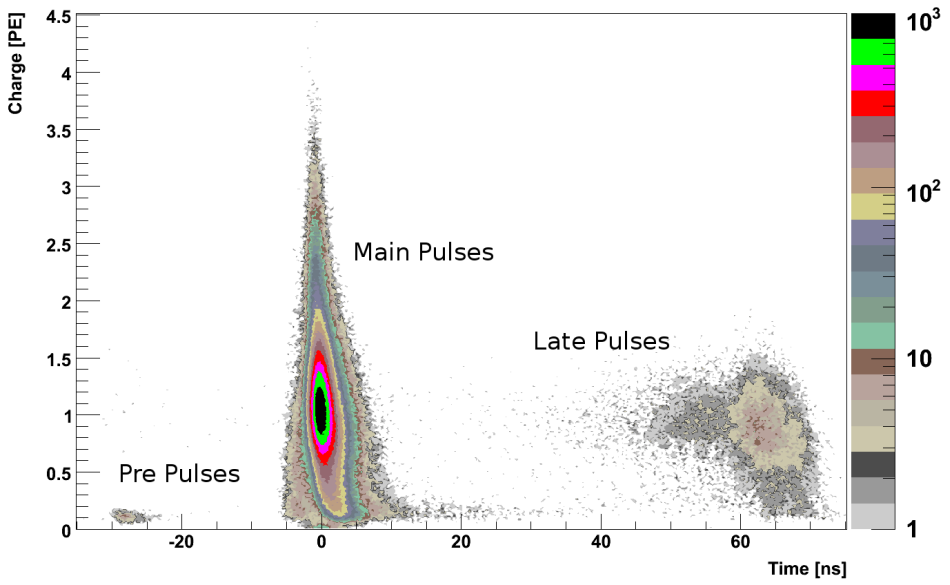

Figure A.4: Measured charge over time distribution.

in the figure. 97 % of all PMT pulses are in the **main peak** which is set to t=0 ns. Roughly 30 ns before so called **pre pulses** occur while up to 70 ns after the main peak the **late pulses** take place. As one can see there is a quite strong correlation between the time and the charge of the pulses.
To include that correlation in the simulation package of Double Chooz (more precisely in RoSS, see section 2.5) in a correct way one first has to understand their physical origin. Both, the analysis and the simulation of the pulses was done during this PhD. Again details are skipped and the interested reader might be referred to [21] where that work is given in more detail. Due to the measurement of time *and* charge of each pulse it was possible to resolve the underlying physical process producing a special kind of charge and time distribution. For example the charge distribution of late pulses could be determined isolated and fitted with an appropriate function. Doing that for every kind of pulse the outcome are different PDFs for the different pulses, which are listed in table A.2 and in figure A.3.
As a result, the simulated time and charge spectrum in the Double Chooz Monte Carlo (DOGS) is now very close to the experimental one and the time and charge correlation is handled in a very accurate way (figure A.4 vs. A.5).

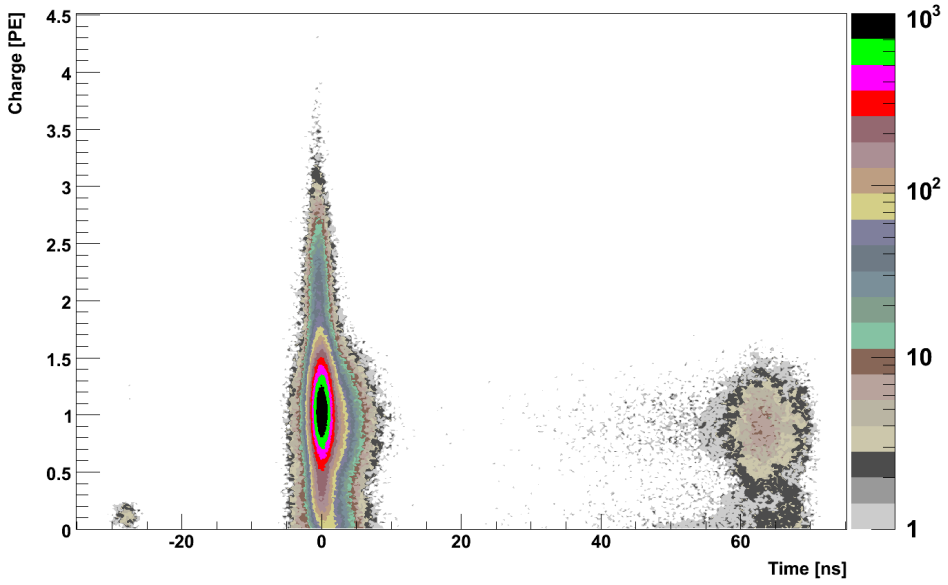

Figure A.5: Simulated charge over time distribution.

Type of Pulse	Process	Time PDF	Charge PDF	Prob.
Pre Pulses	Photon hits 1nd dynode	G	G	0.1%
Early Pulses	Photoelectron is elastic forward scattered at first dynode	G	G+G	1%
Main Pulses	Normally multiplied electrons	G	G+G	77.9%
Later Pulses	Badly amplified electrons	Exp	Exp+G	18%
Inel. Late Pulses	Photoelectron is inelastic backscattered at the first dynode	Exp	Exp+G	2%
El. Late Pulses	Photoelectron is elastic backscattered at the first dynode	G	G	1%

Table A.2: Summary of pulses occurring in the multiplication process of the inner detector PMTs. G stands for a Gaussian and Exp for an exponential PDF.

Bibliography

[1] B. Pontecorvo. Mesonium and Antimesonium. *Sov. Phys. JETP*, 6(5):429, 1957.

[2] M. Gell-Mann and A. Pais. Behavior of neutral Particles under Charge Conjugation. *Phys. Rev.*, 97(5):1387–1389, Mar 1955.

[3] R. Davis. Attempt to detect the Antineutrinos from a Nuclear Reactor by the $Cl^{37}(\overline{\nu}, e^-)A^{37}$ Reaction. *Phys. Rev.*, 97(3):766–769, Feb 1955.

[4] Z. Maki, M. Nakagawa, and S. Sakata. Remarks on the Unified Model of Elementary Particles. *Progress of Theoretical Physics*, 28(5):870–880, 1962.

[5] S. Eliezer and A. R. Swift. Experimental Consequences of $\nu_e - \nu_\mu$ Mixing in Neutrino Beams. *Nuclear Physics B*, 105(1):45 – 51, 1976.

[6] H. Fritsch and P. Minkowski. Vectorlike weak Currents, massive Neutrinos, and Neutrino Beam Oscillations. *Physics Letters B*, 62(1):72 – 76, 1976.

[7] S. Bilenky and B. Pontecorvo. Again on Neutrino Oscillations. *Lettere Al Nuovo Cimento (1971-1985)*, 17:569–574, 1976. 10.1007/BF02746567.

[8] B. Cleveland, T. Daily, R. Davis, J. Distel, K. Lande, C. K. Lee, P. Wildenhain, and J. Ullman. Measurement of the solar Electron Neutrino Flux with the Homestake Chlorine Detector. *The Astrophysical Journal*, 496(1):505, 1998.

[9] W. Hampel et al. GALLEX solar Neutrino Observations: Results for GALLEX IV. *Physics Letters B*, 447(1-2):127 – 133, 1999.

[10] J. Abdurashitov et al. Solar Neutrino Flux Measurements by the Soviet-American Gallium Experiment (SAGE) for Half the 22-year solar Cycle. *Journal of Experimental and Theoretical Physics*, 95:181–193, 2002. 10.1134/1.1506424.

[11] Y. Fukuda et al. Measurements of the solar Neutrino Flux from Super-Kamiokande's first 300 Days. *Phys. Rev. Lett.*, 81(6):1158–1162, Aug 1998.

[12] Q. R. Ahmad et al. Measurement of Day and Night Neutrino Energy Spectra at SNO and Constraints on Neutrino Mixing Parameters. *Phys. Rev. Lett.*, 89(1):011302, Jun 2002.

[13] L. Wolfenstein. Neutrino Oscillations in Matter. *Phys. Rev. D*, 17(9):2369–2374, May 1978.

[14] S. Mikheyev and A. Smirnov. Resonance Enhancement of Oscillations in Matter and solar Neutrino Spectroscopy. *Sov. J. Nucl. Phys.*, 42(6):913–917, December 1985.

[15] Y. Fukuda et al. Evidence for Oscillation of atmospheric Neutrinos. *Phys. Rev. Lett.*, 81(8):1562–1567, Aug 1998.

[16] M. Apollonio et al. Limits on Neutrino Oscillations from the CHOOZ Experiment. *Physics Letters B*, 466(2-4):415 – 430, 1999.

[17] W. Pauli. Offener Brief an die Gruppe der Radioaktiven bei der Gauvereins-Tagung zu Tübingen, 1930.

[18] G. Zacek et al. Neutrino-Oscillation Experiments at the Gösgen Nuclear Power Reactor. *Phys. Rev. D*, 34(9):2621–2636, 1986.

[19] SuperKamiokande Collaboration. SuperKamiokande Webpage http://www-sk.icrr.u-tokyo.ac.jp/sk/physics/solarnu-intro-e.html.

[20] C. Bauer, E. Borger, R. Hofacker, K. Jänner, F. Kaether, C. Langbrandtner, M. Lindner, S. Lucht, M. Reissfelder, S. Schönert, A. Stüken, and C. Wiebusch. Qualification Tests of 474 Photomultipliers for the Inner Detector of the Double Chooz Experiment. *arXiv:1104.0758v1*, Apr 2011.

[21] F. Kaether and C. Langbrandtner. Correlated Charge-Time Measurement and Simulation of the R7081 Photomultipliertube. To be published.

[22] J. Haser, F. Kaether, C. Langbrandtner, M. Lindner, S. Lucht, B. Reinhold, S. Roth, A. Stahl, A. Stüken, and C. Wiebusch. Afterpulse Measurements of 474 Photomultipliers as Qualification Test for the Double Chooz Experiment. *JINST*, 2011. To be published.

[23] M. Lindroos and M. Mezetto. *Beta Beams: Neutrino Beams.* Imperial College Press, 2010.

[24] F. Boehm and P. Vogel. *Physics of Massive Neutrinos.* Cambridge University Press, 1992.

[25] N. Schmitz. *Neutrinophysik.* Teubner Taschenbücher, 1997.

[26] K. Zuber. *Neutrino Physics.* Institute of Physics Publishing, 2004.

[27] S. Bilenky, J. Hosek, and S. Petcov. On the Oscillations of Neutrinos with Dirac and Majorana Masses. *Physics Letters B*, 94(4):495 – 498, 1980.

[28] B. Kayser. On the Quantum Mechanics of Neutrino Oscillation. *Phys. Rev. D*, 24(1):110–116, Jul 1981.

[29] M. Mezzetto and T. Schwetz. θ_{13} : Phenomenology, present Status and Prospect. *Journal of Physics G: Nuclear and Particle Physics*, 37(10):103001, 2010.

[30] T. Schwetz, M. Tortola, and J. Valle. Global Neutrino Data and recent Reactor Fluxes: Status of three-flavour Oscillation Parameters. *arXiv:1103.0734v1*, 2011.

[31] W. Grimus, A. Joshipura, S. Kaneko, L. Lavoura, H. Sawanaka, and M. Tanimoto. Non-vanishing Ue3 and $\cos^2\theta_{23}$ from a broken Z2 symmetry. *Nuclear Physics B*, 713(1-3):151 – 172, 2005.

[32] P. Huber, M. Lindner, T. Schwetz, and W. Winter. Reactor Neutrino Experiments compared to Superbeams. *Nuclear Physics B*, 665:487 – 519, 2003.

[33] F. Soler, C. Froggatt, and F. Muheim. *Neutrinos in Particle Physics, Astrophysics and Cosmology*. Sottish Graduate Series, 2009.

[34] H. Minakata, H. Sugiyama, O. Yasuda, K. Inoue, and F. Suekane. Reactor Measurement of θ_{13} and its Complementarity to long-baseline Experiments. *Phys. Rev. D*, 68(3):033017, Aug 2003.

[35] C. Cowan, F. Reines, F. Harrison, H. Kruse, and A. McGuire. Detection of the free Neutrino: A Confirmation. *Science*, 124(3212):103–104, 1956.

[36] C. Bemporad, G. Gratta, and P. Vogel. Reactor-based Neutrino Oscillation Experiments. *Rev. Mod. Phys.*, 74(2):297–328, Mar 2002.

[37] S. Abe et al. Precision Measurement of Neutrino Oscillation Parameters with KamLAND. *Phys. Rev. Lett.*, 100(22):221803, Jun 2008.

[38] J. Thomas and P. Vahle. *Neutrino Oscillation, Present Status and Future Plans*. World Scientific, 2008.

[39] D. Michael et al. Observation of Muon Neutrino Disappearance with the MINOS Detectors in the NuMI Neutrino Beam. *Phys. Rev. Lett.*, 97(19):191801, Nov 2006.

[40] M. Ahn et al. Measurement of Neutrino Oscillation by the K2K Experiment. *Phys. Rev. D*, 74(7):072003, Oct 2006.

[41] R. Acquafredda et al. First Events from the CNGS Neutrino Beam detected in the OPERA Experiment. *New Journal of Physics*, 8(12):303, 2006.

[42] M. Ahn et al. Search for Electron Neutrino Appearance in a 250 km Long-Baseline Experiment. *Phys. Rev. Lett.*, 93(5):051801, Jul 2004.

[43] P. Adamson et al. Search for Muon-Neutrino to Electron-Neutrino Transitions in MINOS. *Phys. Rev. Lett.*, 103:261802, 2009.

[44] M. Gonzalez-Garcia and M. Maltoni and J. Salvado. Updated global Fit to three Neutrino Mixing: Status of the Hints of $\theta_{13} > 0$. *Journal of High Energy Physics*, 2010:1–20, 2010. 10.1007/JHEP04(2010)056.

[45] S. Dusini. The OPERA Experiment: A direct Search of the $\nu_\mu \rightarrow \nu_\tau$ Oscillations. *Progress in Particle and Nuclear Physics*, 64(2):187 – 189, 2010. Neutrinos in Cosmology, in Astro, Particle and Nuclear Physics, International Workshop on Nuclear Physics, 31st course.

[46] N. Agafonova et al. Observation of a first ν_τ Candidate Event in the OPERA Experiment in the CNGS Beam. *Physics Letters B*, 691(3):138 – 145, 2010.

[47] M. Komatsu, P. Migliozzi, and F. Terranova. Sensitivity to θ_{13} of the CERN to Gran Sasso Neutrino Beam. *Journal of Physics G: Nuclear and Particle Physics*, 29(2):443, 2003.

[48] D. Karlen. Near Detectors for the T2K Experiment. *Nuclear Physics B - Proceedings Supplements*, 159:91 – 96, 2006. Proceedings of the 4th International Workshop on Neutrino-Nucleus Interactions in the Few-GeV Region.

[49] T. Kobayashi. Status of T2K. *Neutrino 2010, XXIV International Conference on Neutrino Physics and Astrophysics, Athens, Greece*, 2010.

[50] Y. Itow et al. The JHF-Kamioka Neutrino Project. *Nucl. Phys. Proc. Suppl.*, 111, 2001.

[51] M. Aoki, K. Hagiwara, and N. Okamura. Measuring the CP-violating Phase by a long base-line Neutrino Experiment with Hyper-Kamiokande. *Physics Letters B*, 554(3-4):121 – 132, 2003.

[52] NOvA-Collaboration. NOvA Proposal to build a 30 Kiloton off-Axis Detector to study Neutrino Oscillations in the Fermilab NuMI Beamline. *arXiv:hep-ex/0503053v1*, 2005.

[53] P. Huber, M. Lindner, M. Rolinec, T. Schwetz, and W. Winter. Prospects of Accelerator and Reactor Neutrino Oscillation Experiments for the coming ten Years. *Phys. Rev. D*, 70(7):073014, Oct 2004.

[54] A. Donini, D. Meloni, and S. Rigolin. Clone Flow Analysis for a Theory inspired Neutrino Experiment planning. *Journal of High Energy Physics*, 2004(06):011, 2004.

[55] S. Rigolin. Physics Reach of Beta-Beams and Neutrino-Factories: The Problem of Degeneracies. *Nuclear Physics B - Proceedings Supplements*, 155(1):33 – 37, 2006. Proceedings to the 7th International Workshop on Neutrino Factories and Superbeams.

[56] A. Rubbia. Neutrino Factories: Detector Concepts for Studies of CP and T Violation Effects in Neutrino Oscillations. *arXiv:hep-ph/0106088v1*, 2001.

[57] The Daya Bay Reactor Antineutrino Experiment. Daya Bay Homepage http://dayawane.ihep.ac.cn/twiki/bin/view/Public/ and Proposal http://arxiv.org/abs/hep-ex/0701029.

[58] P. Huber, M. Lindner, M. Rolinec, and W. Winter. Optimization of a Neutrino Factory Oscillation Experiment. *Phys. Rev. D*, 74(7):073003, Oct 2006.

[59] S. Mikheyev and A. Smirnov. Resonant Amplification of ν-Oscillations in Matter and solar-Neutrino Spectroscopy. *Il Nuovo Cimento C*, 9:17–26, 1986. 10.1007/BF02508049.

[60] J. Hosaka et al. Three Flavor Neutrino Oscillation Analysis of atmospheric Neutrinos in Super-Kamiokande. *Phys. Rev. D*, 74(3):032002, Aug 2006.

[61] M. Mezzetto. Next Challenge in Neutrino Physics: The θ_{13} Angle. *High Energy Physics - Phenomenology (hep-ph)*, 2009.

[62] E. Akhmedov, M. Tórtola, and J. Valle. A simple analytic three-flavour Description of the Day-Night Effect in the solar Neutrino Flux. *Journal of High Energy Physics*, 2004(05):057, 2004.

[63] J. Klein. Results and Prospects for SNO. *Neutrino 2010, XXIV International Conference on Neutrino Physics and Astrophysics, Athens, Greece*, 2010.

[64] F. Calaprice. Solar and terrestrial Neutrino Results from Borexino. *Neutrino 2010, XXIV International Conference on Neutrino Physics and Astrophysics, Athens, Greece*, 2010.

[65] G. Fogli et al. Hints of $\theta_{13} > 0$ from global Neutrino Data Analysis. *Phys. Rev. Lett.*, 101(14):141801, Sep 2008.

[66] C. Lunardini and A. Smirnov. Probing the Neutrino Mass Hierarchy and the 13-mixing with Supernovae. *Journal of Cosmology and Astroparticle Physics*, 2003(06):009, 2003.

[67] P. Dornan. Future Neutrino Experiments. *Proceedings of Science*, 2009.

[68] M. Apollonio et al. Oscillation Physics with a Neutrino Factory. *High Energy Physics - Phenomenology*, 2002.

[69] A. Rubbia. Neutrino Detectors for future Experiments. *Nuclear Physics B - Proceedings Supplements*, 147:103 – 115, 2005. HIF 2004.

[70] C. Amsler et al. The MUNU Experiment: General Description. *Nuclear Instruments and Methods in Physics Research Section A: Accelerators, Spectrometers, Detectors and Associated Equipment*, 396(1-2):115 – 129, 1997.

[71] P. Huber and T. Schwetz. Precision Spectroscopy with Reactor Antineutrinos. *Phys. Rev. D*, 70(5):053011, Sep 2004.

[72] K. Schreckenbach, G. Colvin, W. Gelletly, and F. Von Feilitzsch. Determination of the Antineutrino Spectrum from ^{235}U thermal Neutron Fission Products up to 9.5 MeV. *Physics Letters B*, 160(4-5):325 – 330, 1985.

[73] A. Hahn, K. Schreckenbach, W. Gelletly, F. von Feilitzsch, G. Colvin, and B. Krusche. Antineutrino Spectra from ^{241}Pu and ^{239}Pu thermal Neutron Fission Products. *Physics Letters B*, 218(3):365 – 368, 1989.

[74] N. Haag. Bestimmung des Antineutrinospektrums der Spaltprodukte von ^{238}U. Diploma thesis, TU München, 2008.

[75] B. Achkar et al. Comparison of Anti-Neutrino Reactor Spectrum Models with the Bugey-3 Measurements. *Physics Letters B*, 374(1-3):243 – 248, 1996.

[76] G. Mention, M. Fechner, T. Lasserre, T. Mueller, D. Lhuillier, M. Cribier, and A. Letourneau. The Reactor Antineutrino Anomaly. *arXiv:1101.2755v3*, 2011.

[77] T. Mueller et al. Improved Predictions of Reactor Antineutrino Spectra. *arXiv:1101.2663v3*, 2011.

[78] P. Vogel and J. Beacom. Angular Distribution of Neutron inverse Beta Decay. *Phys. Rev. D*, 60(5):053003, Jul 1999.

[79] Double Chooz Collaboration. Double Chooz: A Search for the Neutrino Mixing Angle θ_{13}. 2006.

[80] M. Apollonio et al. Determination of Neutrino incoming Direction in the CHOOZ Experiment and Supernova Explosion Location by Scintillator Detectors. *High Energy Physics - Experiment*, 61, 1999.

[81] C. Aberle. Optimierung der Fluoreszenzcharakteristik von Flüssigszintillatoren des Double Chooz Reaktorneutrinoexperiments. Diploma thesis, MPIK Heidelberg, 2008.

[82] B. Reinhold. *Development of a Level-1 Trigger and Timing System for the Double Chooz Neutrino Experiment*. PhD thesis, RWTH Aachen, 2009.

[83] T. Akiri. *Test des Flash-ADCs, Optimisation de la Conception du Détecteur et Développement d'un nouveau Concept de Reconstruction spatiale dans l'Expérience d'Oscillation de Neutrinos Double Chooz*. PhD thesis, Universite Paris Diderot, 2010.

[84] DOGS: The Double Chooz Offline Group Software. DOGS Homepage http://doublechooz.in2p3.fr/Private/Working_Groups/MC-Offline/index.php.

[85] Y. Déclais. Neutrino Oscillation Search at Reactors. *Nuclear Physics B - Proceedings Supplements*, 70(1-3):148 – 154, 1999. Proceedings of the Fifth International Workshop on topics in Astroparticle and Underground Physics.

[86] F. Boehm et al. Results from the Palo Verde Neutrino Oscillation Experiment. *Physical Review D*, 62, 2000.

[87] F. Boehm et al. Final Results from the Palo Verde Neutrino Oscillation Experiment. *Physical Review D*, 64, 2001.

[88] M. Ragheb. Neutron Diffusion Theory. 2007.

[89] W. Poenitz and J. Whalen. Measurements of the total Neutron Cross Sections of Hydrogen and Carbon at 0.5, 1.0 and 2.0 MeV. *Nuclear Physics A*, 383(2):224 – 232, 1982.

[90] K. Hochmuth, M. Lindner, and G. Raffelt. Exploiting the directional Sensitivity of the Double Chooz near Detector. *Phys. Rev. D*, 76(7):073001, Oct 2007.

[91] T. Undagoitia et al. Low Energy Neutrino Astronomy with the large liquid Scintillation Detector LENA. *Progress in Particle and Nuclear Physics*, 57(1):283 – 289, 2006. International Workshop of Nuclear Physics 27th course - Neutrinos in Cosmology, in Astro, Particle and Nuclear Physics.

[92] T. Undagoitia et al. LENA: A multipurpose Detector for low Energy Neutrino Astronomy and Proton Decay. *Journal of Physics: Conference Series*, 120(5):052018, 2008.

[93] K. Hochmuth, F. von Feilitzsch, B. Fields, T. Undagoitia, L. Oberauer, W. Potzel, G. Raffelt, and M. Wurm. Probing the Earths Interior with a large-volume liquid Scintillator Detector. *Astroparticle Physics*, 27(1):21 – 29, 2007.

[94] K. Hochmuth, F. von Feilitzsch, T. Undagoitia, L. Oberauer, W. Potzel, M. Wurm, and B. Fields. Probing the Earths Interior with the LENA Detector. *Earth, Moon, and Planets*, 99:253–264, 2006. 10.1007/s11038-006-9111-9.

[95] G. Fiorentini, M. Lissia, and F. Mantovani. Geo-Neutrinos and Earth's Interior. *Physics Reports*, 453(5-6):117 – 172, 2007.

[96] T. Araki et al. Experimental Investigation of geologically produced Antineutrinos with KamLAND. *Nature*, 436, 2005.

[97] G. Bellini et al. Observation of Geo-Neutrinos. *Physics Letters B*, 687(4-5):299 – 304, 2010.

[98] B. Fields and K. Hochmuth. Imaging the Earth's Interior: The Angular Distribution of terrestrial Neutrinos. *Earth, Moon, and Planets*, 99:155–181, 2006. 10.1007/s11038-006-9132-4.

[99] G. Domogatsky, V. Kopeikin, L. Mikaelyan, and V. Sinev. Can radiogenic Heat Sources inside the Earth be located by their Antineutrino incoming Directions? *Physics of Atomic Nuclei*, 69:1894–1898, 2006. 10.1134/S1063778806110135.

[100] L. Cadonati, F. Calaprice, and M. Chen. Supernova Neutrino Detection in Borexino. *Astroparticle Physics*, 2002.

[101] M. Ikeda et al. Search for Supernova Neutrino Bursts at Super-Kamiokande. *The Astrophysical Journal*, 669(1):519, 2007.

[102] H. Yüksel, S. Ando, and J. Beacom. Direct Measurement of Supernova Neutrino Emission Parameters with a Gadolinium-enhanced Super-Kamiokande Detector. *Phys. Rev. C*, 74(1):015803, Jul 2006.

[103] M. Sharp, J. Beacom, and J. Formaggio. Potential for Supernova Neutrino Detection in MiniBooNE. *Phys. Rev. D*, 66(1):013012, Jul 2002.

[104] A. Dighe and A. Smirnov. Identifying the Neutrino Mass Spectrum from a Supernova Neutrino Burst. *Phys. Rev. D*, 62(3):033007, Jul 2000.

[105] C. Lunardini and A. Smirnov. Supernova Neutrinos: Earth Matter Effects and Neutrino Mass Spectrum. *High Energy Physics*, 2001.

[106] J. Beacom. Neutrinos from the next galactic Supernova. *High Energy Physics*, 1999.

[107] SNEWS Collaboration. SNEWS Homepage http://snews.bnl.gov/.

[108] J. Beacom and P. Vogel. Can a Supernova be located by its Neutrinos? *Phys. Rev. D*, 60(3):033007, Jul 1999.

[109] R. Tomàs, D. Semikoz, G. Raffelt, M. Kachelrieß, and A. Dighe. Supernova pointing with low- and high-Energy Neutrino Detectors. *Phys. Rev. D*, 68(9):093013, Nov 2003.

[110] A. Burrows, K. Klein, and R. Gandhi. The Future of Supernova Neutrino Detection. *Phys. Rev. D*, 45(10):3361–3385, May 1992.

[111] J. Beacom. Supernovae and Neutrinos. *Nuclear Physics B - Proceedings Supplements*, 118:307 – 314, 2003. Proceedings of the XXth International Conference on Neutrino Physics and Astrophysics.

[112] J. LoSecco. The Double Chooz Response to Supernova. Double Chooz Document 1801-v1, 2006.

[113] B. Reinhold. Data Production for the Data Challenge. Double Chooz Document 1559-v1, 2010.

[114] A. Cucoanes. *Design Studies for the Double Chooz Trigger*. PhD thesis, RWTH Aachen, 2009.

[115] J. B. Birks. *The Theory and Practice of Scintillation Counting*. Pergamon Press, Oxford, 1964.

[116] S. Wagner. Ionization quenching by low Energy Electrons in the Double Chooz Scintillators. Diploma thesis, MPIK Heidelberg, 2010.

[117] H. Watanabe. Proton Quenching Measurements. To be published.

[118] C. Palomares. Single Rate and Spectrum. Double Chooz Document 1682-v1, 2010.

[119] A. Tonazzo. "Neutron" Background: Could it be due to "near-miss" Muons? Double Chooz Document 622-v1, 2009.

[120] M. Apollonio et al. Search for Neutrino Oscillations on a long base-line at the CHOOZ nuclear Power Station. *The European Physical Journal C - Particles and Fields*, 27, 2003.

[121] C. Palomares. Single Measurements. Private Communication, 2010.

[122] Double Chooz Collaboration. Double Chooz, White Paper: A Search for the Neutrino Mixing Angle θ_{13}. *http://arxiv.org/pdf/hep-ex/0606025*, 2006.

[123] K. Zbiri. Physics Process of cosmogenics ^{9}Li and ^{8}He Production on Muons Interactions with Carbon Target in liquid Scintillator. *Nuclear Instruments and Methods in Physics Research Section A: Accelerators, Spectrometers, Detectors and Associated Equipment*, 597(2-3):219 – 221, 2008.

[124] Y. Chen, T. Tombrello, and R. Kavanagh. Decay Modes of ^{9}Li and States of ^{9}Be. *Nuclear Physics A*, 146(1):136 – 148, 1970.

[125] F. Barker and E. Warburton. The beta-Decay of ^{8}He. *Nuclear Physics A*, 487(2):269 – 278, 1988.

[126] T. Hagner et al. Muon induced Production of radioactive Isotopes in Scintillation Detectors. *Astroparticle Physics*, 14, 1999.

[127] S. Abe et al. Study of the Production of radioactive Isotopes through cosmic Muon Spallation in KamLAND. *Physical Review C*, 2009.

[128] K. Eguchi et al. First Results from KamLAND: Evidence for Reactor Antineutrino Disappearance. *Phys. Rev. Lett.*, 90(2):021802, Jan 2003.

[129] C. Thomas. Background Studies for Double Chooz: Identifying ^{9}Li Decay. Undergraduate Thesis, Boston University and Massachusetts Institute of Technology, 2010.

[130] L. Wen, J. Cao, K.-B. Luk, Y. Ma, Y. Wang, and C. Yang. Measuring cosmogenic ^{9}Li Background in a Reactor Neutrino Experiment. *Nuclear Instruments and Methods in Physics Research Section A: Accelerators, Spectrometers, Detectors and Associated Equipment*, 564(1):471 – 474, 2006.

[131] ROOT: A Data Analysis Framework. http://root.cern.ch/drupal/.

[132] MINUIT: Function Minimization and Error Analysis. MINUIT Homepage http://www.dnp.fmph.uniba.sk/cernlib/asdoc/minuit/minmain.html.

[133] D. Dietrich. Showering Muons. private communication, 2010-2011.

[134] S. Desai. Upward showering Muons in Super-Kamiokande. *AIP Conf. Proc.*, 870:178–180, 2006.

[135] Y.-F. Wang, V. Balic, G. Gratta, A. Fassò, S. Roesler, and A. Ferrari. Predicting Neutron Production from Cosmic-Ray Muons. *Phys. Rev. D*, 64(1):013012, Jun 2001.

[136] R. Hertenberger, M. Chen, and B. Dougherty. Muon-induced Neutron and Pion Production in an organic liquid Scintillator at a shallow Depth. *Phys. Rev. C*, 52(6):3449–3459, Dec 1995.

[137] M. Aglietta et al. Neutron Flux generated by Cosmic-Ray Muons at 5200 hg/cm^2 s.r. Underground. Depth-Neutron Intensity Curve. *Il Nuovo Cimento C*, 12:467–477, 1989.

[138] Y.-F. Wang, L. Miller, and G. Gratta. New Approach to Background Subtraction in low-Energy Neutrino Experiments. *Phys. Rev. D*, 62(1):013012, Jun 2000.

[139] Jollet C., A. Meregaglia, and A. Tonazzo. Fast Neutrons: Simulation and updated Results. Double Chooz Document 1327-v1, 2010.

[140] C. Grieb. *Future Neutrino Detectors and their Impact on Particle- and Astrophysics*. PhD thesis, TUM, 2004.

[141] V.A. Kudryavtsev. Muon Simulation Codes MUSIC and MUSUN for Underground Physics. *Computer Physics Communications*, 180(3):339 – 346, 2009.

[142] A. Tonazzo. Muon Simulation Studies. Double Chooz Document 1259-v1, 2009.

[143] V. Durand. ^{9}Li background from CHOOZ. Double Chooz Document 1330-v1, 2010.

[144] D. Budjas, M. Heider, O. Chkvorets, S. Schönert, and N. Khanbekov. Pulse Shape Analysis with a broad-Energy Germanium Detector for the GERDA Experiment. pages 2513 –2515, 2008.

[145] G. Ranucci, P. Ullucci, S. Bonetti, I. Manno, E. Meroni, and A. Preda. Scintillation Decay Time and Pulse Shape Discrimination of binary Organic liquid Scintillators for the Borexino Detector. *Nuclear Instruments and Methods in Physics Research Section A: Accelerators, Spectrometers, Detectors and Associated Equipment*, 350(1-2):338 – 350, 1994.

[146] C. Aberle. Scintillator Pulse Shapes. Double Chooz Document 1618-v1, 2010.

[147] C. Langbrandtner. Late Light Studies. Double Chooz Document 1462-v1, 2009.

[148] C. Langbrandtner. Other Observables after 1/4 year Data and Impact of the NeutronTH Code. Double Chooz Document 1734-v1, 2010.

[149] T. Mueller. *Expérience Double Chooz : Simulation des Spectres Antineutrinos issus de Réacteurs*. PhD thesis, Université Paris Sud XI-Orsay, 2010.

[150] TRIPOLI4: A 3D Continuous-Energy Monte Carlo Transport Code. TRIPOLI4 description at http://www.oecd-nea.org/tools/abstract/detail/nea-1716.

[151] D. Motta and A. Cucoanes. PSDD. Double Chooz Document 1624-v1, 2010.

[152] G. Feldman and R. Cousins. Unified Approach to the classical statistical Analysis of small Signals. *Phys. Rev. D*, 57(7):3873–3889, Apr 1998.

[153] G. Mention, T. Lasserre, and D. Motta. A unified Analysis of the Reactor Neutrino Program towards the Measurement of the θ_{13} mixing Angle. *arXiv:0704.0498v1*, Apr 2007.

[154] G. Mention. *Étude des Sensibilité et Bruits de Fond de l'Expérience Double Chooz pour la Recherche du Paramétre de Mélange Leptonique* θ_{13}. PhD thesis, Universite Claude Bernard Lyon, 2005.

[155] G. Fogli et al. Getting the most from the statistical Analysis of solar Neutrino Oscillations. *Phys. Rev. D*, 66(5):053010, Sep 2002.

[156] T. Schwetz. C-based program to calculate the sensitivity of Reactor Neutrino Experiments.

[157] B. Achkar et al. Search for Neutrino Oscillations at 15, 40 and 95 meters from a nuclear Power Reactor at Bugey. *Nuclear Physics B*, 434(3):503 – 532, 1995.

[158] S. Lucht. Kalibrierung der Sensitivität und Verstärkung der Photomultiplier für das Double-Chooz-Experiment. Diploma thesis, RWTH Aachen, 2009.

[159] A. Stüken. Kalibration des Rausch- und Nachpuls-Verhaltens von Photomultipliern fur das Double-Chooz-Experiment. Diploma thesis, RWTH Aachen, 2009.

[160] J. Haser. Die Datennahmekette des Double Chooz Experiments und ihre Komponenten. Diploma thesis, MPIK Heidelberg, 2010.

Acknowledgments

Am Ende meiner Doktorarbeit ist es angebracht all jenen zu danken, die Anteil an ihrem Gelingen hatten:
Dies ist an erster Stelle mein Betreuer Prof. Manfred Lindner, dem ich für die Aufnahme in seiner Gruppe, die Freiheiten, die er mir in meiner Arbeit ließ und das Vertrauen, das er mir dadurch geschenkt hat danken möchte.
Dass mir die Zeit der Promotion als eine sehr schöne in Erinnerung bleiben wird, ist vor allem der Double Chooz Gruppe am MPIK zu verdanken: Christoph Aberle, Christian Buck, Benjamin Gramlich, Julia Haser, Florian Kaether, Bernd Reinhold, Ute Schwan, Thomas Schwetz, Stefan Wagner und Hideki Watanabe.
Insbesondere möchte ich Christian Buck, Florian Kaether, Bernd Reinhold, Andreas Schruba, Thomas Schwetz, Friedhelm Serwane und Hideki Watanabe danken, die sich Zeit für die Durchsicht meiner Arbeit genommen haben.

Meinen Eltern danke ich für alles, was sie in meinem Leben für mich getan haben und Gesa für jeden Tag, den ich gemeinsam mit ihr verbringen darf.